Summer 2019

Macrophages and Associated Inflammation Differentially Impact Obesity, Colorectal Cancer and Obesity-Enhanced Colorectal Cancer

Jackie Bader

MACROPHAGES AND ASSOCIATED INFLAMMATION DIFFERENTIALLY IMPACT OBESITY, COLORECTAL CANCER AND OBESITY-ENHANCED COLORECTAL CANCER

by

Jackie Bader

Bachelor of Science
Lynchburg College, 2011

Submitted in Partial Fulfillment of the Requirements

For the Degree of Doctor of Philosophy in

Biomedical Science

School of Medicine

University of South Carolina

2019

Accepted by:

E. Angela Murphy, Major Professor

Mitzi Nagarkatti, Committee Member

Traci Testerman, Committee Member

Daping Fan, Committee Member

Mark Davis, Committee Member

Cheryl L. Addy, Vice Provost and Dean of the Graduate School

DEDICATION

I would like to dedicate this work to my family. To my parents for teaching me hard work, commitment and the importance of having passion in what I do. To my brother for keeping me grounded and humble. You have been my best friend, challenging me to be better and inspiring me to pursue this dream. This would not have been possible without the love and support from you three.

ACKNOWLEDGEMENTS

I have been fortunate enough to have had an incredible and immeasurable support system throughout this process. I would not have gotten to where I am now without the help from several very influential people in my life.

First and foremost, I would like to express my sincerest gratitude to my mentor, Dr. Angela Murphy. Thank you, for molding me into the scientist I am today and supporting me throughout this entire process. Your mentorship has provided me with life changing opportunities for which I am forever indebted to you.

I would also like to acknowledge Drs Reilly Enos and Kandy Velazquez for their mentorship and training. You are, both, incredible scientists that have taken the time to share your knowledge and talent with me. I appreciate all that you have taught me and I am thankful for your friendship and inspiration.

Thank you to the members of my committee, Drs. Mitzi Nagarkatti, Traci Testerman, Daping Fan, and Mark Davis, for donating their time and experience in order to support this work. You have provided unique insight and perspective that has not only strengthened my research but also has made me into a more well-rounded scientist.

To my fellow IBMS graduate students, William Becker, Cody McHale, and Coleman Calva, thank you for your support and friendship. I was incredibly lucky to have shared this journey and experience with you.

ABSTRACT

Colorectal Cancer (CRC) is the third-most common malignancy for men or women, with chronic inflammation considered as a primary risk factor. Obesity is also considered a chronic inflammatory disease and is associated with increased CRC incidence. Further, obesity and CRC occur in men and women differently with the highest incidence of either disease found in men, suggesting that female sex hormones may play a protective role in inflammatory diseases. Macrophages can promote inflammation and are a driving force in obesity-associated metabolic dysfunction. Conversely, macrophages also contribute to pro-tumoral responses including, proliferation, angiogenesis and tissue remodeling. This heterogeneity of macrophage behavior and function within these diseases encourages the need for macrophage targeted studies. Currently, the specific role of macrophages throughout the initiation and progression of these diseases remains unclear. Utilizing clodronate liposomes to target macrophages, we have uncovered that during late stage CRC, macrophage depletion is effective at reducing tumor-promoting macrophage signaling that contributed to reduced tumor burden and a more beneficial microbial composition. However, clodronate mediated macrophage depletion was ineffective at rescuing obesity induced insulin resistance due to compensatory neutrophil associated inflammation. In addition, we examined macrophage behavior within obesity driven CRC. Using a subcutaneous tumor model following diet induced obesity, we found that both insulin resistance and tumor growth presented differently in males, females and ovariectomized (OVX) females. Interestingly, the most severe obesity enhanced tumor

growth was found in the obese OVX mice. This was consistent with increased M2-like tumor associated macrophages, increased subcutaneous adiposity and enhanced macrophage associated adipose tissue inflammation compared to obese females. These results suggest a protective role of female sex hormones in obesity enhanced CRC which is potentially mediated by macrophage associated inflammation. Taken together, our findings confirm a unique role of macrophages and macrophage associated inflammation in CRC, obesity and obesity-enhanced CRC. These findings are significant in further elucidating macrophage behavior through the progression of inflammatory driven diseases and contribute to the mechanistic understanding of sex disparities in obesity associated CRC.

TABLE OF CONTENTS

LIST OF TABLES

LIST OF FIGURES

LIST OF ABBREVIATIONS

CLD..... Clodronate Liposomes

CRC.....Colorectal Cancer

DEXA ..... Dual energy X-ray absorptiometry

H&E ..... Hematoxylin & Eosin

HFD.....High Fat Diet

IFN-γ .....Interferon Gamma

IGF-1.....Insulin-like Growth Factor 1

IL.....Interleukin

JNK ..... Jun Amino-terminal Kinase

LFD ..... Low Fat Diet

M1 ..... Classically Activated Macrophage

M2 .....Alternatively Activated Macrophage

MCP-1..... Monocyte Chemoattractant Protein 1

OVX.....Ovariectomized Female Mice

NF-κB .....Nuclear Factor Kappa B

PMC .....Polymorphonuclear

TAM..... Tumor Associated Macrophage

TGF ..... Tumor Growth Factor

TNF ..... Tumor Necrosis Factor

VEGF ..... Vascular Endothelial Growth Factor

CHAPTER 1

INTRODUCTION

Macrophages are major players in the inflammatory response and are not only the most abundant immune population in a tumor microenvironment, but also are a driving force in obesity-associated inflammation leading to metabolic dysfunction. Macrophages are considered highly plastic immune cells and can assume a variety of functions according to their environment. They can be generally categorized into two broad but distinct subsets as either, classically activated (M1), which are pro-inflammatory/anti-cancer or alternatively activated (M2), which are anti-inflammatory/pro-cancer. However, recent evidence suggests macrophages exist on a spectrum of diverse phenotypic states rather than the rigid dichotomy of M1/M2 phenotypes[1]. Such heterogeneity of macrophage behavior provides uncertainty regarding the role of macrophages in the progression of certain chronic inflammatory diseases. This led us to explore the role of macrophages and macrophage associated inflammation in chronic inflammatory diseases: obesity, colorectal cancer (CRC) and obesity enhanced-CRC.

1.1 Macrophages in Chronic Inflammation

Chronic inflammation is a prolonged condition in which tissue injury and repair simultaneously occur, leading to tissue remodeling and dysfunction. Chronic inflammation often begins as a low-grade, smoldering response which lacks the cardinal signs of inflammation; pain, heat, redness and swelling[2]. Moreover, the continuous progression of tissue injury and repair promotes extensive fibrosis that may eventually cause irreversible tissue dysfunction. This persistent low-grade inflammation has been found responsible for promoting many diseases, specifically obesity associated insulin resistance and CRC[3-5].

Macrophages can enter various tissues in response to chronic inflammation and assume different functions and phenotypes according to the cues they receive from the environment[6]. The infiltration of macrophages within tissues is controlled, in part, through the monocyte chemoattractant protein-1 (MCP-1)[1]. Upon entering the tissue in response to MCP-1, pro-inflammatory cytokines such as IFN-γ, TNF, or Toll-like receptor (TLR) ligands, encourage an M1 phenotype while M2 phenotype is promoted upon IL-4, IL-10, or TGF-β stimulus. M1 macrophages release high levels of pro-inflammatory cytokines, including tumor necrosis factor-α (TNF-α), MCP-1, IL-6, and inducible nitric oxide synthase (iNOS) [7]. On the contrary, M2 macrophages have been demonstrated to express high levels of mannose receptor (CD206), and produce a large amount of IL-10, and arginase-1[8, 9]. In the context of chronic inflammation, the ratio between M1 and M2 macrophages is constantly shifting during bouts of inflammation followed by periods of tissue healing. This fluctuation in macrophage subsets throughout the progression of chronic inflammation makes it unclear which macrophage subsets are truly responsible for disease progression.

1.2 Inflammation induced colorectal cancer

Colorectal cancer is the third most prevalent cancer as well as the third leading cause of cancer related deaths. Although, direct etiology is uncertain, there is an increased risk of colorectal cancer within individuals suffering from chronic inflammatory diseases, particularly, inflammatory bowel diseases (IBD). As discussed previously, macrophages can strongly influence both the onset of inflammation within the colon and conversely, promote tissue remodeling, which can support dysplasia. The intestine is the largest

reservoir of macrophages in the body [10] where they have a close relationship with luminal bacteria. [11] Under inflammatory conditions, monocytes are recruited to the lamina propria and become inflammatory macrophages that secrete cytokines. [12] This macrophage-induced inflammation mediates many pro-tumoral responses. [13-18] Thus, it is no surprise that macrophages have been implicated in tumorigenesis given their propensity to promote inflammation. [18-30]

Although M1 macrophages are heavily involved in initiating colon inflammation, the resulting M2 macrophage mediated tissue remodeling can trigger tumor growth. Within this tumor microenvironment, macrophages are the most abundant immune population. Tumor derived factors such as TGF-β and IL-10 have the potential to polarize infiltrating monocytes mainly into a M2-like phenotype that can then further promote proliferation, invasion and metastasis, angiogenesis, and matrix deposition and remodeling [31]. These macrophages are referred to as tumor-associated macrophages (TAMs). The majority of studies have reported that high levels of TAMs are associated with poor prognosis in CRC [32, 33], with just a few reports indicating an association between macrophage infiltration and increased survival [34, 35]. A crosstalk between TAMs and cancer cells enhances production of inflammatory cytokines, chemokines, proteases, growth factors and angiogenesis-related factors [31]. Additionally, these substances transform the tumor microenvironment to favor the survival, growth and motility of cancer cells. Thus, macrophage-induced inflammation mediates many of the pro-tumoral responses in the tumor microenvironment [13-18]. Given macrophages strong presence within the tumor microenvironment, targeting TAMs can offer beneficial effects for inflammation driven cancers.

1.3 Obesity associated inflammation and insulin resistance

Obesity is considered an epidemic and affects more than 1/3 of the U.S. population. It is largely defined by two primary characteristics: chronic, low-grade inflammation and metabolic dysfunction. It is believed that the main driving force behind the development of type 2 diabetes and insulin resistance is inflammation, particularly macrophage associated inflammation [36]. Infiltrating immune cells are primarily pro-inflammatory macrophages, otherwise classified as M1 macrophages which are responsible for adipose tissue inflammation [37]. Under obese conditions, M1 macrophages may account for approximately 50% of all adipose tissue cells [37]. Conversely, in the lean condition, macrophages only account for approximately 10% of all adipose tissue cells, with the anti-inflammatory, M2 macrophage phenotype being the most predominant. During the onset of obesity, the macrophage presence within adipose tissue shifts from M2, which helps promote homeostasis through efferocytosis, angiogenesis promotion and lipid buffering toward a more M1 dominant phenotype which increases production of inflammatory cytokines and reactive oxygen species resulting in non-esterified fatty acid release [38]. More specifically, M1 adipose tissue macrophages secrete the pro-inflammatory cytokines, TNFα, IL-6 and IL-1β, which act as main effectors of impaired adipocyte function and have been shown to reduce insulin sensitivity in certain tissues [37, 39-41]. Therefore, targeting macrophage-associated inflammation may offer potential benefits in preventing or delaying obesity induced insulin resistance.

1.4 Sex-Disparities in Obesity-Enhanced Colorectal Cancer.

A sex-specific effect is present in the incidence of obesity in CRC patients. Several epidemiological studies have demonstrated that obesity increases the risk of and mortality from CRC in males [42-44]. The relationship in females is somewhat inconsistent, in part due to a potential protective effect that reproductive hormones have on CRC. In postmenopausal women however, this effect may be limited to individuals not currently using hormone replacement therapy (HRT) [45]. A protective effect of HRT on colon cancer has been reported in several epidemiological studies [46, 47]. Taken together, these studies suggest that a woman's risk of colon cancer is affected by hormonal status. Despite these findings, the mechanisms linking estrogen and/or progestins to reduced cancer risk have not been fully elucidated.

The role of estrogen in macrophage polarization under physiological conditions remains unclear. There is evidence that estrogen inhibits the production of Th1 cytokines, while stimulating the production of Th2 cytokines [48]. In this case Th2 cytokines generally promote M2 macrophage polarization however there is little evidence to support a direct effect of estrogen on macrophage polarization. Taken together, current literature does not provide a conclusive role for estrogen in CRC and calls for more research to better understand the mechanism behind this suspected protection. Given the influential role of macrophages in chronic inflammatory diseases and differential incidence within males and females, further investigation to test if estrogen has some influence on macrophage behavior is warranted.

1.5 Summary

Macrophages play a variety of roles during the development of chronic inflammation leading to disease. In the context of obesity, M2 adipose tissue macrophages are most abundant in the lean state but as obesity progresses M1 adipose tissue macrophages predominate. These M1 macrophages are thought to drive inflammation induced insulin resistance. Conversely in the context of inflammation associated CRC, intestinal macrophages are more M1 in the early stages of inflammation but during later stages as tumors begin to form, M2 like TAMs predominate which is associated with poor prognosis. There is further evidence to support that sex disparities within these inflammatory diseases, may be, in part, associated with sex hormones influence on macrophage behavior. Therefore, the overall goal of this research is to examine the role of macrophages in CRC and risk factors associated with CRC including obesity and sex. The central hypothesis is that macrophage associated inflammation enhances progression of CRC and this can be exacerbated among obese populations. Further, it is hypothesized that macrophage associated inflammation may contribute to the sex disparities observed in obesity and CRC. This hypothesis was tested by pursuing three research aims: 1) to determine the effect of macrophage depletion on intestinal inflammation, the gut microbiota profile, and colon tumorigenesis [49]; 2) to determine the effect of macrophage depletion in diet induced obesity associated inflammation and metabolic dysfunction [50]; and 3) to examine sex-specific differences as they relate to macrophage behavior in obesity-enhanced CRC.

The purpose of the first study was to examine the role of macrophages in progression of CRC while also considering the interaction between macrophages and gut

microbiota in CRC. This was done using the chemically-induced, azoxymethane (AOM) and dextran sodium sulfate (DSS), model of CRC. In this AOM/DSS model animals develop tumors following three cycles of a colon irritant, resembling inflammation induced CRC, such as in IBD patients. We used clodronate filled liposomes to deplete macrophages during the late stage (week 7) of this model in order to specifically target TAMs rather than inflammatory macrophages within the early stages [51-53].

In the second study, we sought to examine the role of macrophage associated inflammation in obesity induced insulin resistance. Utilizing HFD feeding, an obese phenotype was established prior to depleting macrophages with clodronate encapsulated liposomes, in order to determine if macrophage depletion could serve as an effective intervention to reduce obesity-driven adipose tissue inflammation and to ameliorate metabolic dysfunction.

In the final study, sex differences in obesity enhanced colorectal cancer were examined. Diet induced obesity was established in male, female, and ovariectomized mice, prior to injection of MC38 colon cancer cells subcutaneously. Tumor associated macrophage phenotype and macrophage associated adipose tissue inflammation were examined to better understand the role of macrophages in sex specific effects on diet induced obesity.

Taken together, the studies described offer unique insight into the differential role that macrophages play in the chronic inflammatory driven diseases of obesity and CRC.

CHAPTER 2

MACROPHAGE DEPLETION USING CLODRONATE LIPOSOMES DECREASES TUMORIGENESIS AND ALTERS GUT MICROBIOTA IN THE AOM/DSS MOUSE MODEL OF COLON CANCER[1]

[1]Bader JE, Enos RT, Velázquez KT, Carson MS, Nagarkatti M, Nagarkatti PS, Chatzistamou I, Davis JM, Carson JA, Robinson CM, Murphy EA. Macrophage depletion using clodronate liposomes decreases tumorigenesis and alters gut microbiota in the AOM/DSS mouse model of colon cancer. Am J Physiol Gastrointest Liver Physiol. 2018 Jan 1;314(1):G22-G31

Reprinted here with permission from publisher

2.1 Abstract

We examined the role of macrophages in inflammation associated colorectal cancer (CRC). Given the emerging evidence on immune-microbiota interactions in CRC, we also sought to examine the interaction between macrophages and gut microbiota. To induce CRC, male C57BL/6 mice (n=32) received a single injection of azoxymethane (AOM) followed by three cycles of dextran sodium sulfate (DSS) supplemented water at weeks 1, 4, and 7, respectively. Prior to the final DSS cycle (week 7) and twice weekly until sacrifice, mice (n=16/group) received either 200μl i.p. of clodronate filled liposomes (CLD) or phosphate buffered saline (PBS) encapsulated liposomes to deplete macrophages. Colon tissue was analyzed for polyp burden, macrophage markers, transcription factors, and inflammatory mediators. Stool samples were collected and DNA was isolated and subsequently sequenced for 16S rRNA. Clodronate liposomes decreased tumor number by ~36% and specifically large (≥1mm) tumors by ~36% ($p<0.05$). This was consistent with a decrease in gene expression of EMR1 in the colon tissue and polyp tissue as well as expression of select markers associated with M1 (IL-6) and M2 macrophages (IL-13, IL-10, TGFβ & CCL17) in the colon tissue ($p<0.05$). Similarly, there was a decrease in STAT3 and MAPK p38 and ERK signaling in colon tissue. Clodronate liposomes increased the relative abundance of the *Firmicutes* phylum ($p<0.05$) and specifically *Lactobacillaceae* and *Clostridiaceae* families, which have been associated with reduced CRC risk. Overall, these data support the development of therapeutic strategies to target macrophages in CRC and provide support for further evaluation of immune-microbiota interactions in CRC.

2.2 Introduction

Colorectal cancer (CRC) is the third most common malignancy for men or women. For CRCs detected in stage I there is a 91% survival rate whereas that drops to 11% if the cancer is detected in stage IV [54]. As CRC progresses, treatment options become more limited and some patients with advanced CRC opt for no treatment given the lack of success of current therapies. Immunotherapy is a relatively recent strategy that has had some success in treating patients with advanced CRC. However, current immunotherapy options are limited. For example, Pembrolizumab, an immune checkpoint inhibitor targeting PD-1 is limited to patients that have tested positive for specific gene changes [55]. There is a critical need to develop new immunotherapy-based strategies for treatment of CRC.

Macrophages are the most abundant immune population in a tumor microenvironment. They are derived from monocytic precursors circulating in blood and are recruited to the tumor site by chemokines such as MCP-1 and TGFβ [56, 57]. These recruited monocytes differentiate into mature macrophages within the tumor microenvironment. While historically it was thought that macrophages possess anti-tumor functions it is now generally accepted that tumor associated macrophages (TAMs) are conditioned by the tumor environment and exert pro-tumoral functions. Factors such as TGF-β and IL-10 have the potential to modulate and polarize monocytes mainly into M2 macrophages that can then promote proliferation, invasion and metastasis, angiogenesis, and matrix deposition and remodeling [31]. The majority of studies have reported that high levels of TAMs are associated with poor prognosis in CRC [32, 33] with just a few reports indicating an association between macrophage infiltration and increased survival [34, 35].

Understanding the importance of macrophages in CRC is likely to have significant therapeutic implications.

Increasing evidence implicates gut microbiota in the initiation and progression of CRC [58]. Mechanistic support for this relationship comes from animal studies; germ-free status and treatment with wide-spectrum antibiotics results in a significant reduction in CRC [59, 60]. In humans, CRC-associated microbiome risk profiles have been generally characterized as changes in certain microbe abundance and/or changes in microbial diversity. Recent discoveries suggest that immune cells play a pivotal role in this response. For example, host-derived inflammatory responses are important driving forces that shape microbial community composition and, when altered, may contribute to dysbiosis and increased CRC risk [61-63]. Conversely, gut microbes also can influence immune responses in the colon. A recent study reported that germ-free mice exhibit decreased populations of intestinal regulatory T cells [64]. Similarly, antibiotic treatment in mice resulted in reduction of Th17 cells within the colon [65]. Despite the increasing evidence supporting an immune-microbiota interaction in CRC, there are no studies that have directly examined the role of macrophages on gut microbiota in a model of CRC.

The purpose of this study was to examine the role of macrophages in progression of CRC. We also sought to examine the interaction between macrophages and gut microbiota in CRC. This was done using a chemically-induced model of CRC, namely the azoxymethane (AOM) and dextran sodium sulfate (DSS) model. In this AOM/DSS model animals develop tumors due to several gene mutations that are consistent with those seen in CRC patients [66]. We used clodronate filled liposomes to deplete macrophages [51-53]. As we were interested in examining the role of macrophages in progression of

tumorigenesis (as opposed to initiation), macrophages were depleted during the last cycle of DSS treatment (i.e. late stage at a time when tumors are already present as confirmed by our laboratory (unpublished)). Our data indicate that clodronate administration during late stage tumorigenesis results in a decrease in polyp number, reduced expression of select macrophage markers, diminished activation of transcription factors known to regulate carcinogenic processes, and alterations in the gut microbiota profile.

2.3 Materials and Methods

Animals and AOM/DSS model: C57BL/6 (wild-type (WT)) male mice (n=32) were purchased from Jackson Laboratories. All experimental mice were fed an AIN-76A diet (Bio-serv) and were provided with water *ad libitum* for the duration of the experiment. At 8-10 weeks of age, all mice were injected i.p. with a single dose of 10 mg/kg of AOM (Sigma) designated as week 0. DSS (MP Biochemicals; 36,000-50,000 mw) was dissolved in filtered drinking water and administered to mice for 7 days during the following weeks: 1 (2% DSS), 4 (1% DSS), and 7 (1% DSS). To deplete macrophages, we administered a 200ul i.p. injection (~1mg) of clodronate encapsulated liposomes (ClodronateLiposomes, Amsterdam, The Netherlands) beginning at week 6.5 and continuing twice weekly until sacrifice (CLD). This dose was selected based on the recommendations of the manufacturer and previously published literature. Phosphate buffered saline (PBS) encapsulated liposomes (ClodronateLiposomes) were administered in the same manner to the vehicle control group (VEH). After 12 weeks, mice (VEH & CLD) were sacrificed, colon contents were collected for microbiota profiling, colons were dissected, and polyps were counted using a stereoscope. For a subset of samples (n=4-8) the distal portion of the

colon was fixed in 4% paraformaldehyde, paraffin embedded, and sectioned for Hematoxylin & Eosin (H&E) staining. Polyps were removed from the remaining colon tissue and flash frozen for RT-PCR analysis. The remaining colon tissue was then divided into two pieces for western blot and RT-PCR analysis. The Institutional Animal Care Committee of the University of South Carolina approved all the animal experimentation.

Morphometric measurements, food and water intake: Body weight, and food and water intake were monitored weekly over the duration of the experiment. Body composition was assessed before AOM injection and prior to sacrifice (week 12) via dual-energy x-ray absorptiometry (DEXA, Lunar PIXImus) as previously described [67].

Symptom Severity: Symptom score was evaluated twice a week beginning at the first cycle of DSS exposure. Briefly, animal health was monitored by combining the scores of weight loss (WL) (>5%WL=0; 6-10%WL=1; 11-15%WL=2); fecal consistency (pellet=0; pasty=2; liquid=4); and blood in stools (assessed with hemoccult kit negative=0, positive=2, and gross bleeding=4) [68].

Gene expression: Quantitative RT-PCR (ABI-7300) was performed in both the polyp and colonic tissue after RNA isolation with trizol reagent and purification from DSS-treated tissues as described in detail [69]. Sample ct values calculated as relative to 18S rRNA internal control and normalized to vehicle control. The following Taq primers from Applied Biosystems were used: MCP-1, TNFa, IL-6, EMR1, NOS2, IL-10, IL-12a, IL-23, IL-13, TGFb, Arg1, and CCL17.

Western blot analysis: The frozen colons were homogenized in mueller buffer [70] and total protein was determined via the Bradford method. All samples were run in triplicate on the same plate with a CV of less than 3%. Equal amounts of crude protein

homogenates (10-40 μg) were fractioned on hand-casted 6.5-12% SDS-polyacrylamide gels and electrophoretically transferred to a PVDF membrane using a Genie Blotter (IDEA Scientific, Minneapolis, MN). Membranes were stained with a Ponceau S solution to verify equal protein loading and transfer efficiency. Subsequently, membranes were blocked for one hour in 5% milk in Tris-buffered saline, 0.1% Tween-20 (TBST). Primary antibodies were diluted 1:1,000 in 5% milk-TBST or 5% BSA-TBST solution according to antibody specifications for either a 1 hour incubation at room temperature [Cell signaling, Danvers, MA: total ERK (#4676) total Stat 3 (#4904) and total p38 (#8690)] or overnight incubation at 4°C [Cell signaling: total (#8242) and phosphorylated (Ser536) NFκB p65 (#3033), phosphorylated (Thr^{180}/Tyr^{182}) p38 (#4631), phosphorylated ERK (#4376), phosphorylated Stat 3 (y705) (#9138)]. An anti-rabbit (Cell signaling: #7047) or anti-mouse (Cell Signaling: #7076) IgG horseradish peroxidase conjugated secondary antibody was diluted 1:2000 in 5% milk and incubated for one hour at room temperature. An enhanced chemiluminescent substrate for detection of horseradish peroxidase (Thermo Scientific, Watham, MA) was used to visualize the antibody-antigen interaction. Autoradiography films were scanned and blots were quantified using scientific imaging software (Image J). After completion of the western blot, all membranes were stained with Amido black, and the densitometry of each lane was calculated using Quantity One Software (Bio-Rad, Hercules, CA) allowing for total protein normalization. This method of normalization has been shown to be more accurate than typically used loading controls [71].

Histology: Paraffin block sections of the distal colon were stained with H&E and subsequently evaluated blindly by a pathologist (I.C.) and characterized according to the

severity of tumor dysplasia when a tumor was present in the section; low-grade dysplasia (LGD) or high-grade dysplasia (HGD).

Microbiome Analysis: Following sacrifice, feces from the colon was removed, snap frozen and stored at -80°C until analysis. Microbial DNA was isolated from feces using a QIAamp Fast DNA Stool Mini Kit (QIAGEN #51604) according to manufacturers' instruction. The DNA concentration was determined using a Nanophotometer Pearl, diluted to 5 ng/ul in 10 mM Tris Buffer pH 8.5 and stored at -20°C until analysis. Amplification of the 16S rRNA V3-V4 hypervariable region was carried out using the 16S V3 314F forward (5′TCGTCGGCAGCGTCAGATGTGTATAAGAGACAGCCTACGGGNGGCWGCAG 3′) and V4 805R reverse primer (5′GTCTCGTGGGCTCGGAGATGTGTATAAGAGACAGGACTACHVGGGTATCT AATCC3′) with added Illumina adapter overhang nucleotide sequences [72]. The PCR conditions used were 3 min at 95 °C followed by 25 cycles of 30 s at 95 °C, 30 s at 55 °C and 30 s at 72 °C, and a final extension at 72 °C for 5 min. Each reaction mixture (25 µl) contained 50 ng of genomic DNA, 0.5 µl of amplicon PCR forward primer (0.2 µM), 0.5 µl of amplicon PCR reverse primer (0.2 µM) and 12.5 µl of 2× KAPA Hifi Hot Start Ready Mix. Each reaction was cleaned up using Agencourt AMPure XP beads. Attachment of dual indices and Illumina sequencing adapters was performed using 5 µl of amplicon PCR product DNA, 5 µl of Illumina Nextera XT Index Primer 1 (N7xx), 5 µl of Nextera XT Index Primer 2 (S5xx), 25 µl of 2× KAPA HiFi Hot Start Ready Mix, and 10 µl of PCR-grade water. Amplification was carried out under the following conditions: 3 min at 95 °C, followed by 8 cycles of 30 s at 95 °C, 30 s at 55 °C, and 30 s at 72 °C, and a final

extension at 72 °C for 5 min. Constructed 16S metagenomic libraries were purified with Agencourt AM Pure XP beads and quantified with Quant-iTPicoGreen. Library quality control and average size distribution were determined using an Agilent Technologies 2100 Bioanalyzer. Libraries were normalized and pooled to 40 nM based on quantified values. Pooled samples were denatured and diluted to a final concentration of 6 pM with a 30% PhiX (Illumina) control. Amplicons were subjected to pyrosequencing using the MiSeq Reagent Kit V3 in the Illumina MiSeq System.

The online 16S analysis software from NIH (https://nephele.niaid.nih.gov/) was used to analyze sequencing data collected on the Illumina Miseq. FASTQ sequences were uploaded to Nephele and the 16S metagenomics application was executed. The groups of related DNA sequences were assigned to operational taxonomic units (OTUs), and output files were analyzed to determine gut microbial composition.

Statistics: Data were analyzed using commercially available statistical software: Prism 5 and SigmaStat (GraphPad Software). Data were analyzed using an unpaired Student t-test or Fisher's exact test (categorical data). Any statistical test that did not pass the equal-variance test (Bartlett's test for equal variances) was log transformed and then re-analyzed. Data are presented as the mean ± SEMs and the level of significance was set at $p<0.05$.

2.4 Results

Effects of clodronate administration on morphometric characteristics in AOM/DSS treated mice.

Body weights and symptom scores over the course of the 12-week AOM/DSS protocol are presented in Figure 2.1. The dashed line represents the initiation of clodronate treatment at week 6.5 and twice weekly i.p. injections for the duration of the study. There was no difference in body weight between treatment groups prior to clodronate administration; however, body weight was reduced in clodronate treated mice following administration at weeks 7-12 ($p=0.079$, 0.066, 0.015, 0.023, 0.002, and 0.007 respectively (Figure 2.1A)). Despite the decrease in body weight, there was no significant difference in symptom scores between treatment groups over the course of the experiment (Figure 2.1B). It is important to note that mice from each treatment had similar starting body weights ($p=0.218$) ensuring that both groups received similar doses of the carcinogen AOM (Figure 2.1A). Additionally, both groups consumed equal amounts of total DSS over the course of the 12-week protocol ($p=0.923$) (data not shown). Regarding food intake, clodronate treatment significantly decreased consumption compared to control mice and this was consistent with a decrease in lean mass, fat mass and fat% in the DEXA body composition measurements (Figure 2.1 C-E).

Effects of clodronate administration on colon polyps and colon inflammation

Clodronate administration resulted in a significant reduction in overall polyp number ($p=<0.001$). When polyps were stratified by size, we found a reduction in large polyps greater than or equal to 1 mm ($p=0.012$) and a slight, but non-significant, reduction in small polyps less than 1 mm ($p=0.100$) following clodronate treatment (Figure 2.2A-B). Following histological analysis, we did not document any colon carcinomas in either group. However, it should be noted that only the distal colon was included in this analysis and for a small subset of mice (n=4-8). To further explore the effects of clodronate

administration on tumorigenesis, distal colon polyps were evaluated for dysplasia and quantitatively represented as low-grade dysplasia (1) or high-grade dysplasia (2). There was no significant difference in severity of dysplasia between treatment groups with both groups exhibiting high-grade dysplasia in polyps scored (Figure 2.2C-D). Similarly, histological inflammation revealed no differences between the groups. To further evaluate the CRC phenotype, spleen and colon weight and colon length to width ratio were determined. The ratio of spleen to body weight and colon weight was reduced in the clodronate treated group ($p=0.007$ and 0.152 respectively), which is consistent with the decreased tumor number (Figure 2.2E-F). However, there was no difference in the colon length to width ratio (Figure 2.2G).

Effects of clodronate administration on cytokine and cell marker expression in the colon

In addition to histological evaluation of the colon, gene expression profiles via qPCR of cytokine and macrophage cell markers for both colon and colon polyp tissue are shown in Figure 2.3. Within the clodronate treated group, the macrophage cell marker F4/80 was significantly reduced in both colon and colon tumor tissue ($p=<0.001$ and $p=0.024$, respectively) confirming that clodronate was effective at depleting F4/80 positive cells in both the target tissue and tumor (Figure 2.3A). This was consistent with a decrease in MCP-1, a strong macrophage chemoattractant, in the colon tissue of clodronate treated mice ($p=0.019$) (Figure 2.3B). Despite the reduction in the macrophage cell marker F4/80 and macrophage chemoattractant, we were not able to characterize this decrease as M1 or M2 phenotype specific as no statistically significant differences were found for NOS2 and Arg 1, M1 and M2 markers, respectively ($p=0.643$ and $p=0.389$). However, within the colon tissue, anti-inflammatory M2 associated cytokines including IL-13, TGF-β, IL-10,

and CCL-17 were significantly reduced (p=<0.001, 0.002, <0.001, and 0.009, respectively) with clodronate treatment. Aside from IL-6 (p=0.01) there were no significant differences in pro-inflammatory M1 associated cytokines. Despite the reduction in F4/80 expression, there were no significant differences in macrophage marker or cytokine expression in the colon tumors (Figure 2.3C). To confirm that changes in gene expression are reflective of changes in downstream signaling pathways, western blot analysis was performed and results are illustrated in Figure 2.4. Consistent with reduced expression of IL-10 and IL-6 in the clodronate treated group, was activation of the downstream transcription factor STAT3 (p=0.026 and 0.005, respectively). There was also a significant reduction in the activated MAPK signaling molecules p38 and ERK for the clodronate treated group (p=0.003 and p=<0.001, respectively). However, there was no significant difference in NFKb expression for phosphorylated, total or calculated ratio, between the groups.

Effects of clodronate administration on microbiota composition

Stool samples were collected at sacrifice and 16S microbial rRNA sequencing was performed (Figure 2.5). Relative abundance of OTUs in the *Firmicutes* phylum were significantly increased in the clodronate treated group compared with the control group (p=0.02) (Figure 2.5A). Specifically, within the *Firmicutes* phylum, the *Lactobacillaceae* and *Clostridiaceae* families were significantly increased in the clodronate treated group contributing to the respective changes at the Phylum level (p=0.04 and 0.009, respectively). Additionally, there was a slight increase in *Erysipelotrichaceae* family in the clodronate treated group although not statistically significant (p=0.08) (Figure 2.5B). Despite differences in relative abundance within phyla and families, there were no significant

differences between alpha or beta diversity, as shown through Chao1 index and weighted UniFrac PCA plots, respectively (Figure 2.5C-D).

2.5 Discussion

TAMs have been associated with CRC progression, metastasis, and poor prognosis [33, 73-75]. However, this relationship is complex given that different macrophage subsets are likely to have stage-specific roles in CRC progression. Using the AOM/DSS mouse model of CRC we sought to better understand the role of macrophages in tumor progression. As emerging evidence implicates immune-microbiota interactions in CRC we also sought to examine the interaction between macrophages and gut microbiota in CRC. Our data indicate that clodronate administration, a well-established method to deplete macrophages [51-53], during late stage tumorigenesis results in a decrease in polyp number, reduced expression of select macrophage markers, diminished activation of transcription factors, and alterations in the gut microbiota profile.

We used clodronate liposomes to deplete macrophages during the final cycle of DSS (i.e. at a time when polyps are present) to specifically determine their role in tumor progression as opposed to tumor initiation. This approach was employed in order to establish the efficacy of targeting macrophages for treatment of CRC. We report a significant reduction in overall polyp number (36%) as well as the number of large polyps (36%). However, as baseline polyps (i.e. prior to clodronate treatment) were not evaluated we were not able to determine whether clodronate treatment decreased size of existing polyps and/or growth of new polyps. These findings are consistent with a previous study from our laboratory showing that deletion of MCP-1, the most important chemokine for

macrophage recruitment, results in a decrease in polyp number and size in in the *Apc*$^{Min/+}$ mouse model of intestinal tumorigenesis. Zhao et al., reported similar findings with a ~45% percent reduction in AOM/DSS induced tumorigenesis when macrophages were depleted during both the initiation and progression of tumorigenesis [76]. However, unlike the current study, stage-specific effects could not be determined from these reports. Despite the differences in polyp number and size, we were not able to detect a difference in severity of dysplasia or histological inflammation between treatment groups. This may not be entirely surprising given that clodronate administration was performed at a time when mice are likely to already exhibit high dysplasia and this analysis was performed on a small sample size. Similarly, and likely for the same reasons, we were not able to identify any differences in disease activity index scores. Contrary to what would be expected with reduced tumorigenesis, the clodronate treated group had a decrease in body weight and body fat percent; typically, body weight loss or fat loss is associated with worsened outcome in this model. However, given the fact that tumorigenesis was decreased with clodronate and that we (unpublished) and others [77] have found a decrease in food consumption and/or body weight with clodronate/macrophage depletion [77, 78], we suggest that this is an effect of clodronate treatment independent of the tumorigenesis outcomes. Given this, it is certainly possible that the reduced tumorigenesis associated with clodronate treatment could be explained, or partially explained, by the reduction in food intake and subsequent decrease in body weight as there is evidence that caloric restriction reduces tumorigenesis [79]. Nonetheless we believe that our findings set the stage for the development of strategies to target macrophages to treat CRC.

Although clodronate liposomes are a well-established method of macrophage depletion in the colon [51-53], we wanted to confirm successful depletion in our hands and further establish whether it was effective at depleting macrophages in the tumor microenvironment. Indeed, we show that compared to PBS, clodronate-filled liposomes successfully decreased expression of F4/80+, a pan macrophage marker, within the colon tissue and corresponding polyp tissue (Figure 2.3A); although it appeared more effective in the colon tissue. This is not surprising given the route of administration and mechanism of action of clodronate [51-53]; macrophages in the intestinal tissue would likely be more available to uptake the liposomes than those deep within the tumor tissue, clodronate does not result in complete depletion of macrophages, and there is evidence to suggest that TAMs may lose their phagocytic activity as tumorigenesis progresses [80]. To further characterize the effects of clodronate on macrophages in the colon and tumor microenvironment we examined M1 and M2 macrophage associated markers. In general, and as for F4/80, clodronate liposomes were more effective at altering expression of macrophage markers in the colon tissue as opposed to the polyp tissue. In the colon tissue clodronate decreased expression of select M1 (IL-6) and M2 (IL-13, IL-10, TGFβ and CCL17) associated markers along with the macrophage chemoattractant MCP-1 indicating its non-selectivity for macrophage phenotype. Thus, a simultaneous/non-specific reduction in markers associated with both M1 and M2 macrophage populations can reduce tumorigenesis. Interestingly, we found an increase in IL-13 in the tumor microenvironment in the clodronate treated group. IL-13 has been shown to be increased in certain cancers and can influence polarization of TAMs [81, 82]. Therefore, it is possible that the spike in IL-13 is compensatory production of IL-13 by T helper 2 cells in response to the overall

decrease in F4/80 positive cells. While we and others have successfully used clodronate to deplete macrophages, the possibility of also impacting dendritic cells has been reported [51] and these cells can influence CRC [83]. Thus, we cannot rule out a role for dendritic cells in this model. While we did not measure systemic cytokine levels in this study it is certainly possible that a reduction in circulating inflammatory mediators by clodronate [84] also may be contributing to the reduced tumorigenesis in this model. Although these findings should be validated using FACS, we conclude that clodronate administration has beneficial effects on tumorigenesis and that even larger effects may be possible if M2 macrophages can be selectively depleted in the tumor microenvironment.

Given the significant effects of clodronate administration on cytokines in the colon tissue we next examined downstream transcription factors in the normal tissue. STAT3, a major mediator of IL-6 and IL-10 signaling, was reduced following clodronate treatment consistent with the decrease in mRNA expression of IL-6 and IL-10. STAT3 has been reported to be deregulated in many cancers including CRC and has been associated with metastasis and poor prognosis [85, 86]. p38 MAPK also was decreased in clodronate-treated mice. Although the p38 pathway is often related to pro-apoptotic effects and tumor suppressor activity in some tissues, it has been suggested that p38 acquires an oncogenic role particularly in established malignancies [87]. Similarly activated ERK MAPK was decreased in the clodronate-treated group. Mutations leading to constitutive activation of ERK pathways are found in >40% of CRC patients and significantly contribute to tumor formation and progression [87, 88]. In support of our findings, Chiacchiera et. al. has shown that combined inhibition of p38 and ERK MAPK pathways efficiently reduces the volume of xenografted tumors and AOM/DSS-induced tumors *in vivo* [88]. On the other

hand, there was no change in activated NF-κB with clodronate treatment although NFκB has been associated with CRC [89]. The failure to detect a difference in NFκB may not be surprising as there was no difference in TNF-α, an activator of the canonical NFκB pathway, and IL-1β was not measured. Alternatively, the failure to see changes in activated NFκB may reflect averaging of this signal in whole colon comprised of an admixture of cells. While not performed for the current study given limitations in tissue, it would have been useful to double-stain colon sections for both p-NFκB p65 and a macrophage marker to determine whether macrophage NFκB signaling is altered. Even so, these data provide strong support for targeting macrophages to prevent the activation of transcription factors associated with CRC.

Emerging evidence implicates immune-microbiota interactions in CRC [90, 91]. Therefore, we next examined the effects of clodronate treatment on the gut microbiota profile. Relative abundance of OTUs in the *Firmicutes* phylum was significantly higher in the clodronate-treated group. *Firmicutes*, represent one of the two most abundant phyla in the gut microbiota and therefore a change within this phylum can have profound effects on intestinal homeostasis. In fact, decreases in *Firmicutes* have been reported in inflammatory bowel disease and CRC [90, 92-95]. The anti-cancer effects of *Firmicutes* are likely due, at least in part, to the production of short chain fatty acids, specifically butyrate, which has documented effects on CRC. Within this phylum, *Lactobacillaceae* represent the known probiotic *Lactobacillus*, and *Clostridiaceae* contain strong butyrate producers in the clusters IV and XIVa. These bacteria were significantly increased in the clodronate treated group. Despite differences in relative abundance within phyla and families, there were no significant differences between alpha or beta diversity, as shown through Chao1 index and

weighted UniFrac PCA plots, respectively. This indicates that overall alpha and beta diversity within stool was unaffected by clodronate treatment. Thus, our data suggest that macrophages may be facilitating the change in *Firmicutes* abundance. However, these findings should be interpreted with caution as it is unclear whether the change in *Firmicutes* is a direct result of macrophage depletion or an indirect effect of the decrease in tumorigenesis. Contributions from both explanations are also a possibility. Nonetheless, we show a strong association between lower frequency of macrophages, increased *Firmicutes*, and decreased tumorigenesis in this model. Together, this supports further evaluation of macrophage-microbiota interactions in CRC.

In summary, we found that clodronate administration during late-stage tumorigenesis is effective at reducing tumor growth. This was associated with a decrease in select M1 and M2 macrophage markers and chemokines in the colon tissue and a decrease in transcription factors that are linked to CRC. Additionally, the clodronate-treated group was found to have an increased abundance of *Firmicutes*, a phylum with documented anti-tumorigenic effects. Overall, these data support the development of therapeutic strategies to target macrophages in CRC and provide further support for further evaluation of immune-microbiota interactions in CRC.

2.6 FIGURES & LEGENDS

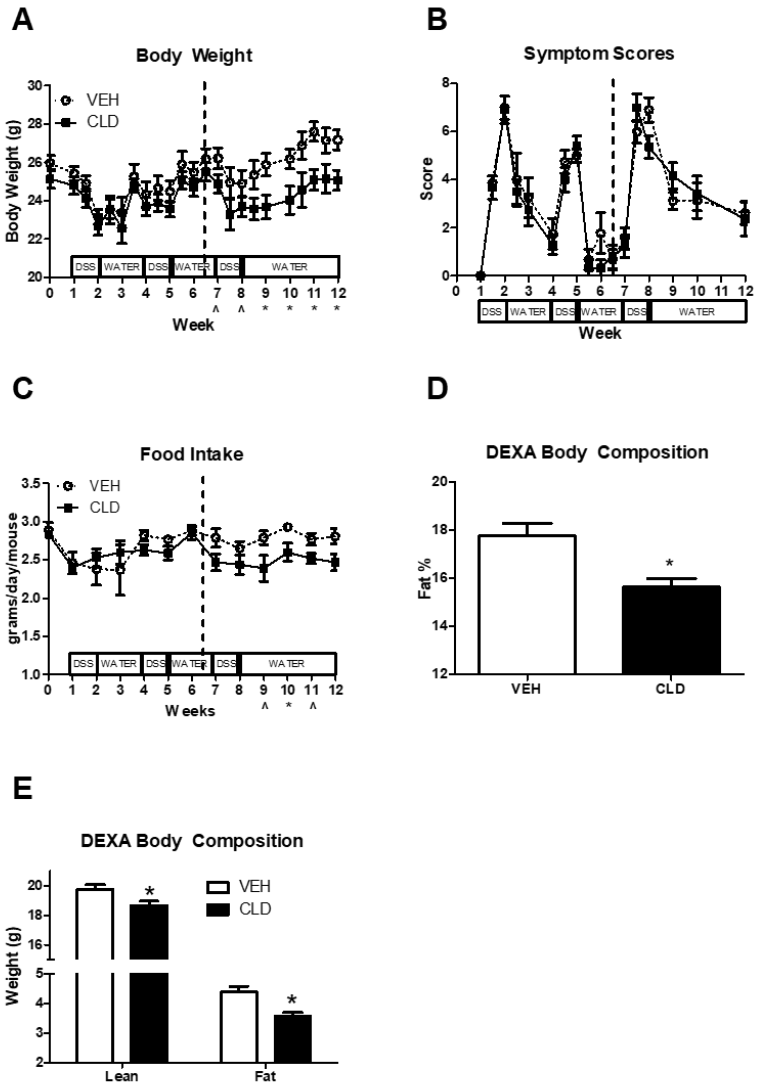

Figure 2.1: Effects of late stage clodronate administration on morphometric characteristics following azoxymethane (AOM) and dextran sulfate sodium (DSS) treatment. The dashed line represents the initiation of clodronate treatment at week 6.5 and twice weekly i.p. injections for the duration of the study. A: Mouse body weight measurements through AOM/DSS protocol and clodronate treatments. B: Symptom score (body weight loss + blood in stool + diarrhea). C: Measured weekly food consumption represented as grams of food per mouse in cage per day. D and E: Body Composition measure via Dual-Energy X-ray Absorptiometry (DEXA) for lean mass, fat mass and fat %. Values are means ± SE; n=16 mice per group. *P < 0.05. ^P < 0.10 unpaired student t-test.

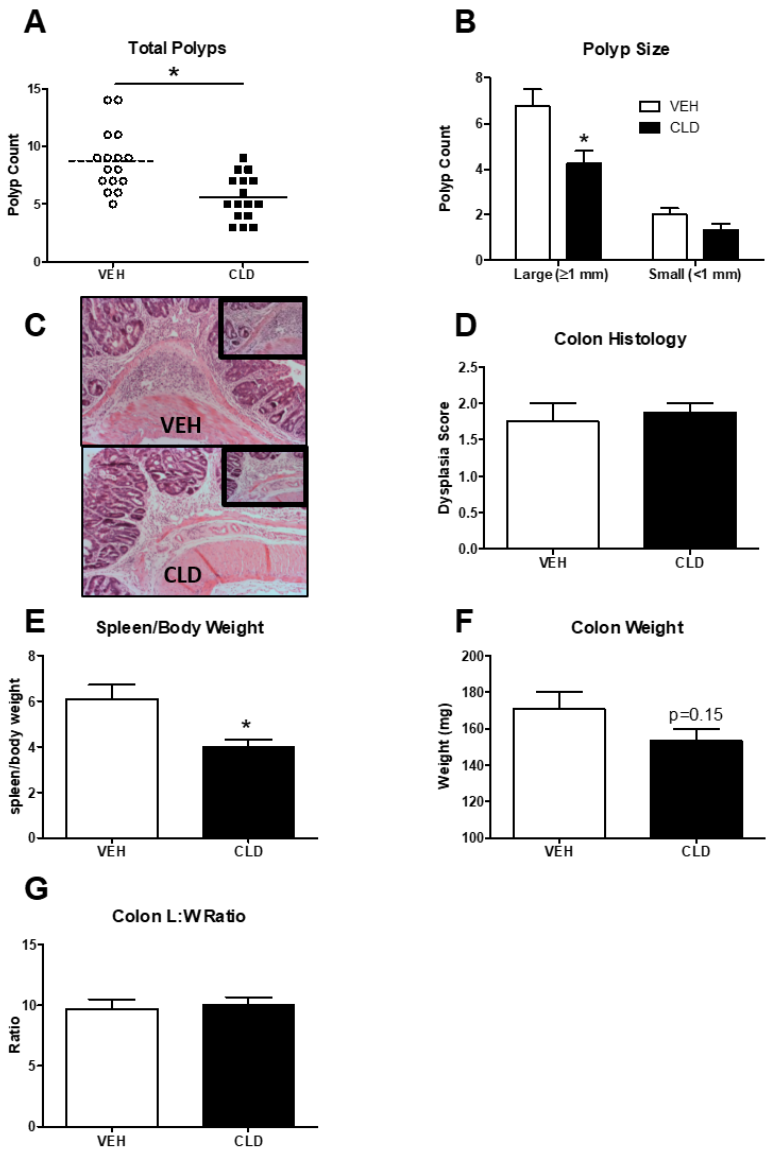

Figure 2.2: Effect of clodronate administration on colon polyps and dysplasia. A and B: Polyp count and size after AOM/DSS treatment. C: Representative hematoxylin-eosin stained sections of distal colon tumor exhibiting high grade dysplasia after AOM/DSS treatment (10X magnification with 20X in upper right box, indicating that dysplastic cells are limited to the mucosa and do not penetrate through the muscularis mucosa). D: Histology evaluation of distal colon tumors (quantitatively represented as low grade dysplasia (1) or high grade dysplasia (2) n=4-8 colons) E: Ratio of spleen weight (mg)/ mouse body weight (g) following AOM/DSS treatment. F: Colon weight (after feces removed). G: Colon length to width ratio. Values are means ± SE; n=16 mice per group unless indicated. *P < 0.05. unpaired student t-test.

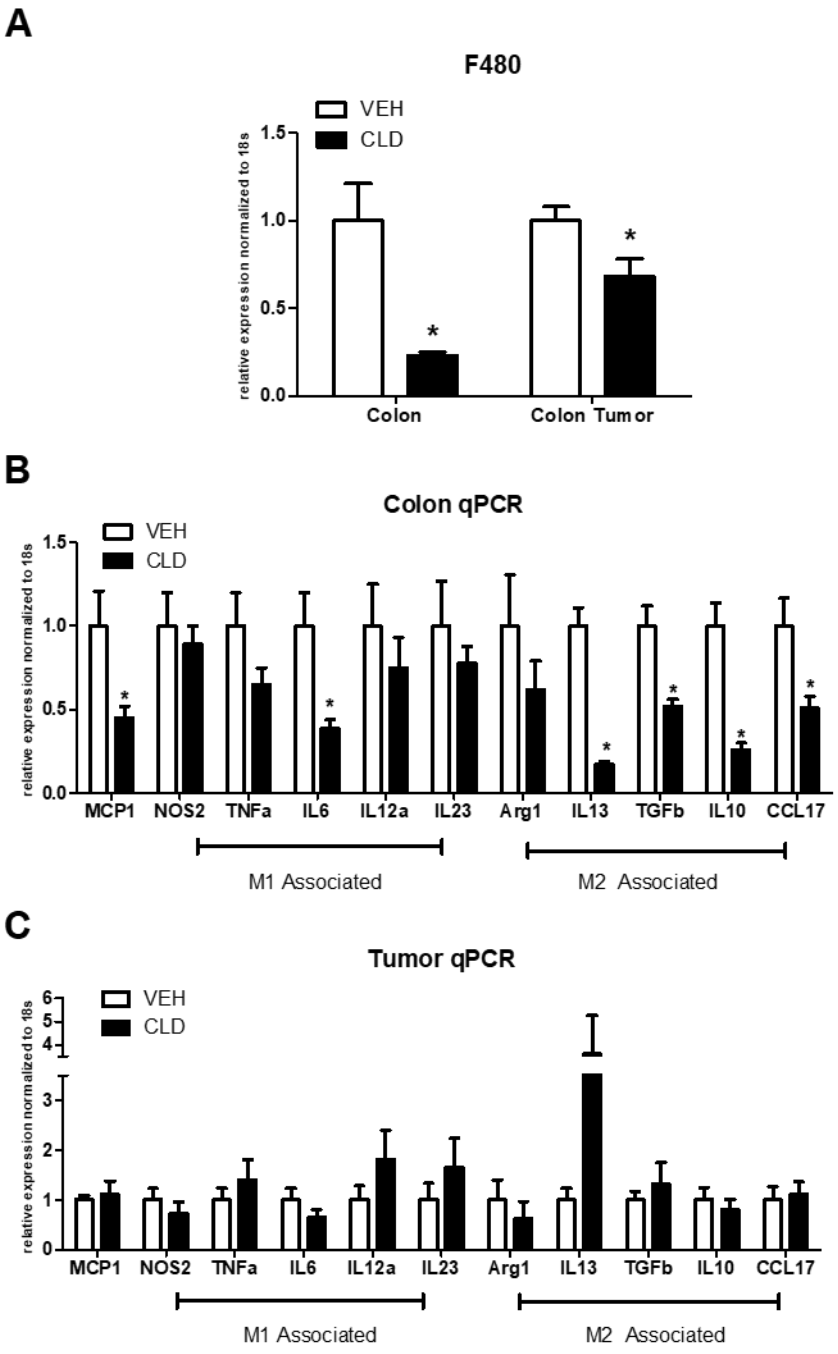

Figure 2.3: Effect of clodronate administration on gene expression in colon and colon polyp tissue. A-C: Quantitative RT-PCR assessment of gene expression in colon and colon tumor tissue. Ct values relative to 18s rRNA internal control and normalized to vehicle control group. Values are means ± SE; n=9 mice per group for colon tissue and n=7 mice per group for colon polyp tissue. *P < 0.05. unpaired student t-test.

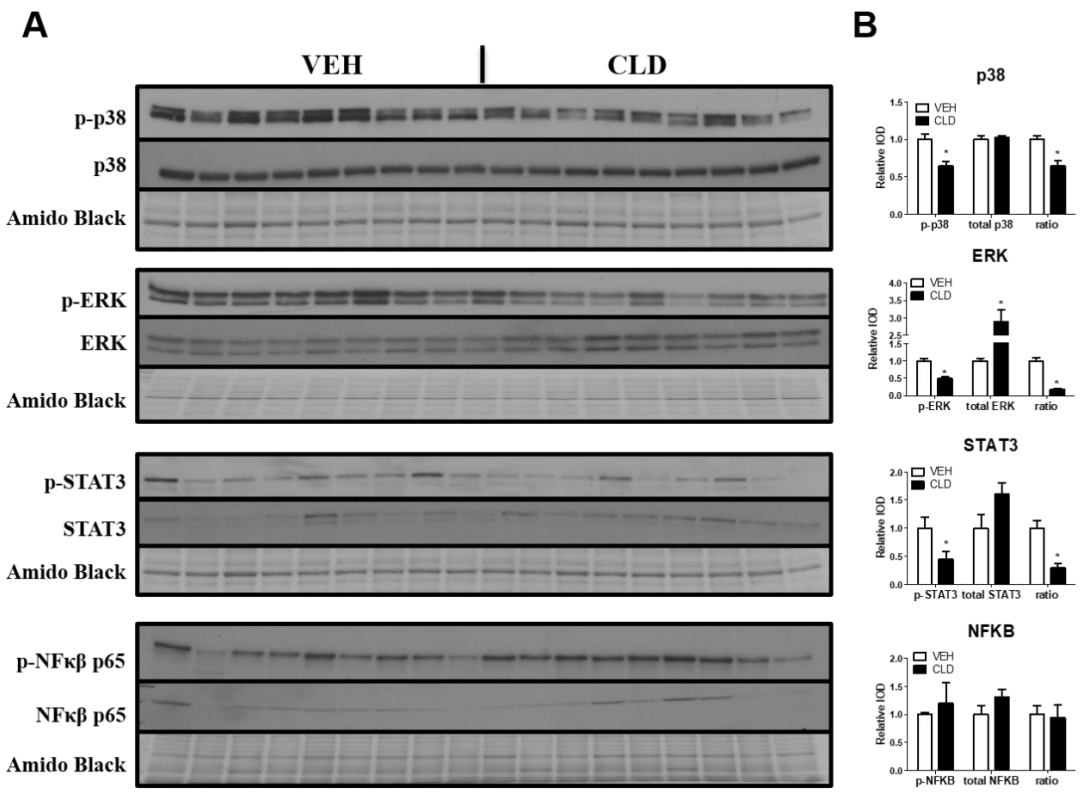

Figure 2.4: Effect of clodronate administration on protein expression in colon tissue. A: Western blot and corresponding amido black membrane stain of colon tissue. B: Quantitative intensity of densitometry relative to total protein normalized to vehicle control. Ratio= total/phosphorylated. Values are means ± SE; n=9 mice per group. *P < 0.05. unpaired student t-test.

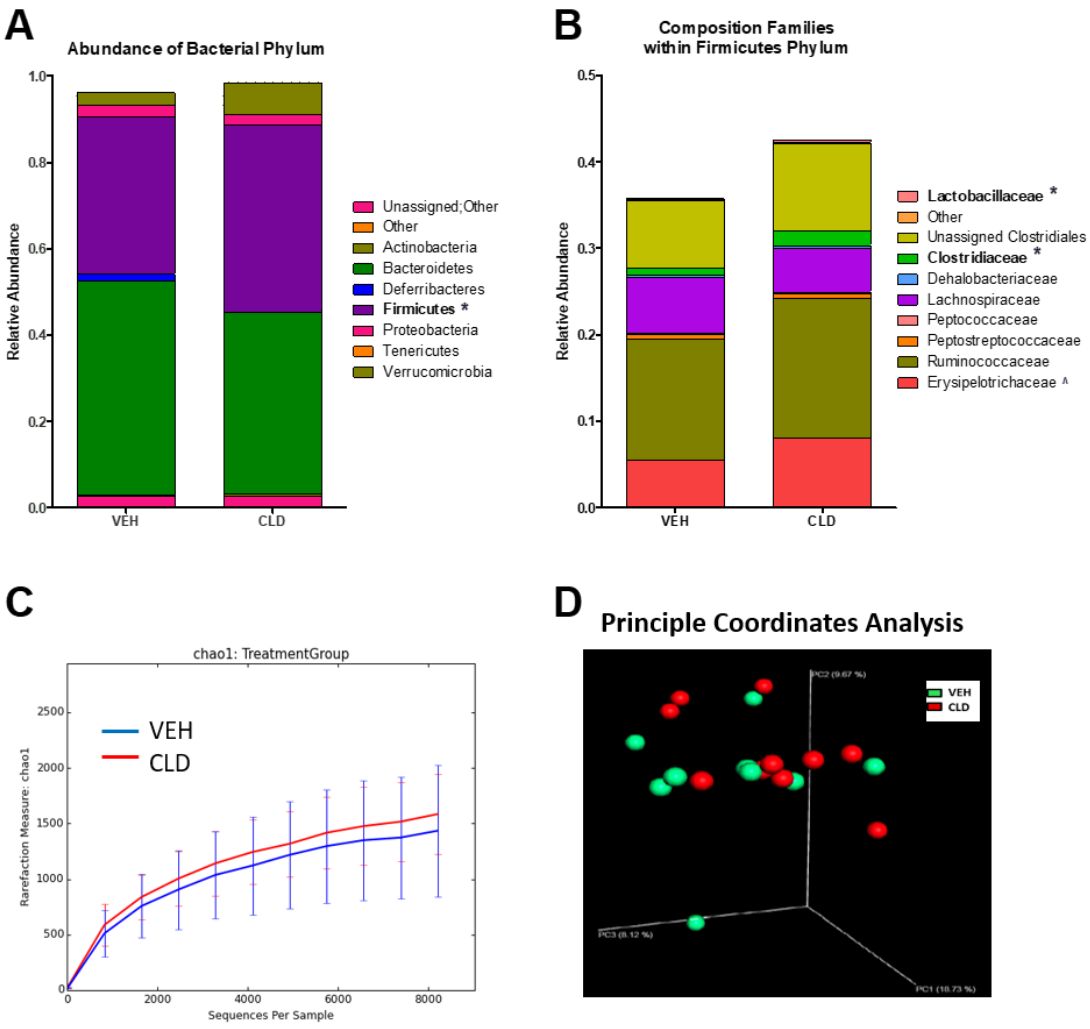

Figure 2.5: Effects of clodronate administration on microbiota composition in stool. A: Relative abundance of OTU in bacterial Phylum following AOM/DSS treatment. B: Composition of Families within the *Firmicutes* phylum (families with abundance less than 0.001 are not shown). C: Rarefraction curve within-sample Chao1 (Alpha Diversity). D: Principal Coordinates Analysis plot of (Beta Diversity) distance between samples matrix. Text in bold indicate significant difference. *p <0.05. n= 10 mice per group.

CHAPTER 3

REPEATED CLODRONATE-LIPOSOME TREATMENT RESULTS IN NEUTROPHILIA AND IS NOT EFFECTIVE IN LIMITING OBESITY-LINKED METABOLIC IMPAIRMENTS[2]

[2]Bader JE, Enos RT, Velázquez KT, Carson MS, Sougiannis AT, McGuinness OP, Robinson CM, Murphy EA. Repeated clodronate-liposome treatment results in neutrophilia and is not effective in limiting obesity-linked metabolic impairments. Am J Physiol Endocrinol Metab. 2019 Mar 1;316(3):E358-E372

Reprinted here with permission from publisher

3.1 ABSTRACT

Objective: Depletion of macrophages is thought to be a therapeutic option for obesity-induced inflammation and metabolic dysfunction. However, whether the therapeutic effect is a direct result of reduced macrophage-derived inflammation or secondary to decreases in fat mass is controversial as macrophage depletion has been shown to disrupt energy homeostasis. This study was designed to determine if macrophage depletion via clodronate-liposome (CLD) treatment could serve as an effective intervention to reduce obesity-driven inflammatory and metabolic impairments independent of changes in energy intake.

Methods: Following 16 weeks of high-fat diet (HFD) or AIN-76A control diet (LFD) (n=30/diet treatment), male *C57BL/6J* mice were assigned to either a CLD or PBS-liposome-treatment (n=15/group) for 4 weeks. Liposomes were administered bi-weekly via intraperitoneal injections (8 administrations in total). PBS-liposome-treated groups were pair-fed to their CLD-treated dietary counterparts. Metabolic function was assessed pre- and post- liposome treatment. Adipose tissue as well as liver were investigated for macrophage infiltration and the presence of inflammatory mediators. Additionally, a complete blood count was performed.

Results: CLD treatment reduced energy intake. When controlling for energy intake, CLD treatment was unable to regress metabolic dysfunction or Non-Alcoholic-Fatty-Liver Disease, and impaired adipose tissue insulin action. Moreover, repeated CLD treatment induced neutrophilia, anemia, increased adipose tissue mRNA expression of the pro-inflammatory cytokines, IL-6 and IL-1β, and augmented circulating IL-6 and MCP-1 concentrations ($p<0.05$).

*Conclusion***:** This study suggests that the repeated administration of CLD treatment to deplete macrophages attenuates obesity by limiting energy intake. Moreover, after controlling for the benefits of weight loss, the accompanying detrimental side effects limit regular CLD treatment as an effective therapeutic strategy

3.2 INTRODUCTION

Obesity has been established as a public health concern given the condition's link to increased health care costs, morbidity, and mortality [96]. The underlying cause of obesity is rooted in a lack of physical activity and an excessive intake of energy-dense foods resulting in the obese phenotype. This phenotype is largely defined by two primary characteristics: chronic, low-grade inflammation and metabolic dysfunction. Although it has been established that these two processes are linked, the degree to which one process regulates the other is still not completely understood. It is believed that a main driving force behind the development of type 2 diabetes and insulin resistance is inflammation [36]. Thus, therapies designed at combating obesity-associated inflammation may protect against the obesity-associated metabolic diseases.

Many different factors are thought to play a role in obesity-associated inflammation including, but not limited to, changes in the gut microbiota, the gut-brain axis, and non-alcoholic-fatty-liver-disease (NAFLD) [97, 98]. However, the immune cells primarily responsible for adipose tissue inflammation are infiltrating pro-inflammatory macrophages, otherwise classified as M1 macrophages [37]. Under obese conditions, macrophages, predominately of the M1 phenotype, may account for approximately 50% of all adipose tissue cells [37]. This is in stark contrast to the lean condition, in which macrophages only account for approximately 10% of all adipose tissue cells, with the anti-

inflammatory, M2 macrophage phenotype being the most predominant. In addition to clearing dead adipocytes, M1 macrophages secrete a variety of pro-inflammatory cytokines, including TNF-α, a cytokine known to negatively impact insulin signaling [39]. As such, depletion of macrophages to reduce macrophage-derived adipose tissue inflammation has been investigated as a potential therapeutic. Depletion of macrophages in an obese setting reduces adipose tissue inflammation and improves insulin sensitivity [99, 100]. Macrophage depletion has also been shown to reduce energy intake [101] and body weight [101-104], and it is well known that energy restriction can attenuate inflammation and improve metabolic function [105-108]. Whether the beneficial impact of macrophage depletion extends beyond weight loss has not been examined.

Therefore, through the utilization of pair-feeding, our study was designed to determine if macrophage depletion could serve as an effective intervention to reduce obesity-driven adipose tissue inflammation and improve metabolic dysfunction beyond the weight loss seen with reduced energy intake.

3.3 METHODS

Animals: Male WT *C57BL/6J* mice were purchased from the Jackson Laboratories (Bar Harbor, ME) and cared for at the Animal Resources Facility at the University of South Carolina. Mice (n=15/group) were housed 5 per cage, maintained on a 12:12-h light-dark cycle in a low stress environment (22°C, 50% humidity, low noise) and given water *ad libitum*. Principles of laboratory animal care were followed, and the Institutional Animal Care and Usage Committee of the University of South Carolina approved all experiments.

Diets: At 6 weeks of age, mice were randomly assigned to either control purified AIN-76A low-fat diet (LFD) (3.77 kcal/g) or a purified HFD (40% of total kcals from fat;

4.57 kcal/g) designed to mimic the standard American diet (BioServ, Frenchtown, NJ, USA). We have used this diet in several of our previous investigations [67, 109-113]. Mice were initially provided the respective LFD or HFD for 16 weeks at which time baseline body composition (DEXA) and metabolic tests were administered. Based upon these outcomes, mice within each diet were separated into one of four treatment groups (LFD phosphate-buffered saline (PBS)-encapsulated liposomes, HFD PBS-encapsulated liposomes, LFD clodronate (CLD)-encapsulated liposomes, and HFD CLD-encapsulated liposomes) to match body weight and composition within each dietary treatment. Subsequently, mice continued their respective diets (LFD or HFD) for another 4 weeks. Thus, in total, mice consumed diets for 20 weeks.

Clodronate treatment & pair feeding: To deplete adipose tissue macrophages, a 200 µl IP injection (~1mg) of CLD-encapsulated liposomes (ClodronateLiposomes, Netherlands) was administered twice a week beginning at week 16 of dietary treatment (8 injections in total) until sacrifice at week 20. The selection of this dose of CLD utilized was based upon pilot work that we conducted. IP administration of CLD liposomes was chosen as this has previously been shown to be a more effective means of depleting adipose tissue macrophages compared to intravenous (IV) administration [114]. We had initially used the manufacturer's recommended dose of 0.05 mg/g body weight. However, the dose was scaled down to ≈0.03 mg/g body weight in an attempt to lessen toxicity, but still elicit significant macrophage depletion as we have previously shown with respect to colonic macrophages [49]. Administration of CLD treatment was initiated after 16 weeks of HFD-feeding, as we have previously shown this length of feeding induces an obese phenotype characterized by adipose tissue inflammation with significant adipose tissue macrophage

recruitment and metabolic dysfunction [67, 109]. PBS-encapsulated liposomes (ClodronateLiposomes, Netherlands) were administered in the same manner as CLD liposomes to serve as a control. The sample size in the LFD CLD and HFD CLD groups was reduced to 9 and 14 mice, respectively, due to apparent toxicity of CLD treatment. In our unpublished and published [49] experiments, we have found that macrophage depletion reduces energy intake. This is in accordance with another published paper, which showed that macrophage depletion (via the use of the diphtheria toxin) resulted in a significant reduction in energy intake [101]. Given this, PBS treated mice were pair-fed to their CLD-treated counterparts so as not to allow energy intake to be a potential confounding factor on the outcomes of the study. As the number of mice in each cage was equal across treatment groups, pair feeding calculations were determined by measuring the food consumption of CLD-treated animals by averaging the food intake/cage each day prior to administering food to the counterpart PBS-treated groups. For example, if the 3 CLD HFD cages consumed 15, 16, and 16.4 grams of food over a 24-hour period, the average of this food consumption (=15.8 grams) was provided to each of the 3 PBS HFD cages.

Body weights, energy intake, and body composition: Body weight was monitored on a weekly basis throughout the study. Energy intake was monitored on a weekly basis prior to CLD treatment and on a daily basis upon the commencement of CLD treatment for pair-feeding purposes. Energy intake was calculated by dividing the total food consumption in grams/cage/week/mouse multiplied by the energy density/gram of the respective diet. Body composition was assessed before and after CLD treatments (weeks 16 and 20). For this procedure, mice were placed under brief anesthesia (isoflurane

inhalation) and were assessed for lean mass, fat mass, and body fat percentage via dual-energy X-ray absorptiometry (DEXA) (Lunar PIXImus, Madison, WI).

Metabolism: Metabolic parameters were assessed pre (16 weeks of dietary treatment) and post CLD treatment (20 weeks of dietary treatment/4 weeks of CLD treatment). After a five-hour fast, blood samples were collected from the tip of the tail. Blood glucose concentrations were determined in whole blood using a glucometer (Bayer Contour, Michawaka, IN). Collected blood was centrifuged at 4,000 rpm for 10 min at 4°C. Plasma was aliquoted and stored at -80°C until analysis. Plasma insulin concentrations were analyzed according to the manufacturer's instructions using a mouse insulin ELISA kit (Mercodia Inc., Winston Salem, NC). For glucose tolerance tests (GTTs) and insulin tolerance tests (ITTs), mice were fasted for 5 hours and glucose or insulin was administered (IP) at a dose of 2 g/kg or 0.75 U/kg lean mass, respectively. Blood glucose concentrations (tail sampling) were measured intermittently over a two hour period (0, 15, 30, 60, 90, and 120 minutes) for GTTs and intermittently over a one-hour period (0, 15, 30, 45, and 60 minutes) for ITTs using a glucometer (Bayer Contour, Michawaka, IN). Area under the curve (AUC) was calculated using the trapezoidal rule. Fasting serum was collected for free-fatty acid (FFA) analysis at the 0- and 30-minute time point of the post-CLD treatment ITT to assess insulin's ability to inhibit lipolysis. FFAs were analyzed using a commercially available kit according to the manufacturer's instructions (Wako Diagnostics, Richmond, VA).

Tissue collection: After 20 weeks of dietary treatment (4 weeks after CLD treatment), mice were sacrificed via isoflurane inhalation for tissue collection. An aliquot of whole blood taken from the inferior vena cava was analyzed for hematology analysis using a VetScan

Hm5 (Abaxis, Union City, CA). The remaining blood was spun at 4,000 RPM x 10 min and plasma was stored -80°C. Epididymal, mesentery, and peri-renal fat pads, as well as the liver were removed, weighed, and immediately snap-frozen in liquid nitrogen and stored at −80°C or fixed in 4% formalin until analysis.

Hepatic lipid content and alanine transaminase activity (ALT) assay: Lipids were isolated from the liver utilizing a modified Folch extraction method and were quantified gravimetrically, as previously described [109, 111, 112, 115, 116]. Plasma ALT activity was assessed using an Infinity ALT liquid reagent (Thermo Fisher, Middletown, VA) following the manufacturer's instructions.

Adipose tissue hydroxyproline assessment: In order to assess the impact of macrophage depletion on adipose tissue fibrosis, epididymal adipose tissue hydroxyproline content (an indirect method for assessing collagen deposition[117]) was examined. Due to limitations in the amount of available epididymal adipose tissue, this assay was limited to the adipose tissue of HFD groups only. Briefly, 100-200 mg of epididymal adipose tissue was acid hydrolyzed overnight at 110ºC using 6N HCL. The solution was then centrifuged (10 min x 10,000 RPM) and the resulting supernatant was collected and dried under nitrogen gas. Subsequently, the dried extract was incubated with 0.625 mLs of a chloramine-T solution for a 30 minute period followed by the addition of 0.625 mLs of Ehrlich's solution as previously described [118]. Samples were then incubated for 20 min at 65ºC, cooled in room temperature water, and then transferred to a 96-well microplate and read using a spectrophotometer at 550 nm. Hydroxyproline purchased from Sigma Aldrich (St. Louis, MO) was used to create a standard curve. Total hydroxyproline content was normalized to the epididymal adipose tissue weight originally used.

Adipose Tissue and Liver Histology: Formalin-fixed tissues were embedded in Paraffin blocks and sectioned. The epididymal and peri-renal fat pads and livers were stained with H&E. Representative images were taken at 20x and 100x. For immunofluorescent and immunohistochemistry staining, the antibodies, antibody dilutions, and antigen-retrieval methods are provided in Table 1. For negative controls, a serial section was assayed exactly the same as the treated-section minus the primary antibody.

Quantitative real-time RT-PCR: RNA was isolated from epidydimal and peri-renal adipose tissue depots as well as liver using an RNeasy Lipid Tissue Mini Kit (Qiagen, Valencia, CA). TaqMan reverse transcription reagents and gene expression assays (Applied Biosystems, Foster City, CA) were used to reverse transcribe and to analyze the expression of the following genes: F4/80, CD68, CD11c, CD206, MCP-1, TNFα, IL-10, IL-6, and IL-1β. Potential reference genes (RPLP2, 18s, HMBS, TBP, B2M, H2AFV, and HPRT) were analyzed for stability using Qbase+ software (Biogazelle, Belgium) for each tissue analyzed. The optimal number of reference genes were determined by Qbase+ and the geometric mean of these genes was used as the normalization factor for each analysis: epididymal adipose tissue (HMBS, TBP, B2M, and H2AFV), peri-renal adipose tissue (HMBS and HPRT), and liver (TBS and B2M) [119]. Gene expression quantification was calculated using the ΔΔCT method and Qbase+ software.

Western Blotting: Briefly, epididymal and peri-renal adipose tissue, as well as a portion of the liver was homogenized in Mueller Buffer containing a cocktail protease inhibitor (Sigma Aldrich, St. Louis, MO) [70]. Total protein concentrations were determined by the Bradford method. Equal amounts of crude protein homogenates were

fractioned on hand-casted 12% SDS-polyacrylamide gel and electrophoretically transferred to a PVDF membrane using a Genie Blotter (IDEA Scientific, Minneapolis, MN). Membranes were stained with a Ponceau S solution in order to verify equal protein loading and transfer efficiency. Subsequently, membranes were blocked for 1 hour in 5% milk in Tris-buffered saline, 0.1% Tween-20 (TBST). The Ly6G primary antibody (Abcam, Cambridge, UK) was diluted 1:1,000 in a 5% milk-TBST overnight at 4ºC. An anti-rat (Cell Signaling, Danvers, MA) IgG horseradish peroxidase conjugated secondary antibody was diluted 1:2000 in 5% milk-TBST and incubated for 1 hour at room temperature. An enhanced chemiluminescent substrate for detection of horseradish peroxidase (Thermo Scientific, Watham, MA) was used to visualize the antibody-antigen interaction. Autoradiography films were scanned and blots were quantified using scientific imaging software (Image J). Due to tissue limitations, only the peri-renal fat from HFD-fed animals was analyzed for Ly6G content. After completion of the western blot, all membranes were stained with Amido black [49, 109, 116], and the densitometry of each lane was calculated using Quantity One Software (Biorad, Hercules, CA) allowing for total protein normalization. This method of normalization has been shown to be more accurate than typically used loading controls [71].

Plasma Cytokines: Plasma collected at sacrifice was analyzed for circulating IL-6 and MCP-1 (LEGEND MAX ELISA kits, Biolegend, San Diego, CA). Due to limitations in the amount of plasma only the plasma of the HFD-treated groups was analyzed for MCP-1 concentration.

Statistical Analysis: Data were analyzed using commercially available statistical software: Prism 6 (GraphPad Software, La Jolla, CA)) and SigmaStat (Systat Software,

San Jose, CA). A two-way ANOVA followed by a Newman-Keuls post-hoc analysis was used to determine differences between diet (HFD vs. LFD) and treatment (CLD vs. PBS). For body weight analysis a two-way (time x group) repeated measures ANOVA was used followed by a Newman-Keuls post-hoc test. A two-way (time x group) repeated measures ANOVA followed by a Newman-Keuls post-hoc test was also used for ITT analysis in order to determine differences in blood glucose levels from baseline (0 minutes) over the duration of the test. A Student's T-Test (two-tailed) was used for western blot analysis of Ly6G, epididymal adipose tissue hydroxyproline content, and plasma MCP-1 concentrations to compare treatment (CLD vs. PBS) within diet. Statistical analysis of energy intake was not assessed given the small sample size (n=3/group). Any statistical test that did not pass the equal-variance test (Bartlett's test for equal variances) was log transformed and then re-analyzed. Data are presented as the mean ± SEMs and the level of significance was set at $p<0.05$.

3.4 RESULTS

16 weeks of HFD consumption leads to an obese phenotype

Prior to CLD or PBS treatment, mice were fed a 40% HFD or a LFD for 16 weeks. An obese phenotype was successfully achieved as the HFD-fed mice gained significantly more body weight, fat mass, and displayed a significantly greater body fat % (Figure 3.1A-B) compared to LFD fed mice ($p<0.05$). HFD-fed mice also displayed elevated fasting blood glucose, insulin, GTT AUC, and impaired insulin sensitivity (Figures 3.1C, 1D, 1E, and 1G, respectively), demonstrating a dysfunctional metabolic phenotype ($p<0.05$).

CLD treatment reduces body weight by eliciting changes in energy intake

After 16 weeks of HFD or LFD consumption, mice were administered either PBS or CLD-encapsulated liposomes for a 4-week period. The PBS-treated groups were pair-fed the same amount of food as their CLD-treated counterparts. All CLD-treated groups displayed a decrease in body weight starting one week after CLD treatment (Figure 3.2A) which was accompanied by a decrease in energy intake (Figure 3.2B) suggesting that CLD treatment induced a reduction in appetite. There was a main effect of the HFD-treatment to increase lean mass, fat mass, and body fat% relative to the LFD-fed mice (Figure 3.2C) ($p<0.05$). Pair feeding was successful in matching the body weight, fat mass and lean mass in the PBS and CLD treatment groups. However, within the LFD groups, CLD treatment significantly reduced body fat% (Figure 3.2C) ($p<0.05$). With respect to intra-peritoneal fat pads, HFD increased all fat pad weights (epididymal, mesentery, and peri-renal) relative to the LFD-fed mice (Figure 3.2D) ($p<0.05$). Interestingly, within the HFD-treated mice, CLD-treated mice exhibited an increase in epididymal, but not peri-renal or mesenteric, fat pad weight. Consequently, the sum of all three fat pads was also increased (Figure 3.2D) ($p<0.05$). We found this surprising, and in order to potentially explain this discrepancy, we examined a marker of extracellular matrix (Collagen) accumulation, hydroxyproline content, in epididymal adipose tissue (HFD groups only). However, no significant difference was found in hydroxyproline content (data not shown) between these groups, suggesting that some other mechanisms are responsible for the expansion of epididymal fat pad weight between the HFD groups.

CLD-liposome treatment does not reduce epididymal adipose tissue macrophage populations in a HFD setting, yet results in an exacerbated cytokine profile, and significant increases in circulating and infiltrating neutrophils

We initially examined epididymal adipose tissue to assess the effectiveness of CLD treatment to deplete macrophages as the epididymal fat pad has been shown to develop signs of inflammation and insulin resistance prior to other intraperitoneal fat pads [120]. Interestingly, while as expected, the HFD increased adipose tissue macrophage markers, no significant difference was found with respect to gene expression of overall macrophage markers, F4/80 and CD68, or M1 (CD11c) and M2 (CD206) macrophage markers between the HFD groups (Figure 3.3A). This lack of difference in macrophage populations was substantiated when we performed immunofluorescence staining in the epididymal fat pad (Figure 3.3B). However, within the LFD groups, CLD treatment significantly decreased F4/80 (-58%), CD68 (-52%), and CD206 (-72%) gene expression, but not CD11c mRNA expression (Figure 3.3A) ($p<0.05$).

We then proceeded to examine the gene expression of various inflammatory cytokines in the epididymal fat pad (Figure 3.4A) ($p<0.05$). As expected, HFD treatment significantly increased the gene expression of the monocyte chemoattractant, MCP-1, the pro-inflammatory cytokine, TNF-α, as well as the anti-inflammatory cytokine, IL-10, relative to the LFD groups ($p<0.05$). However, within the HFD groups, CLD treatment further elevated gene expression of MCP-1 and IL-10 ($p<0.05$). An additional interest was the finding that CLD treatment, independent of diet, resulted in substantial increases in mRNA expression of the pro-inflammatory cytokines, IL-6 and IL-1β ($p<0.05$). In fact, IL-1β mRNA induction was further augmented in the CLD LFD group relative to the CLD HFD group, whereas its expression was downregulated in the HFD PBS group relative to the LFD PBS group ($p<0.05$).

Based on these findings, we performed H&E staining to histologically assess the epididymal fat pads (Figure 3.4B). We found clear evidence of infiltrating polymorphonuclear cells (PMCs) in the CLD-treated groups relative to the PBS-treated groups. Additionally, in whole blood collected at sacrifice, we found significant increases in circulating neutrophils in the CLD-treated groups (Figure 3.5A). This finding led us to believe that the tissue PMCs we examined histologically, were neutrophils. As such, we performed a western blot for Ly6G, a neutrophil marker, and found significant increases in Ly6G in the CLD-treated groups relative to their PBS controls (Figure 3.5B) ($p<0.05$). This discovery was corroborated with immunohistochemistry staining of Ly6G (Figure 3.5C).

Macrophage populations are significantly diminished in peri-renal adipose tissue, yet a pro-inflammatory environment including neutrophil infiltration is evident

Because we did not find any significant decreases in macrophage populations in the epididymal fat pad, we decided to assess the peri-renal fat pad with respect to macrophage infiltration. Contrary to the finding in the epididymal fat pad, CLD treatment significantly decreased F4/80 (-30%), CD68 (-35%), CD11c (-40%), and CD206 (-42%) in the CLD HFD group relative to the PBS HFD group (Figure 3.6A) ($p<0.05$), which was corroborated with immunofluorescent staining for F4/80 (Figure 3.6B). In the LFD groups, a similar pattern was found as CLD treatment reduced mRNA content of F4/80 (-43%), CD68 (-35%), and CD206 (-47%) (Figure 3.6A) ($p<0.05$). However, similar to the epididymal adipose tissue, CLD treatment did not influence CD11c gene expression.

Since we found reduced macrophage populations in the CLD-treated groups, we moved on to explore the gene expression of several pro-inflammatory cytokines (TNF-α,

MCP-1, IL-1β, and IL-6). As expected, there was a HFD effect to increase TNF-α and MCP-1 expression (Figure 3.7A) ($p<0.05$). On the other hand, IL-6, similar to the finding in epididymal adipose tissue, was downregulated as a result of HFD consumption ($p<0.05$). In a HFD setting, CLD treatment significantly decreased TNF-α gene expression (-31%), which corresponded with the similar decrease (-30%) in F4/80 mRNA (Figure 3.7A) ($p<0.05$). However, analogous to what was observed in the epididymal adipose tissue, MCP-1, IL-1β, and IL-6 were all increased as a result of CLD treatment among the HFD groups (Figure 3.7A) ($p<0.05$). A similar finding was observed with CLD treatment in a LFD setting as both IL-1β and IL-6 expression were significantly increased ($p<0.05$). This outcome, paired with no change in MCP-1 gene expression, paralleled what was observed in epididymal adipose tissue.

We followed up the qRT-PCR analysis with a histological assessment of the peri-renal fat pad and, similar to what was observed in the epididymal fat pad, discovered an abundance of infiltrating PMCs surrounding adipocytes. Immunohistochemistry confirmed that these cells were Ly6G positive cells (Figure 3.7B). A western blot analysis of Ly6G verified that Ly6G content was greater in the CLD-treated mice (Figure 3.7C) ($p<0.05$).

CLD treatment does not regress early-stage NAFLD development

HFD treatment resulted in early-stage NAFLD development as characterized by hepatomegaly (Figure 3.8A), hepatic steatosis (Figure 3.8B & 8D), and elevated plasma ALT activity (Figure 3.8C) ($p<0.05$). However, the disease had not progressed to steatohepatitis as the HFD PBS group, although it did display an increase in F4/80 expression relative to the LFD PBS group (Figure 3.8E & 8F) ($p<0.05$), did not

histologically present significant evidence of immune cell infiltration. Moreover, nor were there any significant increases in any of the pro-inflammatory cytokines measured, including MCP-1, TNF-α, IL-6, and IL-1β (Figure 3.8G). In fact, there was a main effect for HFD consumption to decrease MCP-1 gene expression, and the HFD PBS group displayed less TNF-α gene expression relative to the LFD PBS group ($p<0.05$).

Regardless of the lack of HFD-induced hepatic inflammation, CLD treatment significantly reduced gene expression of F4/80 (-59%) in a HFD setting (Figure 3.8E). This was substantiated by F4/80 staining (Figure 3.8F) and occurred independent of any changes to liver weight or hepatic lipid accumulation. Surprisingly, this decrease in F4/80 did not impact gene expression of MCP-1 or TNF-α (Figure 3.8G). Additionally, CLD treatment in a LFD setting did not significantly reduce macrophages as substantiated by F4/80 gene expression and immunohistochemistry (Figures 8E & 8F, respectively), yet there was a main effect for CLD treatment to decrease TNF-α and IL-1β (Figure 3.8G) ($p<0.05$). Despite these reductions in TNF-α and IL-1β, CLD treatment, independent of diet, resulted in higher IL-6 gene expression (Figure 3.8G) ($p<0.05$).

Macrophage depletion elicits significant increases in circulating IL-6 and MCP-1

Because we found a main effect of CLD treatment to increase gene expression of IL-6 in all tissues analyzed and an interaction for CLD treatment to increase epididymal and peri-renal MCP-1 gene expression among the HFD groups, we examined circulating IL-6 and MCP-1 levels (Figure 3.9). Consistent with the gene expression, CLD treatment, irrespective of diet, induced significant increases in the plasma IL-6 concentration (Figure 3.9A) ($p<0.05$). Additionally, CLD-treated HFD mice displayed >2-fold increases in circulating MCP-1 relative to HFD PBS mice (Figure 3.9B) ($p<0.05$).

Macrophage depletion does not rescue impaired glucose metabolism or insulin resistance and exacerbates adipose tissue insulin action

CLD treatment had no effect at improving glucose metabolism or insulin resistance as fasting blood glucose (Figure 3.10A), fasting insulin (Figure 3.10B), and GTT AUC (Figure 3.10C), were not reduced with CLD treatment in either the LFD or HFD groups. Similarly, insulin's ability to decrease blood glucose levels (Figure 3.10D) was not enhanced with CLD treatment in either the LFD or HFD setting. With respect to FFA metabolism, basal serum FFAs were significantly increased in the LFD PBS group compared to all other groups (Figure 3.10E) ($p<0.05$). Thirty minutes after exogenous insulin administration there was a main effect of diet ($p<0.05$) for the LFD-fed mice to exhibit significantly lower serum FFAs than HFD-fed mice (Figure 3.10F). When examining the absolute change of serum FFAs over the thirty-minute period, there was a main effect of CLD treatment to impair the decrease in serum FFAs compared to PBS treatment. Among the groups, the LFD PBS group displayed the greatest drop in serum FFAs compared to all other groups (Figure 3.10G) ($p<0.05$). LFD CLD mice exhibited a more significant drop in serum FFAs than the HFD CLD mice ($p<0.05$), but not when compared to the HFD PBS mice. Although not statistically significant, there was a trend ($p=0.08$) for the HFD PBS mice to decrease serum FFAs more so than the HFD CLD group.

CLD treatment results in anemia

It is well established that macrophages play a central role in heme-iron metabolism [121-123]. Therefore, we analyzed whole blood to see if CLD treatment impacted hemoglobin levels. Data from the hematology analysis showed that CLD treatment,

independent of diet, decreased absolute hemoglobin levels and the hematocrit (Table 3.2) ($p<0.05$).

3.5 DISCUSSION

Due to the prominent role macrophages play in obesity-associated inflammation, they have become the target for therapies aimed at mitigating the chronic inflammatory environment and impaired metabolic processes. As others have reported, adipose tissue macrophages (peri-renal) were successfully reduced with CLD-liposome treatment [99, 100, 114, 124]. However, relative to weight-matched control animals, CLD treatment did not rescue HFD-induced impaired glucose metabolism. Moreover, CLD treatment, irrespective of diet, increased circulating and adipose tissue infiltrating neutrophils. Additionally, we found that CLD treatment resulted in reduced energy intake and significant body weight loss.

Interestingly, others who have utilized CLD liposomes to decrease obesity-induced adipose tissue macrophage infiltration have not reported similar findings of neutrophilia, an inability to rescue impaired metabolism, and reduced energy intake [99, 100, 104, 124]. However, our results are consistent with those of Lee *et. al.*, who found that macrophage depletion utilizing a Lysozyme M promoter-directed CRE ($LysM^{Cre}$) diphtheria toxin model resulted in significant neutrophil infiltration, decreased energy intake, and reduced body weight in both HFD and standard-chow-fed mice [101]. Similarly, Gordy *et. al.* developed a $LysM^{Cre}$ floxed FLICE-like inhibitory protein ($LysM^{Cre}$ c-$FLIP^{f/f}$) mouse model which results in mice lacking splenic marginal zone, bone marrow, and thioglycolate-elicited peritoneal macrophages and found that neutrophilia is secondary to macrophage depletion and macrophages regulate neutrophil homeostasis [102]. Although

energy intake was not measured in the study by Gordy *et. al.*, it was discovered that these mice exhibit a decreased body weight. Similar results of neutrophilia and a loss of body weight were reported by Wu *et. al.* when conditional macrophage depletion via the use of a transgenic mouse model was used to study the impact of macrophages on osteoarthritis in obesity [103]. The results of Lee *et. al.*, Gordy *et. al.*, and Wu *et. al.* and the mouse models utilized in their studies provide support that our findings are a direct result of macrophage depletion and not of CLD liposome treatment alone.

It was surprising that we did not find significant decreases in macrophage populations in the epididymal adipose tissue of the HFD CLD group. It was our initial hypothesis that epididymal adipose tissue would be the most sensitive to CLD treatment given the route of liposome administration and that the epididymal fat pad exhibits exacerbated inflammation and impaired insulin action at an earlier time point than other intra-peritoneal fat pads [120]. However, the fact that CLD treatment significantly depleted epididymal and peri-renal adipose tissue macrophages in a LFD setting and resulted in significant peri-renal adipose tissue macrophage depletion in a HFD setting leads us to believe that perhaps epididymal adipose macrophages are more sensitive to the pair feeding. Prior work demonstrated that restricting food intake in obese animals reverses macrophage accumulation in peri-gonadal adipose tissue [125]. As we are comparing the CLD treatment to pair-fed animals who lost weight, it is possible that CLD could not reduce macrophage populations beyond that seen with caloric restriction. Alternatively, the inability to detect a difference in epididymal adipose tissue macrophage populations may be due to the immune system's ability to compensate for the effects of CLD treatment in order to recruit more monocytes to the inflamed area resulting in a repopulation of

macrophages. This is supported by the significant increase in epididymal mRNA expression of the potent monocyte chemokine, MCP-1 (as has been previously shown with acute IP CLD liposome treatment [114]), a higher concentration of circulating MCP-1 as well as tissue neutrophilia in the HFD CLD group. However, a time-course study with CLD treatment would be necessary to confirm this.

It is important to consider that dendritic cells, another phagocytic immune cell, are also known to be affected by CLD-liposome treatment [126]. Thus, the neutrophil infiltration makes physiological sense as they are the only primary professional phagocytic cell remaining after macrophage and dendritic cell depletion. Neutrophil infiltration into the adipose tissue serves two probable functions: 1) remove dead immune cells affected by CLD treatment, and 2) adopt the role of macrophages by cleaning up dead adipocytes. This is supported by the observation of Ly6G positive cells surrounding adipocytes in the CLD-treated mice. Additionally, it is likely that the increased expression of adipose tissue IL-6 and IL-1β as well as the circulating IL-6 concentration originates from these infiltrating neutrophils as the HFD PBS treatment did not induce significant increases in these cytokines relative to the LFD PBS group. Furthermore, both Lee *et. al.* and Gordy *et. al.* found that macrophage-depletion-induced neutrophilia resulted in significant increases in circulating plasma cytokines, including IL-6 [101, 102] and IL-1β [102]. However, we cannot rule out the possibility that other immune cells, such as T-Cells, or adipocytes could be producing these cytokines.

There is a clear discrepancy between the results of our study and the studies of others who have shown macrophage depletion to improve metabolic processes through the use of CLD treatment [99, 100, 104, 124, 127]. In particular, our results are in direct

contradiction of Lee *et. al.* who have suggested that "long-term" obesity-associated insulin resistance, as would be induced after 16 weeks of HFD consumption, is largely mediated by macrophage-induced pro-inflammatory actions [124]. These discrepancies may be explained by many factors including, but not limited to, the type of HFD utilized, the mode of CLD administration (IP vs. IV), as well as the dose, timing, and duration of CLD treatment. For instance, the mode of CLD liposome administration can have a significant effect on the tissue specificity of macrophage depletion. Lanthier *et. al.* showed that IV administration of CLD liposomes selectively depletes Kupffer cells (liver macrophages), whereas IP administration is more advantageous for adipose tissue macrophage depletion [114]. With this being said, the majority of previous studies employing CLD liposomes to deplete adipose tissue macrophages have utilized IP administration [99, 100, 104, 124, 127] as was used in our experiment. However, the CLD dose (≈0.03 mg/g body weight) utilized in our study was significantly less than what others have used (≈0.1 mg/g body weight) [99, 100, 124]. Furthermore, the degree to which the duration of CLD liposome treatment impacts the effectiveness of macrophage depletion and the resulting impact on metabolic function is conflicting. Studies that have employed IP administration of CLD liposomes for a relatively short period (1-2 weeks), such as Feng *et. al.* [100], Choe *et. al.* [127] (2 treatments/week x 1 week) and Lee *et. al.* ("5 injections every 3 days for 14 days" (provided in supplementary data of their paper)) [124] have shown effective macrophage depletion and beneficial effects on metabolic outcomes. The duration (2 treatments/week x 4 weeks) of CLD liposome administration in our study was significantly longer than these previous studies and may be largely responsible for the discrepancy in outcomes between studies. However, Bu *et. al.* used CLD liposome treatment for a significantly longer

duration (2 treatments/week x 9 weeks) than what was used in our study yet showed beneficial effects on adiposity and metabolism [99].

A potential confounding factor for the majority of the previous studies utilizing IP CLD-liposome treatment, however, is the failure to examine/report energy intake or body weight changes with CLD treatment [100, 124, 127]. Moreover, those studies that did report significant changes in body weight did not report energy intake as exemplified in a recent publication by Kumar *et. al.* who used a similar dose of CLD liposome as the dose utilized in our study (≈0.03 mg/g body weight administered weekly for 4 weeks) and found that CLD liposome treatment significantly depleted adipose tissue macrophages, improved metabolic outcomes, and dramatically reduced adiposity by >50% [104]. In the publication by Bu *et. al.*, food intake was reported, however, the authors did not specify the number of mice housed/cage, the means by which energy intake was calculated if multiple mice were housed/cage, and the statistical analysis utilized to assess a potential difference in energy intake [99]. Thus, in these previous studies any potential benefits with respect to decreases in adiposity, inflammation, insulin resistance, and hepatic steatosis as a consequence of macrophage depletion, may in reality simply be a secondary effect resulting from decreased energy intake.

Although it was beyond the scope of our investigation, it is likely that the reduced energy intake and consequential body weight loss resulting from CLD-liposome treatment is due to neutrophilia, an exacerbated circulating pro-inflammatory environment, and brain inflammation. However, it cannot be ruled out that liposome treatment, alone, may have reduced food intake as previously discussed [128]. With this being said, in our previous publication we did not find any effect of PBS-liposome treatment to impact body weight

or food intake [49]. Moreover, the concept that reduced energy intake is due to CLD-liposome treatment and subsequent macrophage depletion and not liposome treatment, in general, is supported by the findings of Lee *et. al.* who showed that macrophage-depleted mice present hypothalamic inflammation and reduced energy intake [101]. It has also been shown that IL-1β plays a key role in regulating this effect as Gordy *et. al.* found that administration of IL-1Ra to macrophage-deficient mice rescued the decreased body weight [102]. Consistent with this, both in the present investigation and in that of Lee *et. al.*, decreased energy intake was observed with macrophage depletion as was increases in adipose tissue IL-1β gene expression, which Lee *et. al.* also found to be elevated in the hypothalamus [101].

Others have shown that hepatic resident macrophage (Kupffer cells) activation has been shown to impair insulin signaling in the early stages of HFD consumption [129]. As such, we assessed whether or not CLD treatment reduced Kupffer cell accumulation in our model. Although there was evidence of NAFLD, as assessed by hepatic steatosis, elevated plasma ALT activity, and an increased macrophage content, there was no effect of the HFD to induce robust hepatitis as substantiated by no significant increases in various inflammatory markers (MCP-1, TNF-α, IL-6, and IL-1β). It is likely that a longer feeding period would be necessary to develop a more advanced NAFLD phenotype. Nonetheless, CLD treatment significantly decreased macrophages (F4/80) in a HFD setting. However, glucose metabolism was not improved. Lanthier *et. al.* found similar results and concluded that Kupffer cell depletion does not provide a therapeutic effect on detrimental metabolic changes induced by a HFD [114]. Thus, our results provide further support that ectopic lipid accumulation resulting from a positive energy balance may be a more important

instigator if impaired metabolic processes than inflammation as has been previously shown [130].

A limitation of our study is that CLD treatment is a non-specific means of depleting macrophage populations. It is well established that different macrophage subsets exist, that are generally categorized into two extreme phenotypes – pro-inflammatory and anti-inflammatory. Although this dichotomy does not fully reflect the heterogeneity of macrophage populations, it is still a widely used distinguishing characteristic. Therapies specifically targeting individual macrophage phenotypes or specific tissue macrophage may be more effective than general systemic macrophage depletion [131]. However, the establishment of such models and tissue specificity is still in its infancy.

It is important to note that CLD-treated groups displayed symptoms of anemia. Macrophages play an essential role in heme and iron metabolism [121-123]. Iron can also modulate glucose homeostasis and adipose tissue function [132]. Thus, it is imperative that a complete blood count be part of a routine assessment when interventions aimed at modulating macrophage populations are utilized. This is especially true in an obese setting as obesity is emerging as a risk factor for iron deficiency [133]. It is also evident from our results that severe macrophage depletion and subsequent compensatory immune responses can be lethal in certain conditions. This is consistent with other macrophage-depletion models [134, 135]. We hypothesize that the larger degree of toxicity observed in the LFD CLD group is the result of an immunocompromised state from severe macrophage depletion not reached in the HFD CLD group. This is likely the case given that adipose tissue macrophage populations of the LFD group would have been significantly less than the HFD-fed mice after 16 weeks of dietary treatment, as we have previously shown [67,

109]. Future assessments to evaluate potential toxicity of macrophage depletion - even in the short-term - are necessary prior to any clinical interventions aimed at macrophage diminution.

In conclusion, our study shows that when controlling for energy intake, depleting macrophages using CLD in an obese setting is not an effective therapy for rescuing metabolic dysfunction and may increase the risk for anemia, neutrophilia, and exacerbated adipose tissue inflammation. Thus, the utilization of pro-longed repeated IP CLD liposome treatment to deplete macrophages does not seem to be a viable option as a potential clinical therapy. Future studies are necessary to better understand the role that the timing, tissue-specificity, and phenotype of macrophage depletion has on obesity outcomes.

3.6 FIGURES & LEGENDS

Table 3.1. Primary and secondary antibodies as well as conditions used for immunofluorescence and immunohistochemistry.

Primary Antibody (Vendor)	Dilution (Incubation)	Antigen-Retrieval	Secondary Antibody/Incubation
Rat-Anti-Mouse F4/80 (Biorad, Hercules, CA)	1:200 (Overnight at 4°C)	Proteinase-K (10 minutes)	Alexa Fluor 555 Goat-Anti-Rat (Thermo Fisher, Waltham, MA) (1:200 at 37°C for 30 minutes)
Rat-Anti-Mouse Ly6g (Biolegend, San Diego, CA)	1:100 (Overnight at 4°C)	Heat-Induced (Citrate Buffer, 10 mmol)	Goat-Anti-Rat HRP Conjugated (Abcam, Cambridge, UK) (1:200 at Room Temp for 1 Hour). DAB was used for visualization.
Rat-Anti-Mouse F4/80 (Biorad, Hercules, CA)	1:200 (Overnight at 4°C)	Proteinase-K (10 minutes)	Goat-Anti-Rat HRP Conjugated (Abcam, Cambridge, UK) (1:200 at Room Temp for 1 Hour). DAB was used for visualization.

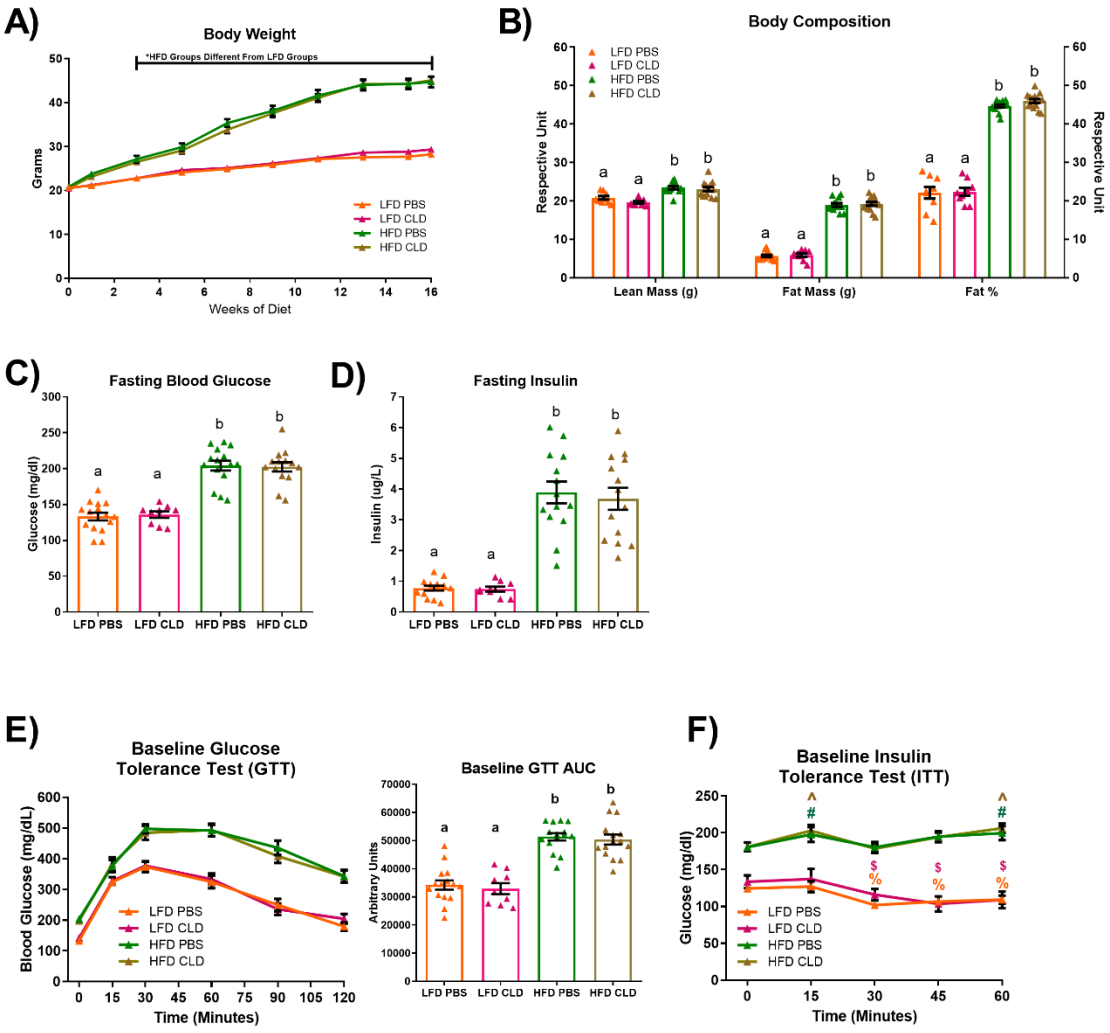

Figure 3.1. Body composition and metabolic data after 16 weeks of dietary treatment prior to start of liposome treatment. Mice were fed a high-fat diet (HFD) or (LFD) for 16 weeks. A) Mouse body weight, B) body composition, C) fasting (5 hour) blood glucose levels, D) fasting (5 hour) plasma insulin levels, E) intraperitoneal (IP) glucose tolerance test (GTT) and corresponding area under the curve (AUC), F) IP insulin tolerance test (ITT) following a 5-hour fast. Values are means ± SE; n=9-15 mice per group. * and bar graphs not sharing a common letter are significantly different from one another ($p<0.05$). %, $, #, ^ represent statistically significant differences ($p<0.05$) in blood glucose levels from baseline (0 minutes) for the LFD PBS, LFD CLD, HFD PBS, and HFD CLD groups, respectively.

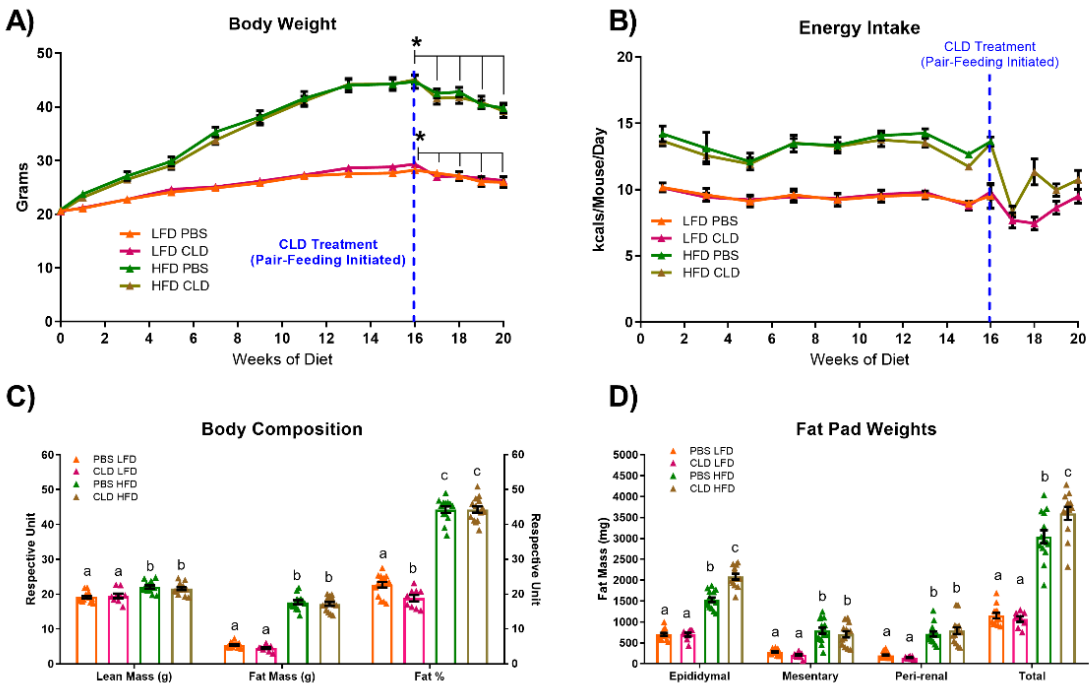

Figure 3.2. Body morphology following dietary and liposome treatment. A) Mouse body weight, B) energy (kcal) intake throughout the experimental protocol, C) terminal body composition analysis as assessed by DEXA, and D) intra-peritoneal adipose tissue depot weights (epididymal, peri-renal, mesentery) and total intra-peritoneal fat weight measured at sacrifice. Values are means ± SE; n=9-15 mice per group. *Signifies significant difference from start of liposome treatment at 16 weeks. Bar graphs not sharing a common letter are significantly different from one another ($p<0.05$).

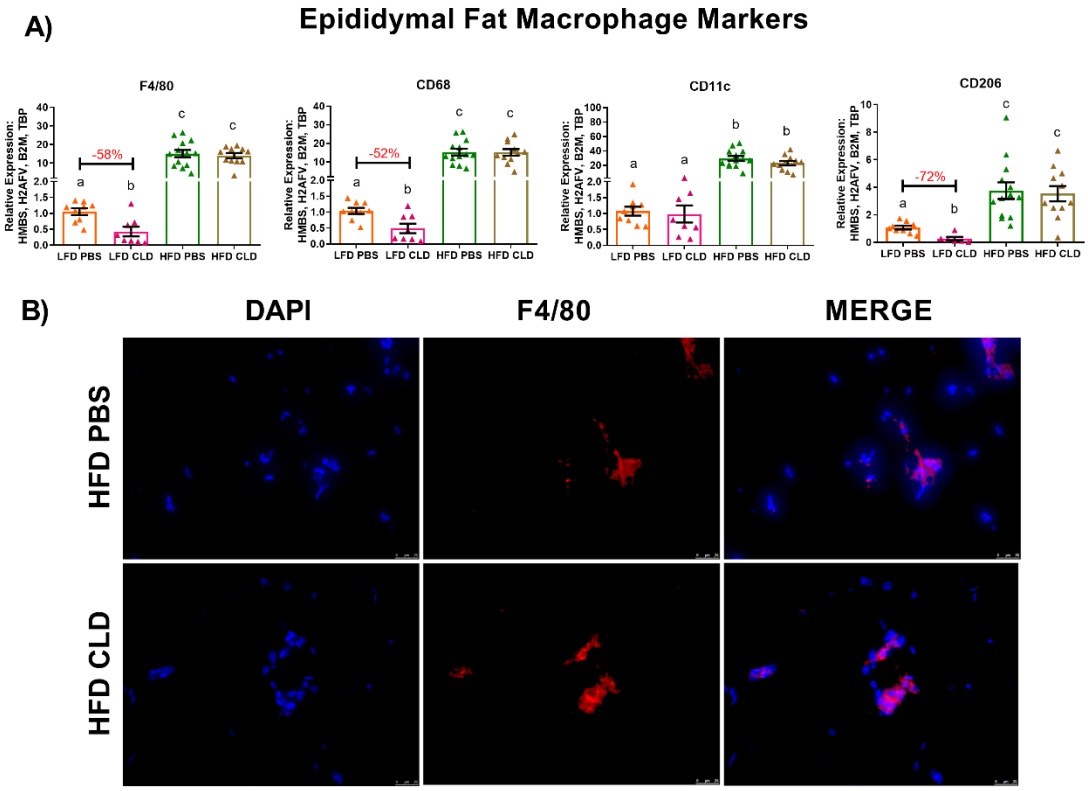

Figure 3.3. Four weeks of CLD treatment depletes epididymal adipose tissue macrophages in a low-fat diet (LFD) setting, but not under high-fat diet (HFD) conditions. (A) Epididymal adipose tissue mRNA expression of macrophage markers (F4/80, CD68, CD11c, and CD206) normalized to the most stable internal reference genes calculated using Qbase+ software, and B) representative immunofluorescent images (40X) of DAPI and F4/80 in epididymal adipose tissue of HFD-treated mice. Values are means ± SE; n=9-15 mice per group. Bar graphs not sharing a common letter are significantly different from one another ($p<0.05$).

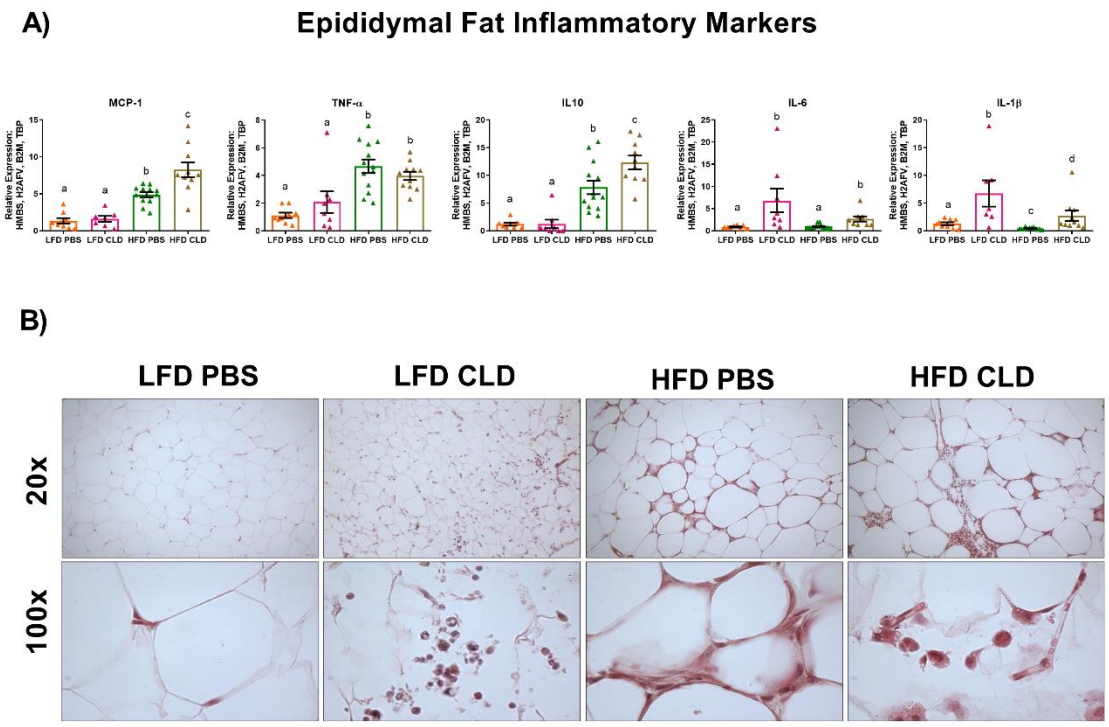

Figure 3.4. Despite not affecting epididymal adipose tissue macrophage populations in a HFD setting, CLD treatment augments epididymal adipose tissue inflammation and polymorphonuclear cell (PMC) infiltration. A) Epididymal adipose tissue mRNA expression of inflammatory mediators (MCP-1, TNF-α, IL-10, IL-6, and IL-1β) normalized to the geometric mean of the most stable internal reference genes calculated using Qbase+ software, and B) representative images (20X and 100X) of H&E stained epididymal adipose tissue sections showing increased (PMC) infiltration in the CLD-treated groups. Values are means ± SE; n=9-15 mice per group. Bar graphs not sharing a common letter are significantly different from one another ($p<0.05$).

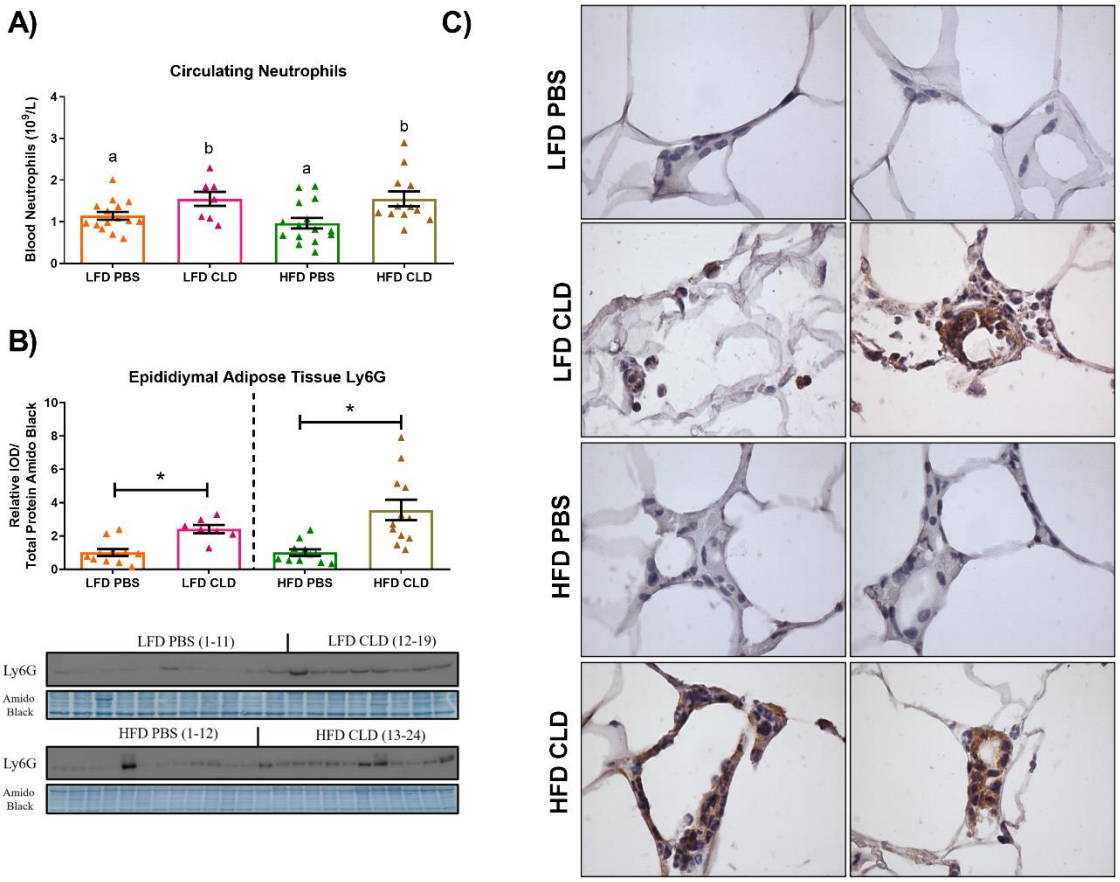

Figure 3.5. CLD treatment increases circulating and epididymal adipose tissue neutrophils. A) Circulating neutrophils determined in whole blood by a VetScan HM5, B) western blot analysis of Ly6G (neutrophil marker) in epididymal adipose tissue normalized to total protein stain (amido black), and C) two representative images of immunohistochemistry staining (100x) of Ly6G in epididymal adipose tissue. Values are means ± SE; n=9-15 mice per group. Bar graphs not sharing a common letter and the * represent a statistically significant difference between groups ($p<0.05$).

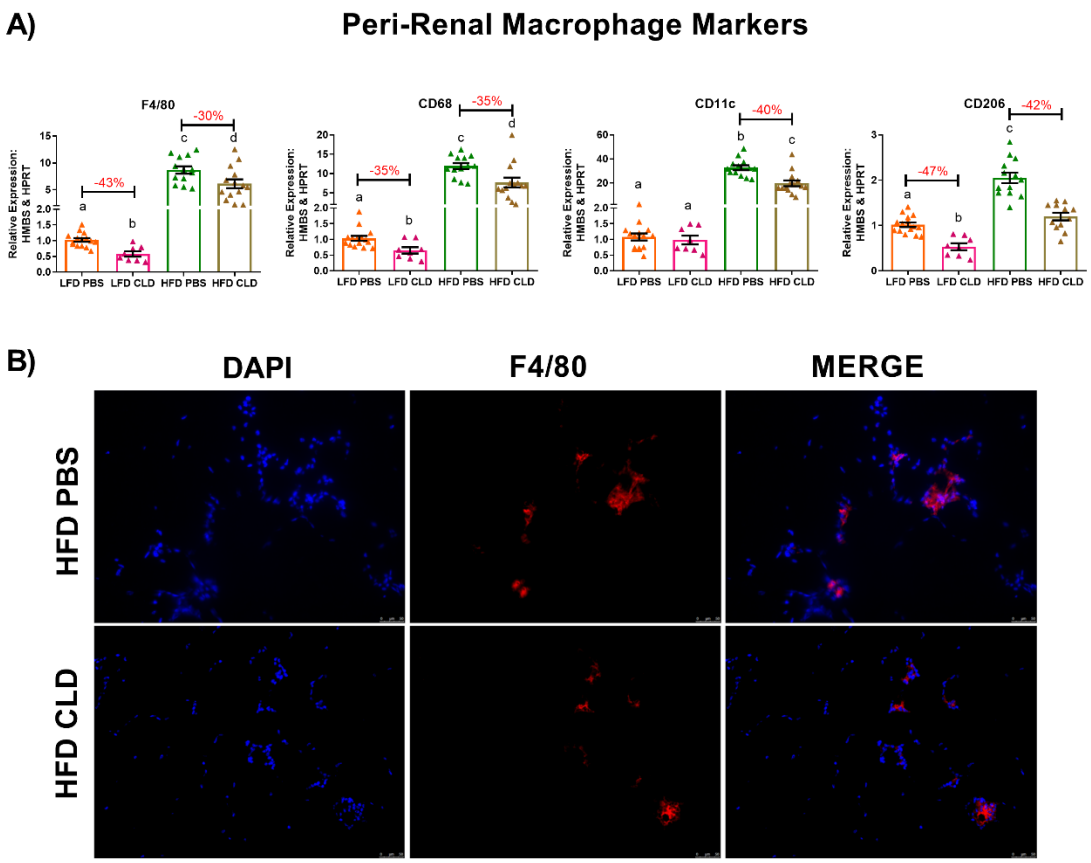

Figure 3.6. Four weeks of CLD treatment depletes macrophages in the peri-renal fat pad. A) Peri-renal adipose tissue mRNA expression of macrophage markers (F4/80, CD68, CD11c, and CD206) normalized to the geometric mean of the most stable internal reference genes using QBase+ software, and B) representative immunofluorescent images (40X) of DAPI and F4/80 in peri-renal adipose tissue of HFD-treated mice. Values are means ± SE; n=9-15 mice per group. Bar graphs not sharing a common letter are significantly different from one another ($p<0.05$).

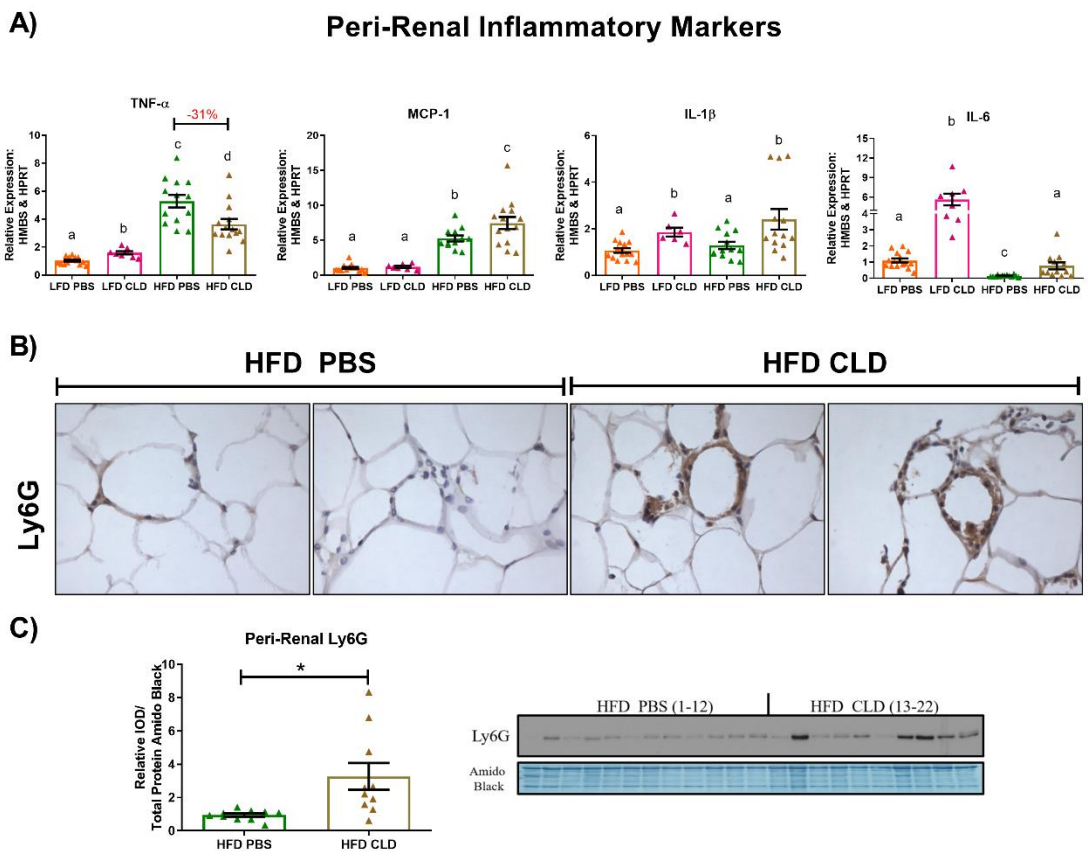

Figure 3.7. An increase in peri-renal adipose tissue inflammation is paired with an increase in infiltrating neutrophils. A) Peri-renal adipose tissue mRNA expression of inflammatory mediators (TNF-α, MCP-1, IL-1β, and IL-6) normalized to the geometric mean of the most stable internal reference genes using QBase+ software, B) two representative images of immunohistochemistry staining (100x) of Ly6G in peri-renal adipose tissue of HFD-treated groups, C) western blot analysis of Ly6G in epididymal adipose tissue normalized to total protein stain (amido black). Values are means ± SE; n=9-15 mice per group. Bar graphs not sharing a common letter and the * represent a statistically significant difference between groups ($p<0.05$).

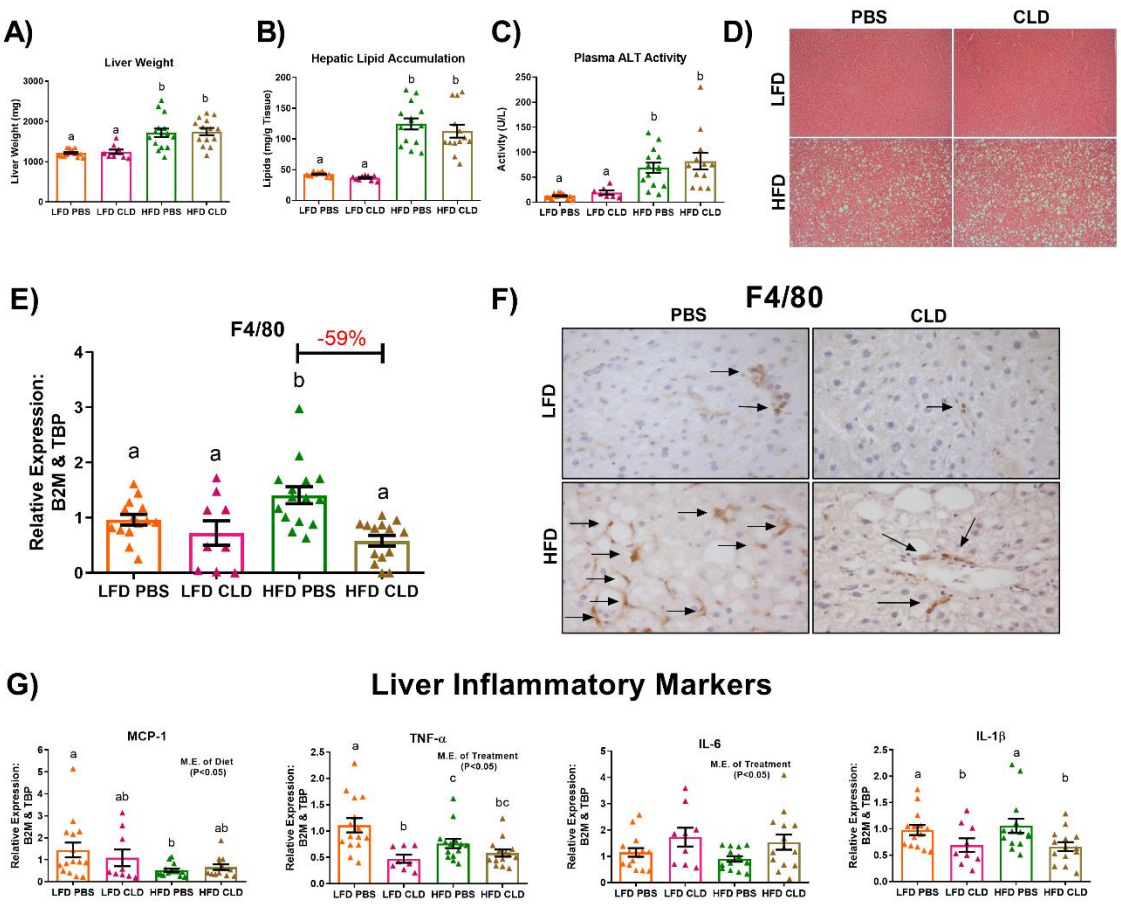

Figure 3.8. CLD treatment has no affect at regressing early-stage NAFLD development. A) Liver weight following sacrifice, B) hepatic lipid accumulation, C) plasma Alanine Transaminase (ALT) Activity, D) representative hepatic H&E (20x) images, E) hepatic gene expression of F4/80, F) representative F4/80 staining (60x, arrows indicate examples of positive staining), and G) mRNA expression of hepatic inflammatory mediators (MCP-1, TNF-α, IL-6, and IL-1β) normalized to the geometric mean of the most stable internal reference genes using QBase+ software. Values are means ± SE; n=9-15 mice per group. Bar graphs not sharing a common letter are significantly different from one another ($p<0.05$). %, $, #, ^ represent statistically significant differences ($p<0.05$) in blood glucose levels from baseline (0 minutes) for the LFD PBS, LFD CLD, HFD PBS, and HFD CLD groups, respectively.

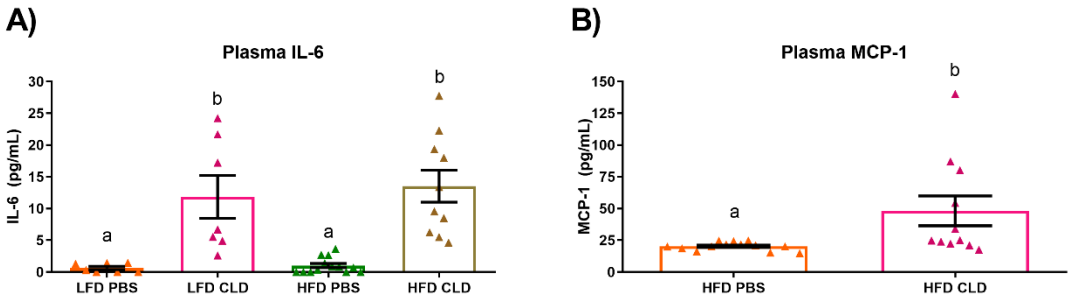

Figure 3.9. CLD treatment significantly increases circulating pro-inflammatory cytokine concentrations. After 20 weeks of diet/4 weeks of clodronate liposome treatment, plasma was assessed for circulating pro-inflammatory cytokines: A) IL-6 and (B) MCP-1. Due to limitations in the amount of plasma, only the plasma of HFD-treated groups was assessed for the concentration of circulating MCP-1. Values are means ± SE; n=7-14 mice per group. Bar graphs not sharing a common letter are significantly different from one another ($p<0.05$).

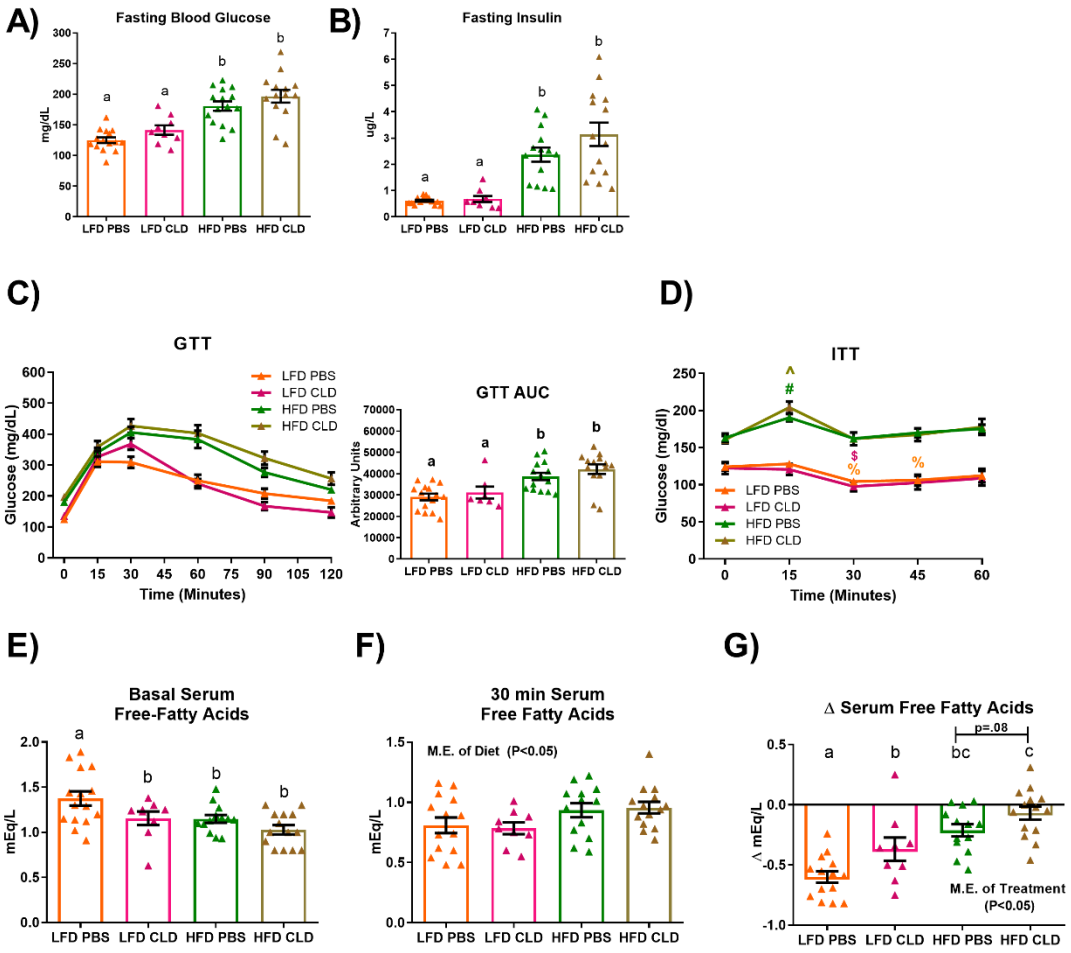

Figure 3.10. CLD treatment does not rescue impaired glucose metabolism or insulin resistance and exacerbates adipose tissue insulin action. After 20 weeks of diet/4 weeks of clodronate liposome treatment, metabolic outcomes were assessed: A) fasting (5 hour) blood glucose levels, B) fasting (5 hour) plasma insulin levels, C) intraperitoneal (IP) glucose tolerance test (GTT) and corresponding area under the curve (AUC), D) IP insulin tolerance test (ITT) following a 5-hour fast, E) serum free-fatty-acid (FFA) concentration following a 5-hour fast measured at the 0 and F) 30-minute time point of the ITT, and G) change in serum FFAs from 0-30 minutes of the ITT. Values are means ± SE; n=9-15 mice per group. Bar graphs not sharing a common letter are significantly different from one another ($p<0.05$).

Table 3.2. CLD treatment results in anemia. Whole blood collected at sacrifice (4 weeks after liposome treatment) was assessed for mean corpuscular hemoglobin concentration, as well as hemoglobin, and % hematocrit. Values are means ± SE; n=9-15 mice per group. Groups not sharing a common letter differ significantly from one another ($p<0.05$).

	LFD PBS	LFD CLD	HFD PBS	HFD CLD
Mean Corpuscular Hemoglobin Concentration (g/l)	36.5±0.42	35.1±0.35	35.2±0.23	35.6±0.59
Hemoglobin (g/dl)	13.7±0.21[a]	11.6±0.22[b]	13.2±0.18[a]	11.8±0.24[b]
Hematocrit (%)	37.7±0.62[a]	33±0.55[b]	37.5±0.52[a]	33.3±0.81[b]

CHAPTER 4

SEX DISPARITIES IN OBESITY-ENHANCED COLON CANCER: DETRIMENT OF ADIPOSITY AND MACROPHAGE ASSOCIATED INFLAMMATION[3]

[3]Bader JE, Carson MS, Enos RT, Velázquez KT, Sougiannis AT, Singh UP, Becker WJ, Nagarkatti M, Robinson CM, Murphy EA. Sex Disparities in obesity-enhanced Colon Cancer: Detriment of Fat Distribution and Macrophage Associated Inflammation. Manuscript in Preparation

4.1 ABSTRACT

Given the high prevalence of colorectal cancer (CRC) in the United States and the increased risk for of CRC in the obese population, it is important to understand the underlying mechanisms that link obesity to CRC. Currently, there is increased incidence within obese males compared to obese females, and evidence suggests that female sex hormones may offer certain protection against obesity enhanced CRC. In this study, MC38 murine colon adenocarcinoma cells were injected subcutaneously ($2x10^5$cells/100μL) in obese mice with associated metabolic dysfunctions following 20 weeks of high fat diet feeding to better elucidate the mechanisms behind tumor growth in an obese state. This was performed in C57BL/6J males, females and females that underwent ovariectomy (OVX), in order to further examine the influence of female sex hormones in this obesity enhanced CRC model. Our results indicate that enhanced tumor growth occurs following diet induced obesity and insulin resistance. Among mice fed a high fat diet, OVX mice exhibited the most significant tumor growth compared to males and females ($p=0.036$ and 0.001 respectively). Furthermore, OVX mice presented with increased CD206 and decreased CD11c gene expression of macrophages isolated from tumors compared to those of female mice. This increase in tumor growth and altered tumor associated macrophage phenotype were attributed to increased subcutaneous adipose tissue and adipose tissue inflammation present in the high fat diet OVX group following 20 weeks of diet feeding. This study provides evidence suggesting adiposity and macrophage associated adipose inflammation as potential mechanisms underlying female derived protection against obesity-associated CRC.

4.2 INTRODUCTION

It has been established that there is a positive relationship between obesity and CRC. Obese men have a higher risk of CRC compared with normal weight men, but this association is much weaker in women [136]. On the other hand, postmenopausal women have an increased risk of obesity, insulin resistance and consequently have an increased incidence of CRC compared to premenopausal women [137, 138]. Interestingly, hormone replacement therapy (HRT), has been shown to reduce the risk of CRC in postmenopausal women although some studies have shown inconclusive effects [139].

Epidemiological studies have shown that distribution of fat increases susceptibility to inflammation induced insulin resistance, which enhances CRC risk. Although females have a larger proportion of body fat mass compared to males, the distribution of adipose tissue in males is primarily abdominal which is more closely linked to worsened insulin sensitivity [140]. Visceral adipose tissue, as opposed to subcutaneous or total body fat is presumed as the particular location for which these metabolic risk factors for CRC arise [141]. Furthermore, visceral adiposity correlates with increased circulating pro-inflammatory adipokines, which can promote cellular proliferation, and angiogenesis [142]. This evidence suggests that adiposity, specifically location of adiposity, is strongly associated with obesity induced insulin resistance and CRC.

This obesity associated inflammation is strongly influenced by immune cell populations, particularly macrophages present in the adipose tissue depots. Studies by our laboratory (unpublished) show a sex-specific association of obesity with macrophage phenotype. This data indicates that male mice have a significant increase in pro-

inflammatory M1 macrophages in response to high fat diet whereas minimal increases are seen in female mice. The ovariectomy of female mice results in increased M1 macrophages similar to males, which is reversed upon estrogen replacement. This suggests that a combination of differential fat distribution and adipose tissue macrophage associated inflammation between men, women, and postmenopausal women may provide a mechanism for the differential incidence of CRC within those populations.

Additional evidence supports a potentially protective role of estrogen against inflammation and obesity associated insulin resistance [143]. However, current literature does not provide a conclusive role for estrogen in CRC. Further, there are few studies that have examined the role of estrogen in CRC in the settings of obesity. This is largely due to the difficulties in choosing appropriate methods for either establishing obesity or inducing CRC. Studies from our laboratory have shown that diet induced obesity increases the mucin production within the colon in the chemically induced AOM/DSS colon cancer model and thus affect the effectiveness of DSS induced inflammation to cause CRC [144]. Furthermore the transgenic $Apc^{Min/+}$ mouse model for intestinal cancer is ineffective at testing obesity enhanced CRC because the genetic mutation of APC gene is present and expressed at birth. This results in development of intestinal polyps before obesity or associated metabolic dysfunctions can be established [113]. Due to these limitations in more commonly used CRC models, we utilized the subcutaneous MC38 tumor model, which allowed us to establish an obese phenotype with associated metabolic dysfunction prior to the initiation of cancer in order to better elucidate the mechanisms behind increased colon cancer risk in an obese population.

Given the high prevalence of CRC in the United States and the increased risk for of CRC in the obese population, it is important to elucidate the mechanistic link between obesity and CRC. In this study, we examined adiposity and macrophage associated inflammation as potential mechanisms influencing sex disparities within colon derived tumor growth following diet-induced obesity.

4.3 MATERIALS & METHODS

Animals: Male and female WT *C57BL/6J* mice were purchased from the Jackson Laboratories (Bar Harbor, ME) and cared for at the Department of Laboratory Animal Resources at the University of South Carolina. Mice (n=15/group) were housed 5 per cage, maintained on a 12:12-h light-dark cycle in a low stress environment (22°C, 50% humidity, low noise) and given water *ad libitum*. Principles of laboratory animal care were followed, and the Institutional Animal Care and Usage Committee of the University of South Carolina approved all experiments. At 9 weeks of age male mice underwent a sham surgery and female mice underwent either a sham or ovariectomy (OVX) surgery. Briefly, mice underwent anaesthesia maintained with 2% isoflurane and oxygen before a dorsal incision was made to the skin then the muscle layers. Both uterine horns were tied with non-absorbable suture 5-0 (cat # S-G518R13) and ovaries were removed. In case of the sham-operated mice, the ovaries were exteriorized and then placed back intact into the abdominal cavity. The muscle wall was sutured with with 5-0 absorbable suture (cat # S-G518R13-U) and wound clips were used to close skin incision. Buprenorphine was given as pain reliever subcutaneously at a dose of 0.043 mg/kg. Wound clips were removed 1 week after surgery and mice were allowed to recover for an additional week prior to initiation of diet

feedings. The experiment was performed over 3 independent blocks, with n=5 mice/group/block for a total of n=15/group.

Diets: At 11 weeks of age, mice (Male, Female and OVX) were randomly assigned to either control purified AIN-76A low-fat diet (LFD) (3.77 kcal/g) or a purified HFD (40% of total kcals from fat; 4.57 kcal/g) designed to mimic the standard American diet (BioServ, Frenchtown, NJ, USA). We have used this diet in several of our previous studies [50, 67, 109-113]. Mice were initially provided the respective LFD or HFD for 20 weeks at which time baseline body composition (DEXA) and metabolic tests were performed. Following MC38 colon cancer cell injection (described below), mice continued their respective diets (LFD or HFD) for another 3 weeks. Thus, in total, mice consumed the assigned diets for 23 weeks.

Body weights, body composition and metabolism: Body weight was monitored on a weekly basis throughout the study. Body composition was assessed before cancer cell injection at 20 weeks of diet feeding. For this procedure, mice were placed under brief anesthesia (isoflurane inhalation) and were assessed for lean mass, fat mass, body fat percentage and bone mineral density via dual-energy X-ray absorptiometry (DEXA) (Lunar PIXImus, Madison, WI). Metabolic parameters were assessed at 20 weeks of dietary treatment. After a five-hour fasting, blood samples were collected from the tip of the tail. Blood glucose concentrations were determined in whole blood using a glucometer (Bayer Contour, Michawaka, IN). Collected blood was centrifuged at 4,000 rpm for 10 min at 4°C. Plasma was aliquoted and stored at -80°C until analysis. Plasma insulin concentrations were analyzed using a mouse insulin ELISA kit according to the manufacturer's instructions (Mercodia Inc., Winston Salem, NC). Insulin resistance was estimated by HOMA index

according to the following formula: insulin resistance index = fasting insulin (μU/ml) x fasting glucose (mmol/l)/22.5. For glucose tolerance tests (GTTs) and insulin tolerance tests (ITTs), mice were fasted for 5 hours and glucose or insulin was administered (IP) at a dose of 2 g/kg or 0.75 U/kg lean mass, respectively. Blood glucose concentrations (tail sampling) were measured intermittently over a two-hour period (0, 15, 30, 60, 90, and 120 minutes) for GTTs and intermittently over a one-hour period (0, 15, 30, 45, and 60 minutes) for ITTs using a glucometer (Bayer Contour, Michawaka, IN). Area under the curve (AUC) was calculated using the trapezoidal rule.

Subcutaneous Tumor Model: MC38, murine colon adenocarcinoma cells (Kerafast), were maintained in complete DMEM 4.5g/L glucose with 10% fetal bovine serum, 2mM glutamine, and 1% penicillin/streptomycin. Cells were routinely passaged when 80% confluence was reached under sterile conditions and maintained in a 37°C, 5% CO2 incubator. Prior to injection, cells (passage <20) were trypsinized, washed, counted with a hemocytometer and resuspended at $2x10^6$ cells/mL in phosphate buffered saline. Mice were briefly anesthetized (isoflurane inhalation), and 100μL of MC38 cell suspension ($2x10^5$cells/100μL/mouse) was injected subcutaneously using a 0.3mL 29G syringe into the left dorsal lumbar region of each mouse. Viability of the cell suspension was confirmed >95% using trypan blue staining before and after all injections were completed.

Tissue collection: After 23 weeks of dietary treatment (3 weeks after tumor injection), mice were sacrificed via isoflurane inhalation for tissue collection. Whole blood taken from the inferior vena cava was analyzed for hematology analysis using a VetScan Hm5 (Abaxis, Union City, CA). The blood was spun at 4,000 RPM x 10 min and aliquoted plasma was stored -80°C. Gonadal, mesentery, and peri-renal fat pads, as well as the liver and spleen

were removed, weighed, and immediately snap-frozen in liquid nitrogen and stored at −80°C until analysis. Subcutaneous tumors were removed, weighed and measured (length and width) using calipers. Half of the tumor was placed in complete DMEM to be used for cell sorting. The other half was snap frozen and stored at -80°C until analysis.

Flow Cytometry and Cell Sorting: Tumors were mechanically disrupted in PBS with 5% FBS using the gentleMACS dissociate and tumor associated macrophages (TAMs) were isolated using FACS as described [145]. Briefly tumor isolates underwent RBC lysis and filtered through a 100μM then 70μM cell strainer prior to being stained with CD45-APC, F4/80-PE, and CD11b-FITC (Biolegend, San Diego, CA) antibodies for 30 minutes. Following compensation using unstained and single stained controls, tumor associated macrophages were quantified by gating for CD45+ cells followed by F480 and CD11b double positive gate. TAMs were sorted into a separate tube containing PBS with 5% FBS and kept on ice until all samples were sorted. Data were acquired using a BD FACS Aria II cell sorter and analyzed using DIVA software. Freshly sorted TAMs were spun at 2000 RPM x 5min, resuspended in trizol reagent and stored at -20ºC until RNA isolation.

Quantitative real-time RT-PCR: RNA was isolated from fluorescent activated cell sorted TAMs, and gonadal and subcutaneous adipose tissue depots using trizol reagent. TaqMan reverse transcription reagents and gene expression assays (Applied Biosystems, Foster City, CA) were used to reverse transcribe and to analyze the expression of the following genes: F4/80, CD11c, CD206, MCP-1, NOS, ARG, TNFα, and TGFβ. Potential reference genes (18s, HMBS, TBP, B2M, H2AFV, and HPRT) were analyzed for stability using Qbase+ software (Biogazelle, Belgium) for each tissue analyzed. The optimal number of reference genes were determined by Qbase+ and the geometric mean of these genes was

used as the normalization factor for each analysis: TAM (B2M and H2AFV), gonadal adipose tissue (H2AFV, 18S, HPRT, HMBS, TBP), and subcutaneous adipose tissue (B2M, TBP, HMBS) [50, 119]. Gene expression quantification was calculated using the ΔΔCT method and Qbase+ software. Values were normalized to the LFD female group.

Micro Computed Tomography (CT) Quantification of Fat Volume: Following 20 weeks of diet feeding mice were placed under brief anesthesia (isoflurane inhalation) and positioned with both legs fully extended on the bed. The torso was scanned at an isotropic voxel size of 44 mm FOV (70kVp, 114uA) for 18seconds using Quantum GX micro CT Imaging System (Perkin Elmer). Using, AccuCT micro CT analysis software, all scans were calibrated to Hounsfield Unites (HU) based on the standard densities of plastic (40) and air (-1000) plotted against the measured density at the time of scanning. All scans underwent low pass filter to remove background noise and cropped to a region of interest between L1 and L5 of each mouse. Threshold objects of bone (>500 HU), soft tissue (75-500 HU) and adipose tissue (<75 HU) were applied to all scans. Subcutaneous and visceral adipose tissue was differentiated using the abdominal wall as an anatomical landmark (adipose superficial to the soft tissue layer was marked subcutaneous and all adipose deep marked as visceral). Volumes of specified objects (bone, soft tissue, visceral fat and subcutaneous fat) were calculated using AccuCT micro CT analysis software. Volumes of adipose tissue were then normalized to the soft tissue volume calculated within each scan [146].

Statistical Analysis: Data were analyzed using commercially available statistical software: Prism 6 (GraphPad Software, La Jolla, CA). A two-way ANOVA followed by a turkey post-hoc analysis was used to determine differences between diet (HFD vs. LFD) and hormone status (female intact estrogen+/testosterone-; female OVX estrogen-

/testosterone-; and male estrogen-/testosterone+). For correlation calculations values were plotted on an XY plot and a Pearson correlation was performed with a two tailed 95% confidence interval and significance set to $p<0.05$. Any statistical test that did not pass the equal-variance test (Bartlett's test for equal variances) was log transformed and then re-analyzed. Data are presented as the mean ± SEMs and the level of significance was set at $p<0.05$.

4.4 RESULTS

20 weeks of HFD feeding leads to an obese phenotype that is exacerbated in male and OVX mice

At 9 weeks of age mice received either a sham or ovariectomy surgery to establish male, female, or OVX groups. Two weeks following surgery, mice were fed a 40% HFD or a purified LFD for 20 weeks. An obese phenotype was successfully achieved as the HFD-fed mice gained significantly more body weight, fat mass, and displayed a significantly greater body fat % (Figure 4.1 A-B) compared to LFD fed mice ($p<0.05$). HFD-fed mice also displayed elevated fasting blood glucose, insulin, HOMA-Index, GTT AUC, and impaired insulin sensitivity (Figures 4.1 D-J), demonstrating a dysfunctional metabolic phenotype ($p<0.05$). Further, within a high fat diet, male mice exhibited increased body fat mass ($p=0.01$), lean mass ($p<0.0001$) and HOMA-Index ($p<0.0001$) compared to intact female mice, indicating that females exhibit a slight protection against diet induced obesity. However, this observed protection was not as prevalent in the HFD OVX group, which exhibited increased body weight and fat mass ($p<0.0001$) with trending increased body fat%, GTT, and HOMA-index although these were not significantly increased compared to HFD females. Further, this OVX group resulted in decreased bone

mineral density compared to intact females or males, independent of diet, a common consequence of estrogen depletion as estrogen is important for bone calcium reabsorption (Figure 4.1 C).

Tumor weight is increased in obese mice and is most severe in HFD OVX group

Following MC38 cell injection, tumors were allowed to grow for 3 weeks before weights were measured. Consistent with epidemiological evidence, HFD resulted in increased tumor weight compared to LFD (Figure 4.2 A). This was consistent with increases in spleen and liver weight of the HFD mice compared to LFD (Figure 4.2 B-C). As expected, adipose tissue of all depots measured was significantly increased as a result of 23-week HFD feeding (Figure 4.2 E). Additionally, HFD feeding significantly increased white blood cells, specifically lymphocytes and neutrophils within whole blood (Figure 4.2 F). Interestingly, the HFD OVX group presented with the largest tumors of any group, significantly larger compared to female and male groups within the same diet treatment (Figure 4.2 A $p=0.036$ and 0.001 respectively). This increase in tumor weight within HFD OVX was consistent with increased white blood cells, specifically neutrophils ($p=0.005$) (Figure 4.2 F). However, contrary to the epidemiological data, HFD feeding in male mice did not significantly increase tumor weight. Further, the tumor challenge resulted in reduced gonadal adipose tissue and subsequent total adipose weights measured 3 weeks following tumor initiation compared to female and OVX mice within the same diet ($p<0.0001$) (Figure 4.2 E). Despite the reduced tumor weight and gonadal adipose tissue, HFD male mice presented with increased white blood cells, specifically lymphocytes and neutrophils, similar to the HFD OVX mice. The phenotypic differences between female

and OVX groups were further confirmed by significant decreases in uterus weight of the OVX groups compared to the female groups ($p<0.0001$) as shown in figure 4.2 D.

Tumor associated macrophages isolated from female and OVX tumors exhibited different phenotypes

Due to the unchanged tumor growth observed in the lean compared to obese male mice, we decided to focus on the interaction solely between female intact and OVX mice within respective diets. Following tumor excision, TAMs were defined as double positive F4/80 and CD11b cells from a CD45 positive gate and were collected using FACS (Figure 4.3 A). Although there were differences in tumor weight as seen in Figure 4.2 A, between HFD OVX and female mice, there were no significant differences in the TAM percentage within these tumors (Figure 4.3 B). However, upon further investigation of the gene expression in these isolated TAMs, CD11c, an M1 macrophage marker was significantly increased in female mice ($p=0.05$), consistent with a significant decrease in expression of CD206, an M2-macropahge marker ($p=0.02$) (Figure 4.3 C-D). This indicates that irrespective of tumor size or diet, female mice possess more pro-inflammatory/ anti-tumor macrophages within the tumor microenvironment compared to OVX mice. However, because TAMs were isolated from tumors of different sizes it is unclear whether this altered macrophage phenotype directly impacted tumor growth or is simply a consequence of the difference in tumor size.

Spleen, total fat and fasting insulin levels are positively correlated with tumor weight of female and OVX mice.

In order to further examine potential mechanisms of the increased tumor size within OVX mice, tumor weight was plotted against spleen, total fat and fasting insulin levels (Figure 4.4). Consistent with other cancer models, tumor size was strongly correlated with increased spleen size (R^2=0.6017, p<0.0001), confirming that an increased immune response is present following tumor challenge. Additionally, there was a significant positive, albeit weak, correlation between total visceral fat (R^2=0.294, p=0.0008) compared to tumor weight as well as fasting plasma insulin levels (R^2=0.4151, p<0.0001) compared to tumor weight suggesting a potential link between fat distribution or insulin sensitivity and tumor growth.

Differential fat distribution of visceral and subcutaneous fat among female and OVX mice following 20-week diet feedings

The significant correlation between tumor weight and total fat shown in Figure 4.4 B, led us to initiate a new cohort of female and OVX mice subjected to the same low fat or high fat diet treatment for 20 weeks. This helped us understand the environment at the time of MC38 injection as opposed to 3 weeks following tumor growth. As reflected in the DEXA analysis in the previous study (Figure 4.1B), 20 weeks of HFD feeding resulted in significantly increased body fat %. Although within the HFD, no difference in body fat % was observed between OVX and female mice. To better understand distribution of fat rather than total body fat%, the new cohort of mice were scanned using micro CT which is considered more accurate and sensitive than DEXA and can distinguish between visceral and subcutaneous fat [146]. As seen in the representative images in Figure 4.5 A, bone, soft tissue, visceral fat and subcutaneous fat were able to be distinguished based on differing densities, and quantified by volume within the region of interest, L1 and L5. The

micro CT analysis in Figure 4.5 B-C, confirmed, that in addition to increased visceral adipose tissue, HFD mice had significantly increased subcutaneous adipose tissue compared to LFD mice ($p<0.0001$). Further, OVX mice had significantly increased subcutaneous fat distribution compared to female mice within either LFD or HFD groups ($p=0.04$ and $p=0.03$, respectively). In order to confirm the accuracy of the micro CT analysis to measure adipose volume, a correlation between visceral adipose tissue weight taken at sacrifice and visceral adipose volume calculated via micro CT scan revealed a strong positive correlation ($R2= 0.9793$ and $p<0.0001$) (Figure 4.5 D).

Increased macrophage infiltration and associated inflammation in adipose tissue of HFD OVX mice

As expected, a main effect of diet was achieved through increased F480, MCP1, CD11c, CD206, NOS, ARG-1, TNFα and TGFβ gene expression within HFD parametrial adipose tissue compared to LFD adipose tissue ($p<0.05$) (Figure 4.6). Additionally, within the HFD group, OVX mice presented with greater adipose inflammation with significant increased F480, MCP1, CD11c, CD206, NOS, ARG-1, TNFα and TGFβ compared to female mice ($p<0.01$). This severe inflammation presented only in the adipose tissue of HFD OVX mice, supporting that intact female mice are to a certain extent protected against obesity induced adipose tissue inflammation. The subcutaneous adipose tissue gene expression revealed no significant difference in F4/80 macrophage gene expression in contrast to a significant increase in MCP-1 within HFD compared to LFD ($p=0.01$). Among HFD fed mice, OVX mice had significantly increased MCP-1 concentrations compared to female ($p=0.05$). Additionally, OVX mice displayed a significant increase in the pro-inflammatory macrophage marker CD11c compared to female mice within HFD

(p=0.001). These differences indicate that inflammation is unique within visceral and subcutaneous adipose tissue depots and that HFD OVX mice have greater adipose tissue inflammation compared to HFD female mice.

4.5 DISCUSSION

Given the established link between obesity and CRC along with a suggested interaction of sex specific hormones, we examined sex disparities within colon derived cancer growth following diet-induced obesity. Using the subcutaneous MC38 tumor model, we were able to replicate some epidemiological data, as we observed enhanced tumor growth following diet-induced obesity and insulin resistance. Within female mice on a high fat diet, some protection against obesity-enhanced tumor growth was observed compared to ovariectomized mice. However, male mice failed to coincide with epidemiological data and did not exhibit increased tumor growth compared to females fed the same diet. It was revealed in a follow up study, that following 20 weeks of high fat diet feeding, OVX mice had significantly increased visceral and subcutaneous fat compared to female mice. These adipose tissue depots within HFD OVX exhibited more severe macrophage associated inflammation through observed increases in CD11c, M1 macrophage gene expression. Taken together these data suggest that accelerated subcutaneous tumor growth within obese OVX mice may be due to the increase in subcutaneous adiposity combined with increased M1, pro-inflammatory adipose tissue macrophages.

The association between obesity and CRC has been suggested in both epidemiological and in-vivo mouse studies. Epidemiological evidence has further uncovered a more significant relationship in men than in women [42-44]. A meta-analysis of 18 observational studies showed a 20% reduction in colon cancer incidence among women who had ever used HRT, indicating a specific association between female sex hormones and CRC [47]. Utilizing in-vivo subcutaneous tumor models, many have reported that obesity enhances colorectal tumor growth [147-150]. Consistent with our findings, Yakar et al, revealed similar increases in tumor growth of obese OVX mice compared to female mice [137]. However, contrary to what we found, this group was able to show obesity-enhanced tumor growth in males in addition to female and OVX mice although they did not directly compare all 3 groups within the same experiment [150]. Our study is the first to include male, female and OVX mice in an obesity-enhanced subcutaneous tumor model in order to directly examine sex disparities within this cancer model.

Although there is evidence to support sex differences in obesity enhanced CRC, a clear mechanism has yet to be elucidated. Macrophage associated inflammation has been implicated in obesity induced insulin resistance and CRC which may offer an explanation for the large tumors present in HFD OVX mice. We observed that in addition to large tumors, HFD OVX mice presented with more pro-inflammatory macrophages within both the visceral and subcutaneous adipose tissue depots. M1 macrophage derived inflammatory cytokines, including NOS and TNF-α which were both increased in our HFD OVX parametrial adipose tissue, can activate the inflammatory pathways NFκB and STAT3 to mediate proliferation, invasion, angiogenesis, survival and metastasis [151,

152]. This is consistent with our findings that pro-inflammatory adipose tissue macrophages present at the time of MC38 injection in HFD OVX mice may have resulted in the increased tumor weight that was observed 3 weeks post injection.

In addition to inflammation, distribution of adiposity may play an important role in colon carcinogenesis [153]. In the present study, utilizing highly accurate micro CT analysis, we found increased visceral and subcutaneous adipose tissue within HFD OVX mice compared to female mice. There is emerging evidence that adipose stromal cells may be a source of stromal cells in tumor microenvironments. In animal models of obesity, adipose stromal cells from inflamed visceral adipose tissue can migrate to tumor sites [154]. These, stromal cells present in the tumor microenvironment can promote angiogenesis and support tumor progression[18]. This offers evidence that increased adiposity within HFD OVX mice may have resulted in increased adipose derived stromal cells in the tumor and these stromal cells promoted tumor growth. However additional studies are necessary to confirm this hypothesis.

There is some evidence that female sex hormones may offer a protection against CRC. In vitro findings have shown that estradiol in addition to estrogen receptor β agonist can inhibit proliferation and migration of MC38 cells [155, 156]. In several in-vivo studies, exposure of ovariectomized rats to estrogen reduced the rate of colon tumors by 71% [138, 157]. In addition, in the $Apc^{Min/+}$ mice ovariectomy resulted in an increased number of polyps, whereas estrogen replacement in these mice reduced the number of polyps to the baseline levels [158]. Our data is consistent with these findings, as the female mice presented with smaller tumors compared to ovariectomized mice. Moreover, the tumor-associated macrophages within female tumors had higher expression of CD11c with

reduced expression of CD206 compared to OVX mice. This shift in the M1/M2 like TAM ratio suggests a more tumoricidal environment that coincides with the reduced tumor size of female mice. Taken together our results indicate a potential for sex hormones present in females to influence tumor growth and TAM phenotype.

In addition to macrophage associated inflammation, adiposity and estrogen influencing CRC, emerging evidence indicates insulin as a mechanism for cancer proliferation. Obesity leads to insulin resistance and results in increased circulating insulin. A proliferative role of insulin has been reported in various cancers including breast cancer, pancreatic cancer and CRC [159, 160]. Hvid et al, reports that treatment with insulin accelerates tumor growth, specifically in the MC38 subcutaneous tumor model [161]. Additionally reducing circulating insulin levels may be beneficial in cancer prevention, as treatment with metformin, a type 2 diabetes drug, is associated with reduced incidence of breast cancer in women [162]. Consistent with primary literature, we report a positive correlation between tumor weight and fasting insulin levels in female and OVX mice, although we did not explore this potential mechanism further in this study.

An unexpected finding that conflicts with the previously stated evidence was that tumor growth in HFD males was not increased compared to LFD males despite the significantly high level of fasting insulin. One possible explanation could be that in addition to fasting insulin levels, macrophage infiltration and pro-inflammatory macrophages in the adipose tissue of obese male mice were also significantly increased compared to both the OVX and female mice within the high fat diet (data not shown). Although chronic low-grade inflammation is often cancer promoting, perhaps severe acute inflammation induces apoptosis. It is possible that the chronic mild inflammatory

environment of the high fat diet OVX mice combined with the high levels of circulating insulin was conducive to cancer growth while the severe inflammation in the male mice offset any proliferative effects of the increased circulating insulin. Of course, additional studies, involving insulin, insulin knockout mice, or insulin antagonists would be required in order to test this hypothesis.

In conclusion, our study confirms that obesity enhanced CRC was achieved following 20 weeks of a high fat diet using a subcutaneous MC38 tumor model, thus validating this model for future studies. We established that diet induced obesity and associated insulin resistance present differently in male, female and OVX mice. Additionally, increased accumulation of subcutaneous fat and increased pro-inflammatory adipose tissue macrophages at the time of tumor challenge, are likely responsible for the accelerated tumor growth observed in the high fat diet OVX mice. This study provides insight into potential mechanisms behind female associated protection against obesity associated CRC.

4.6 FIGURES & LEGENDS

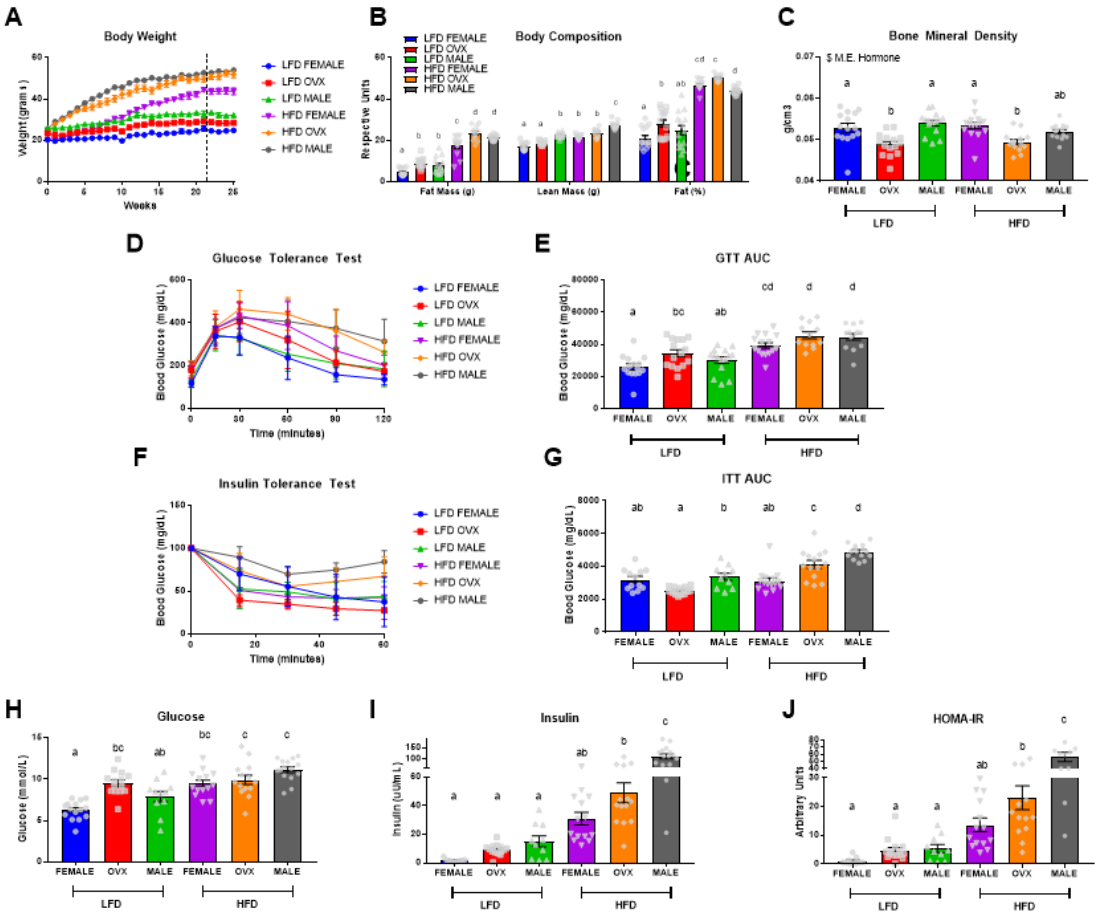

Figure 4.1 Body composition and metabolic assessment after 20 weeks of dietary treatment prior to injection of MC38 cells. A) Mouse body weight, B-E) body composition, fat mass, lean mass, fat%, and bone mineral density, respectively F-G) intraperitoneal (IP) glucose tolerance test (GTT) and corresponding area under the curve (AUC), H-I) IP insulin tolerance test (ITT) following a 5-hour fast and corresponding AUC. J) fasting (5 hour) blood glucose levels, K) fasting (5 hour) plasma insulin levels, L) Homeostatic Model Assessment Index – Insulin Resistance (HOMA-IR) calculated as fasting insulin (μU/ml) x fasting glucose (mmol/l)/22.5. Values are means ± SE; n=12-15 mice per group. Bar graphs not sharing a common letter are significantly different from one another ($p<0.05$).

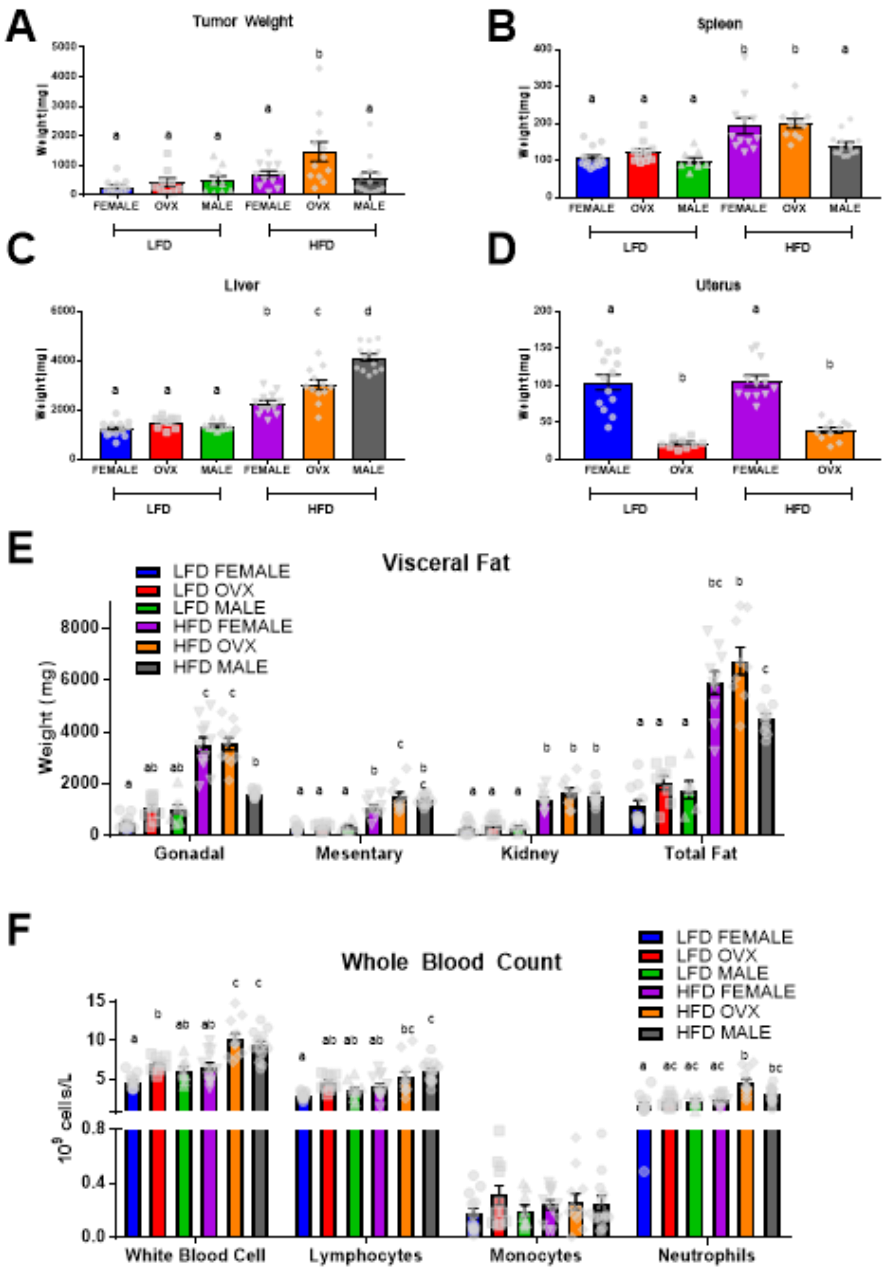

Figure 4.2 High fat diet feeding increased tumor weight with enhance growth in OVX group. A) Tumor weight measurements 3 weeks post injection B-D) Organ weights of spleen, liver, and uterus (females only), respectively. E) Weight of various adipose depots with total fat as the sum of gonadal, mesentery and kidney weights. F) Complete blood count of whole blood. Values are means ± SE; n=9-15 mice per group. Bar graphs not sharing a common letter are significantly different from one another ($p<0.05$)

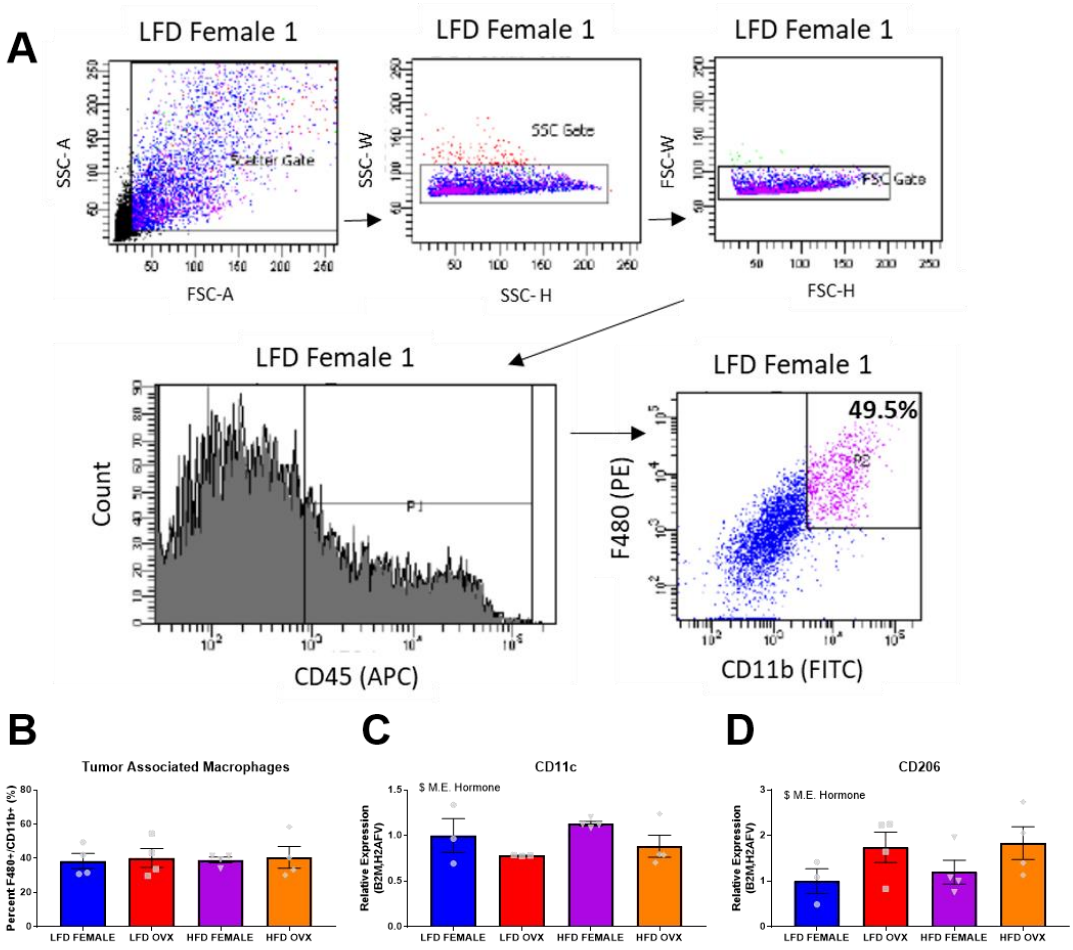

Figure 4.3 Differential tumor associated macrophage phenotype in female and OVX groups. A) Representative gating strategy for collection of tumors associated macrophages, defined as CD45+ F4/80+ CD11b+ cells. B) Percentage of tumor associated macrophages within tumors at time of sort. C-D) Quantitative RT-PCR assessment of gene expression in sorted tumor associated macrophages. Ct values relative to average of multiple internal controls determined using qBASE pro software analysis. Values are means ± SE; n=3-4 mice per group. Bar graphs not sharing a common letter are significantly different from one another ($p<0.05$)

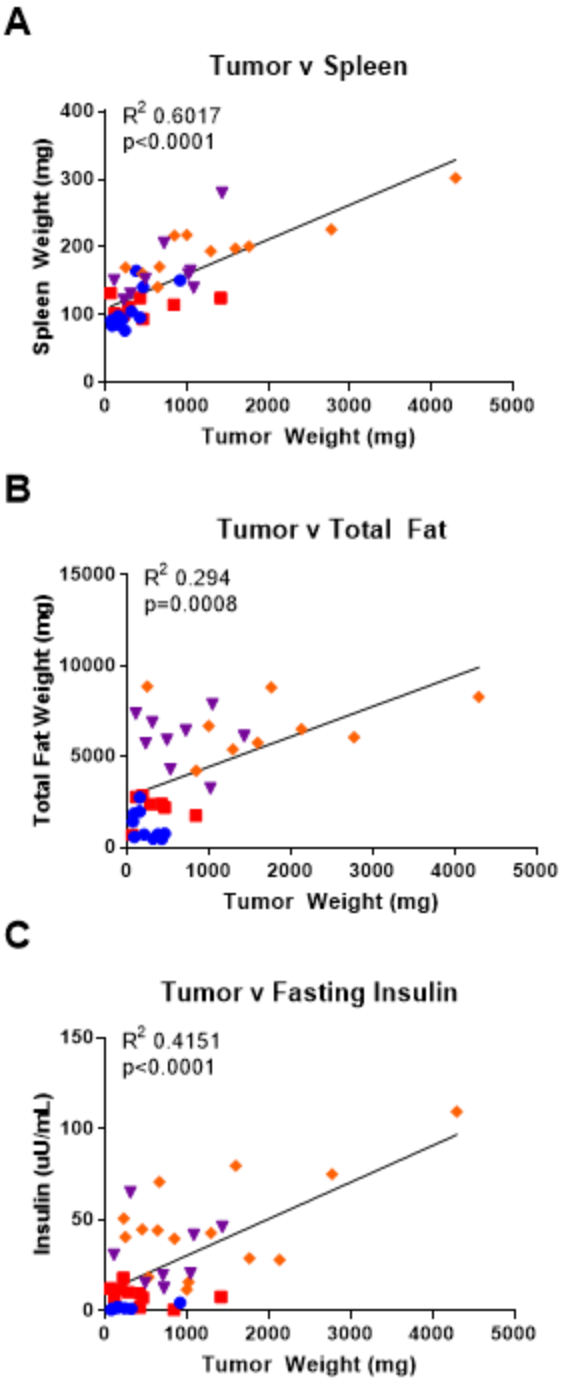

Figure 4.4 Tumor weight positive correlated with spleen, fat and fasting insulin levels among female and OVX mice. Correlation between tumor weight and A) spleen weight, B) total fat weight, C) fasting insulin from plasma. Data analyzed using Pearson correlation set to 95% confidence two tailed with significance set to <0.5)

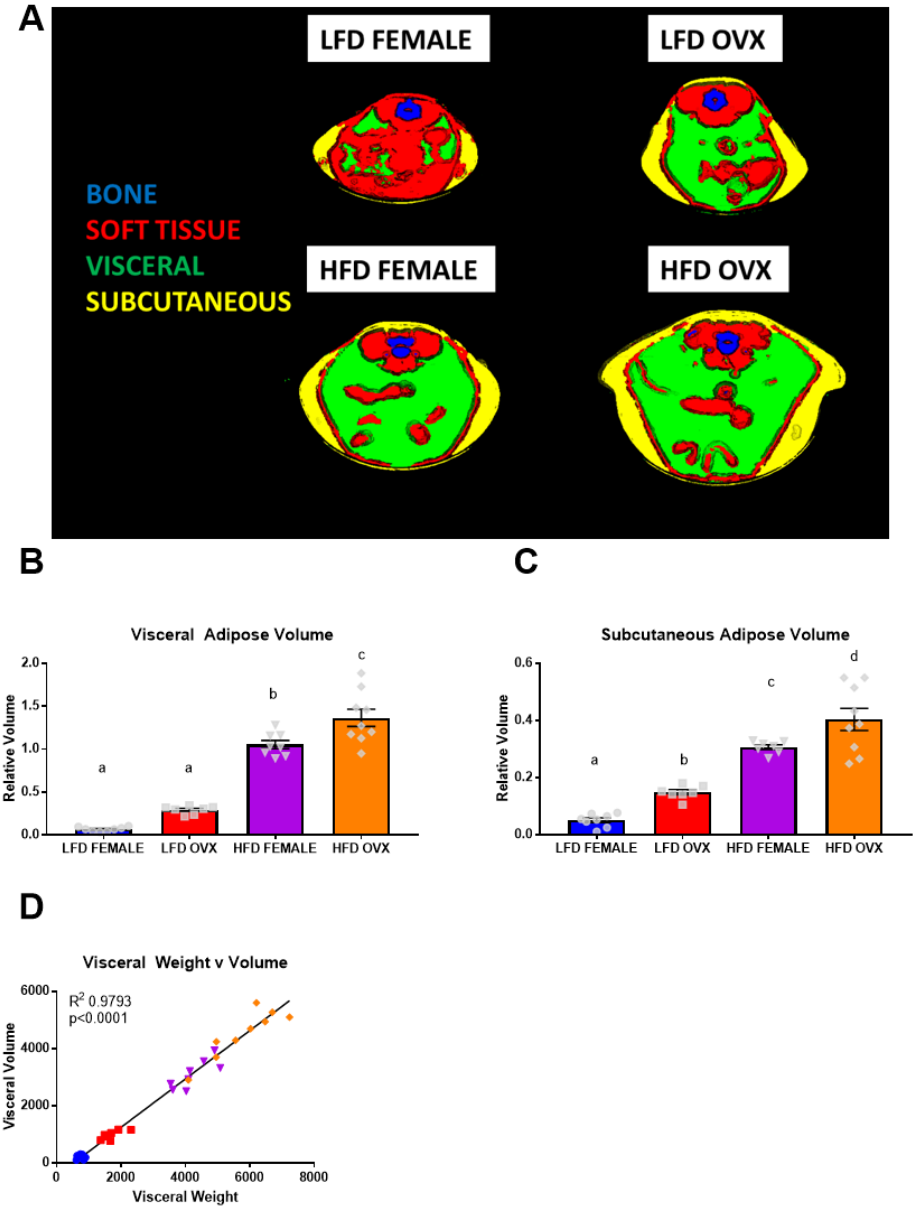

Figure 4.5 Micro CT imagining of mice at 20weeks DIO reveals differential fat distribution. A) Representative micro CT images of defined objects based on density thresholds, bone, soft tissue, visceral fat, subcutaneous fat, B-C) Quantification of adipose volume based on defined objects within micro CT scans. Volumes relative to soft tissue volumes, D) Pearson Correlation between quantified volume of visceral adipose tissue via micro CT and visceral adipose tissue weight taken at sacrifice. Values are means ± SE; n=8-9 mice per group. Bar graphs not sharing a common letter are significantly different from one another ($p<0.05$)

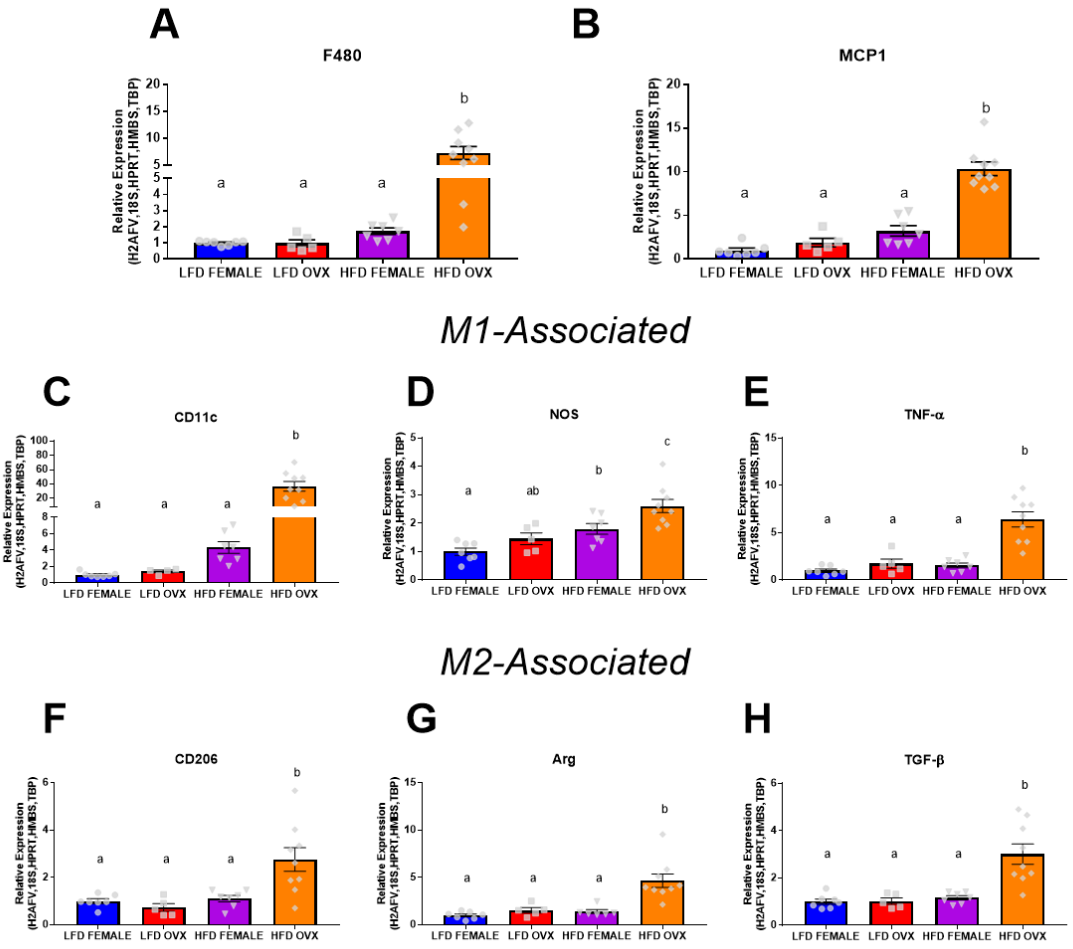

Figure 4.6 Gene expression of macrophage markers and associated inflammation in parametrial adipose tissue. Relative gene expression of F480, MCP-1, CD11c, NOS, TNF, CD206, ARG, TGF of mRNA isolated from parametrial adipose tissue. Ct values relative to average of multiple internal controls determined using qBASE pro software analysis. Values are means ± SE; n=8-9 mice per group. Bar graphs not sharing a common letter are significantly different from one another ($p<0.05$)

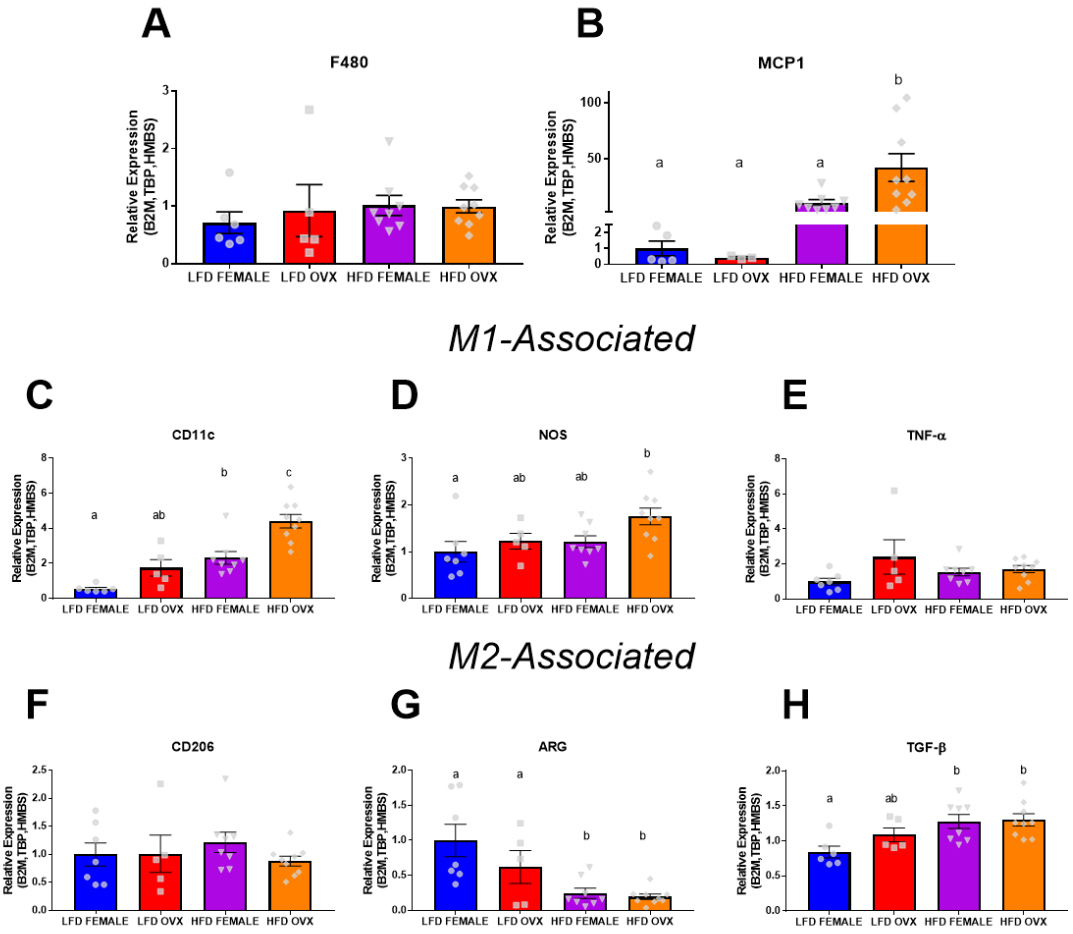

Figure 4.7 Gene expression of macrophage markers and associated inflammation in subcutaneous adipose tissue. Relative gene expression of F480, MCP-1, CD11c, NOS, TNF, CD206, ARG, TGF of mRNA isolated from the dorsal-lumbar portion of the inguinal adipose tissue. Ct values relative to average of multiple internal controls determined using qBASE pro software analysis. Values are means ± SE; n=8-9 mice per group. Bar graphs not sharing a common letter are significantly different from one another ($p<0.05$)

CHAPTER 5

SUMMARY AND CONCLUSIONS

Macrophages play a variety of roles during the development of chronic inflammation and are a driving force behind inflammation induced insulin resistance and inflammation association CRC. There is further evidence to support that sex disparities within these inflammatory diseases may be in part associated with the influence of sex hormones on macrophage behavior. In the present study, I have examined the effect of eliminating macrophage associated inflammation in either the context of CRC or obesity as a potential therapeutic treatment for these inflammatory driven diseases. I have also uncovered a possible mechanism for sex disparities within obesity enhanced CRC attributed to differential fat distribution and adipose inflammation.

As presented in my first study, reducing macrophages using clodronate encapsulated liposomes during the late stage of the chemically induced AOM/DSS CRC model, was effective at a reducing both colon polyp number and size compared to vehicle treated AOM/DSS mice. Although clodronate was not able to rescue tumor grade, through histopathological evaluation of dysplasia or disease symptom scores. This reduction in colon polyp number was attributed to reduced colon macrophages, in particular pro-tumoral TAM cytokines. Consistently, there was reduced activation of oncogenic proliferation pathways including p38, ERK and STAT3 observed in the colon of macrophage depleted mice. Lastly, macrophage depleted mice, presented with a unique gut microbiota composition rich in beneficial, butyrate producing flora. This study concluded that in the late stages of CRC, TAMs predominate, and that decreasing these macrophages and associated cytokines through CLD-liposomes resulted in a reduced diseased state with improved outcome.

Conversely, in the context of the inflammatory driven disease obesity, depletion of macrophages resulted in a compensatory reaction that exacerbated and worsened the disease state. This rationale that if macrophage depletion is in fact beneficial in late stage CRC perhaps, it would offer similar benefits in obesity associated insulin resistance, since insulin resistance is closely linked to CRC. However, depletion of adipose tissue macrophages, following diet induced obesity, was ineffective at rescuing obesity associated metabolic function. In fact, macrophage depletion exacerbated inflammation and resulted in neutrophilia observed through increased adipose tissue and circulating neutrophils. We concluded that in the absence of macrophages during the obese state, neutrophils infiltrate into the adipose tissue in response to MCP1, exacerbating tissue specific and systemic inflammation. This compensatory reaction therefore negates any potential benefit of macrophage depletion in the context of obesity. These results highlight the importance of macrophage presence within adipose tissue and encourage therapies that specifically target macrophage associated inflammation without affecting macrophage number.

Lastly, in Chapter 4, we used mouse models of obesity and CRC, to examine macrophage associated inflammation on obesity enhanced CRC with respect sex disparities. It was observed that high fat diet feeding accelerated tumor growth with HFD OVX exhibiting the largest tumors. We proposed that this increase in tumor growth in the OVX group is related to increased adiposity and macrophage associated inflammation within the adipose tissue. Although, these results did not completely agree with epidemiological data, they were able to uncover sex differences in adipose tissue distribution and macrophage associated adipose inflammation. This study provides insight

into potential mechanisms underlying protection of females against obesity associated CRC.

Taken together, these data suggest that macrophages differentially impact obesity and CRC. While clodronate mediated macrophage depletion may not provide a global treatment for all inflammatory driven diseases, it provided further insight into the diverse functions of macrophages in the context of obesity and CRC. Additionally, a potential mechanism for sex-disparities in CRC may involve macrophage associated inflammation. Due to the prevalence of obesity and CRC worldwide, any evidence that suggests potential mechanisms for these inflammatory driven diseases are profoundly important. However, further studies are needed to explore therapies targeting macrophage associated inflammation in obesity and CRC.

CHAPTER 6

FUTURE DIRECTIONS

In these studies, we focused primarily on the progression of CRC or diet-induced obesity in the absence of macrophages in order to better understand the role of macrophages in these diseases. Although it was effective at depleting macrophages, clodronate treatment resulted in significantly decreased food intake of mice. In order to confirm that the results we observed in chapters 2 and 3 were specifically related to macrophage depletion and not the clodronate treatment, it would be important to further test our hypotheses using an alternative method to deplete macrophages. Further, given the differential importance of macrophage phenotype in obesity and CRC, it would be interesting to focus our approach by targeting macrophage subsets or tissue specific macrophages rather than total macrophages. Although specific M1 or M2 targeted macrophage depletions are difficult, the utilization of LysM Cre- crossed with a loxP site targeted to NOS or ARG, the common M1 and M2 expressing macrophage gene, respectively, could prove effective at phenotype specific targeting within either the obesity or CRC models previously used.

Our results in Chapter 4 indicate that sex specific differences are observed in an obesity enhanced tumor model and that macrophage associated inflammation may play a role. It would be important to follow up this study to include the addition of both an estrogen and progesterone to further validate our hypothesis that female sex hormones offer some protection. Additionally, emerging evidence supports the influence of insulin in tumorigenesis and cancer risk. Targeting insulin, either through addition of insulin, insulin inhibitors or by transfecting the MC38 cells to become insulin receptor deficient would offer a more mechanistic approach to examine insulin specific effects on tumorigenesis.

REFERENCES

1. Parisi, L., E. Gini, D. Baci, M. Tremolati, M. Fanuli, B. Bassani, G. Farronato, A. Bruno, and L. Mortara, *Macrophage Polarization in Chronic Inflammatory Diseases: Killers or Builders?* J Immunol Res, 2018. **2018**: p. 8917804.
2. Oishi, Y. and I. Manabe, *Macrophages in age-related chronic inflammatory diseases.* NPJ Aging Mech Dis, 2016. **2**: p. 16018.
3. Donath, M.Y. and S.E. Shoelson, *Type 2 diabetes as an inflammatory disease.* Nat Rev Immunol, 2011. **11**(2): p. 98-107.
4. Cox, T.R. and J.T. Erler, *Remodeling and homeostasis of the extracellular matrix: implications for fibrotic diseases and cancer.* Dis Model Mech, 2011. **4**(2): p. 165-78.
5. Markert, E.K., A.J. Levine, and A. Vazquez, *Proliferation and tissue remodeling in cancer: the hallmarks revisited.* Cell Death Dis, 2012. **3**: p. e397.
6. Ariel, A., I. Maridonneau-Parini, P. Rovere-Querini, J.S. Levine, and H. Muhl, *Macrophages in inflammation and its resolution.* Front Immunol, 2012. **3**: p. 324.
7. Sica, A. and A. Mantovani, *Macrophage plasticity and polarization: in vivo veritas.* J Clin Invest, 2012. **122**(3): p. 787-95.
8. Martinez, F.O., L. Helming, and S. Gordon, *Alternative activation of macrophages: an immunologic functional perspective.* Annu Rev Immunol, 2009. **27**: p. 451-83.
9. Galvan-Pena, S. and L.A. O'Neill, *Metabolic reprograming in macrophage polarization.* Front Immunol, 2014. **5**: p. 420.
10. Lee, S.H., P.M. Starkey, and S. Gordon, *Quantitative analysis of total macrophage content in adult mouse tissues. Immunochemical studies with monoclonal antibody F4/80.* J Exp Med, 1985. **161**(3): p. 475-89.
11. Jung, C., J.P. Hugot, and F. Barreau, *Peyer's Patches: The Immune Sensors of the Intestine.* Int J Inflam, 2010. **2010**: p. 823710.
12. Gren, S.T. and O. Grip, *Role of Monocytes and Intestinal Macrophages in Crohn's Disease and Ulcerative Colitis.* Inflamm Bowel Dis, 2016. **22**(8): p. 1992-8.
13. Aggarwal, B.B., S. Shishodia, S.K. Sandur, M.K. Pandey, and G. Sethi, *Inflammation and cancer: how hot is the link?* Biochem Pharmacol, 2006. **72**(11): p. 1605-21.
14. Balkwill, F., K.A. Charles, and A. Mantovani, *Smoldering and polarized inflammation in the initiation and promotion of malignant disease.* Cancer Cell, 2005. **7**(3): p. 211-7.
15. Balkwill, F. and A. Mantovani, *Inflammation and cancer: back to Virchow?* Lancet, 2001. **357**(9255): p. 539-45.

16. Goede, V., L. Brogelli, M. Ziche, and H.G. Augustin, *Induction of inflammatory angiogenesis by monocyte chemoattractant protein-1.* Int J Cancer, 1999. **82**(5): p. 765-70.
17. Neumark, E., O. Sagi-Assif, B. Shalmon, A. Ben-Baruch, and I.P. Witz, *Progression of mouse mammary tumors: MCP-1-TNFalpha cross-regulatory pathway and clonal expression of promalignancy and antimalignancy factors.* Int J Cancer, 2003. **106**(6): p. 879-86.
18. Coussens, L.M. and Z. Werb, *Inflammation and cancer.* Nature, 2002. **420**(6917): p. 860-7.
19. Sica, A. and V. Bronte, *Altered macrophage differentiation and immune dysfunction in tumor development.* J Clin Invest, 2007. **117**(5): p. 1155-66.
20. Bingle, L., N.J. Brown, and C.E. Lewis, *The role of tumour-associated macrophages in tumour progression: implications for new anticancer therapies.* J Pathol, 2002. **196**(3): p. 254-65.
21. Ueno, T., M. Toi, H. Saji, M. Muta, H. Bando, K. Kuroi, M. Koike, H. Inadera, and K. Matsushima, *Significance of macrophage chemoattractant protein-1 in macrophage recruitment, angiogenesis, and survival in human breast cancer.* Clin Cancer Res, 2000. **6**(8): p. 3282-9.
22. Lin, E.Y., A.V. Nguyen, R.G. Russell, and J.W. Pollard, *Colony-stimulating factor 1 promotes progression of mammary tumors to malignancy.* J Exp Med, 2001. **193**(6): p. 727-40.
23. Gouon-Evans, V., E.Y. Lin, and J.W. Pollard, *Requirement of macrophages and eosinophils and their cytokines/chemokines for mammary gland development.* Breast Cancer Res, 2002. **4**(4): p. 155-64.
24. Lin, E.Y., V. Gouon-Evans, A.V. Nguyen, and J.W. Pollard, *The macrophage growth factor CSF-1 in mammary gland development and tumor progression.* J Mammary Gland Biol Neoplasia, 2002. **7**(2): p. 147-62.
25. Lin, E.Y. and J.W. Pollard, *Macrophages: modulators of breast cancer progression.* Novartis Found Symp, 2004. **256**: p. 158-68; discussion 168-72, 259-69.
26. Steele, R.J., O. Eremin, M. Brown, and R.A. Hawkins, *A high macrophage content in human breast cancer is not associated with favourable prognostic factors.* Br J Surg, 1984. **71**(6): p. 456-8.
27. Mantovani, A., P. Allavena, A. Sica, and F. Balkwill, *Cancer-related inflammation.* Nature, 2008. **454**(7203): p. 436-44.
28. Mantovani, A., F. Marchesi, C. Porta, A. Sica, and P. Allavena, *Inflammation and cancer: breast cancer as a prototype.* Breast, 2007. **16 Suppl 2**: p. S27-33.
29. Mantovani, A., F. Marchesi, C. Portal, P. Allavena, and A. Sica, *Linking inflammation reactions to cancer: novel targets for therapeutic strategies.* Adv Exp Med Biol, 2008. **610**: p. 112-27.
30. Mantovani, A. and M.A. Pierotti, *Cancer and inflammation: a complex relationship.* Cancer Lett, 2008. **267**(2): p. 180-1.
31. Ono, M., *Molecular links between tumor angiogenesis and inflammation: inflammatory stimuli of macrophages and cancer cells as targets for therapeutic strategy.* Cancer Sci, 2008. **99**(8): p. 1501-6.

32. Jedinak, A., S. Dudhgaonkar, and D. Sliva, *Activated macrophages induce metastatic behavior of colon cancer cells.* Immunobiology, 2010. **215**(3): p. 242-9.
33. Kang, J.C., J.S. Chen, C.H. Lee, J.J. Chang, and Y.S. Shieh, *Intratumoral macrophage counts correlate with tumor progression in colorectal cancer.* J Surg Oncol, 2010. **102**(3): p. 242-8.
34. Forssell, J., A. Oberg, M.L. Henriksson, R. Stenling, A. Jung, and R. Palmqvist, *High macrophage infiltration along the tumor front correlates with improved survival in colon cancer.* Clin Cancer Res, 2007. **13**(5): p. 1472-9.
35. Zhang, Q.W., L. Liu, C.Y. Gong, H.S. Shi, Y.H. Zeng, X.Z. Wang, Y.W. Zhao, and Y.Q. Wei, *Prognostic significance of tumor-associated macrophages in solid tumor: a meta-analysis of the literature.* PLoS One, 2012. **7**(12): p. e50946.
36. Boutens, L. and R. Stienstra, *Adipose tissue macrophages: going off track during obesity.* Diabetologia, 2016. **59**(5): p. 879-94.
37. Weisberg, S.P., D. McCann, M. Desai, M. Rosenbaum, R.L. Leibel, and A.W. Ferrante, Jr., *Obesity is associated with macrophage accumulation in adipose tissue.* J Clin Invest, 2003. **112**(12): p. 1796-808.
38. Russo, L. and C.N. Lumeng, *Properties and functions of adipose tissue macrophages in obesity.* Immunology, 2018. **155**(4): p. 407-417.
39. Hotamisligil, G.S., D.L. Murray, L.N. Choy, and B.M. Spiegelman, *Tumor necrosis factor alpha inhibits signaling from the insulin receptor.* Proc Natl Acad Sci U S A, 1994. **91**(11): p. 4854-8.
40. Chen, L., R. Chen, H. Wang, and F. Liang, *Mechanisms Linking Inflammation to Insulin Resistance.* Int J Endocrinol, 2015. **2015**: p. 508409.
41. Guilherme, A., J.V. Virbasius, V. Puri, and M.P. Czech, *Adipocyte dysfunctions linking obesity to insulin resistance and type 2 diabetes.* Nat Rev Mol Cell Biol, 2008. **9**(5): p. 367-77.
42. Dai, Z., Y.C. Xu, and L. Niu, *Obesity and colorectal cancer risk: a meta-analysis of cohort studies.* World J Gastroenterol, 2007. **13**(31): p. 4199-206.
43. Ning, Y., L. Wang, and E.L. Giovannucci, *A quantitative analysis of body mass index and colorectal cancer: findings from 56 observational studies.* Obes Rev, 2010. **11**(1): p. 19-30.
44. Larsson, S.C. and A. Wolk, *Obesity and colon and rectal cancer risk: a meta-analysis of prospective studies.* Am J Clin Nutr, 2007. **86**(3): p. 556-65.
45. Pischon, T., P.H. Lahmann, H. Boeing, C. Friedenreich, T. Norat, A. Tjonneland, J. Halkjaer, K. Overvad, F. Clavel-Chapelon, M.C. Boutron-Ruault, G. Guernec, M.M. Bergmann, J. Linseisen, N. Becker, A. Trichopoulou, D. Trichopoulos, S. Sieri, D. Palli, R. Tumino, P. Vineis, S. Panico, P.H. Peeters, H.B. Bueno-de-Mesquita, H.C. Boshuizen, B. Van Guelpen, R. Palmqvist, G. Berglund, C.A. Gonzalez, M. Dorronsoro, A. Barricarte, C. Navarro, C. Martinez, J.R. Quiros, A. Roddam, N. Allen, S. Bingham, K.T. Khaw, P. Ferrari, R. Kaaks, N. Slimani, and E. Riboli, *Body size and risk of colon and rectal cancer in the European Prospective Investigation Into Cancer and Nutrition (EPIC).* J Natl Cancer Inst, 2006. **98**(13): p. 920-31.

46. Grodstein, F., P.A. Newcomb, and M.J. Stampfer, *Postmenopausal hormone therapy and the risk of colorectal cancer: a review and meta-analysis.* The American Journal of Medicine, 1999. **106**(5): p. 574-582.
47. Nelson, H.D., L.L. Humphrey, P. Nygren, S.M. Teutsch, and J.D. Allan, *Postmenopausal Hormone Replacement Therapy.* Jama, 2002. **288**(7): p. 872.
48. Salem, M., *Estrogen, A Double-Edged Sword: Modulation of TH1- and TH2-Mediated Inflammations by Differential Regulation of TH1 / TH2 Cytokine Production.* Current Drug Target -Inflammation & Allergy, 2004. **3**(1): p. 97-104.
49. Bader, J.E., R.T. Enos, K.T. Velazquez, M.S. Carson, M. Nagarkatti, P.S. Nagarkatti, I. Chatzistamou, J.M. Davis, J.A. Carson, C. Robinson, and E.A. Murphy, *Macrophage depletion using clodronate liposomes decreases tumorigenesis and alters gut microbiota in the AOM/DSS mouse model of colon cancer.* Am J Physiol Gastrointest Liver Physiol, 2017: p. ajpgi 00229 2017.
50. Bader, J.E., R.T. Enos, K.T. Velazquez, M.S. Carson, A.T. Sougiannis, O.P. McGuinness, C.M. Robinson, and E.A. Murphy, *Repeated clodronate-liposome treatment results in neutrophilia and is not effective in limiting obesity-linked metabolic impairments.* Am J Physiol Endocrinol Metab, 2019. **316**(3): p. E358-E372.
51. Weisser, S.B., N. van Rooijen, and L.M. Sly, *Depletion and reconstitution of macrophages in mice.* J Vis Exp, 2012(66): p. 4105.
52. Watanabe, N., K. Ikuta, K. Okazaki, H. Nakase, Y. Tabata, M. Matsuura, H. Tamaki, C. Kawanami, T. Honjo, and T. Chiba, *Elimination of local macrophages in intestine prevents chronic colitis in interleukin-10-deficient mice.* Dig Dis Sci, 2003. **48**(2): p. 408-14.
53. Zhao, H., X. Zhang, X. Chen, Y. Li, Z. Ke, T. Tang, H. Chai, A.M. Guo, H. Chen, and J. Yang, *Isoliquiritigenin, a flavonoid from licorice, blocks M2 macrophage polarization in colitis-associated tumorigenesis through downregulating PGE2 and IL-6.* Toxicol Appl Pharmacol, 2014. **279**(3): p. 311-21.
54. Society, A.C., *Colorectal Cancer Facts & Figures 2017-2019.* 2017.
55. Basile, D., S.K. Garattini, M. Bonotto, E. Ongaro, M. Casagrande, M. Cattaneo, V. Fanotto, E. De Carlo, F. Loupakis, F. Urbano, F.V. Negri, N. Pella, M. Russano, O. Brunetti, M. Scartozzi, D. Santini, N. Silvestris, A. Casadei Gardini, M. Puzzoni, L. Calvetti, N. Cardarelli, and G. Aprile, *Immunotherapy for colorectal cancer: where are we heading?* Expert Opin Biol Ther, 2017. **17**(6): p. 709-721.
56. McClellan, J.L., J.M. Davis, J.L. Steiner, R.T. Enos, S.H. Jung, J.A. Carson, M.M. Pena, K.A. Carnevale, F.G. Berger, and E.A. Murphy, *Linking tumor-associated macrophages, inflammation, and intestinal tumorigenesis: role of MCP-1.* Am J Physiol Gastrointest Liver Physiol, 2012. **303**(10): p. G1087-95.
57. Li, J., Y. Liu, B. Wang, Y. Xu, A. Ma, F. Zhang, C. Ge, Z. Yang, J. Li, and Y. Liu, *Myeloid TGF-beta signaling contributes to colitis-associated tumorigenesis in mice.* Carcinogenesis, 2013. **34**(9): p. 2099-108.
58. Wroblewski, L.E., R.M. Peek, Jr., and L.A. Coburn, *The Role of the Microbiome in Gastrointestinal Cancer.* Gastroenterol Clin North Am, 2016. **45**(3): p. 543-56.
59. Vannucci, L., R. Stepankova, H. Kozakova, A. Fiserova, P. Rossmann, and H. Tlaskalova-Hogenova, *Colorectal carcinogenesis in germ-free and conventionally*

reared rats: different intestinal environments affect the systemic immunity. Int J Oncol, 2008. **32**(3): p. 609-17.
60. Grivennikov, S.I., K. Wang, D. Mucida, C.A. Stewart, B. Schnabl, D. Jauch, K. Taniguchi, G.Y. Yu, C.H. Osterreicher, K.E. Hung, C. Datz, Y. Feng, E.R. Fearon, M. Oukka, L. Tessarollo, V. Coppola, F. Yarovinsky, H. Cheroutre, L. Eckmann, G. Trinchieri, and M. Karin, *Adenoma-linked barrier defects and microbial products drive IL-23/IL-17-mediated tumour growth.* Nature. **491**(7423): p. 254-8.
61. Arthur, J.C. and C. Jobin, *The complex interplay between inflammation, the microbiota and colorectal cancer.* Gut Microbes. **4**(3): p. 253-8.
62. Hooper, L.V., D.R. Littman, and A.J. Macpherson, *Interactions between the microbiota and the immune system.* Science. **336**(6086): p. 1268-73.
63. Arthur, J.C., E. Perez-Chanona, M. Muhlbauer, S. Tomkovich, J.M. Uronis, T.J. Fan, B.J. Campbell, T. Abujamel, B. Dogan, A.B. Rogers, J.M. Rhodes, A. Stintzi, K.W. Simpson, J.J. Hansen, T.O. Keku, A.A. Fodor, and C. Jobin, *Intestinal inflammation targets cancer-inducing activity of the microbiota.* Science. **338**(6103): p. 120-3.
64. Ostman, S., C. Rask, A.E. Wold, S. Hultkrantz, and E. Telemo, *Impaired regulatory T cell function in germ-free mice.* Eur J Immunol, 2006. **36**(9): p. 2336-46.
65. Ivanov, II, K. Atarashi, N. Manel, E.L. Brodie, T. Shima, U. Karaoz, D. Wei, K.C. Goldfarb, C.A. Santee, S.V. Lynch, T. Tanoue, A. Imaoka, K. Itoh, K. Takeda, Y. Umesaki, K. Honda, and D.R. Littman, *Induction of intestinal Th17 cells by segmented filamentous bacteria.* Cell, 2009. **139**(3): p. 485-98.
66. Chen, J. and X.F. Huang, *The signal pathways in azoxymethane-induced colon cancer and preventive implications.* Cancer Biol Ther, 2009. **8**(14): p. 1313-7.
67. Enos, R.T., J.M. Davis, K.T. Velazquez, J.L. McClellan, S.D. Day, K.A. Carnevale, and E.A. Murphy, *Influence of dietary saturated fat content on adiposity, macrophage behavior, inflammation, and metabolism: composition matters.* J Lipid Res, 2013. **54**(1): p. 152-63.
68. Kim, J.J., M.S. Shajib, M.M. Manocha, and W.I. Khan, *Investigating intestinal inflammation in DSS-induced model of IBD.* J Vis Exp, 2012(60).
69. Viennois, E., F. Chen, H. Laroui, M.T. Baker, and D. Merlin, *Dextran sodium sulfate inhibits the activities of both polymerase and reverse transcriptase: lithium chloride purification, a rapid and efficient technique to purify RNA.* BMC Res Notes, 2013. **6**: p. 360.
70. Carson, J.A., W.J. Lee, J. McClung, and G.A. Hand, *Steroid receptor concentration in aged rat hindlimb muscle: effect of anabolic steroid administration.* J Appl Physiol (1985), 2002. **93**(1): p. 242-50.
71. Aldridge, G.M., D.M. Podrebarac, W.T. Greenough, and I.J. Weiler, *The use of total protein stains as loading controls: an alternative to high-abundance single-protein controls in semi-quantitative immunoblotting.* J Neurosci Methods, 2008. **172**(2): p. 250-4.
72. Klindworth, A., E. Pruesse, T. Schweer, J. Peplies, C. Quast, M. Horn, and F.O. Glockner, *Evaluation of general 16S ribosomal RNA gene PCR primers for*

classical and next-generation sequencing-based diversity studies. Nucleic Acids Res, 2013. **41**(1): p. e1.
73. WANG, W., X. LI, D. ZHENG, D. ZHANG, X. PENG, X. ZHANG, F. AI, X. WANG, J. MA, W. XIONG, G. LI, Y. ZHOU, and S. SHEN, *Dynamic changes and functions of macrophages and M1/M2 subpopulations during ulcerative colitits-associated carcinogenesis in an AOM/DSS mouse model.* . Molecular Medicine Reports, 2015. **11**: p. 2397-2406.
74. Mantovani, A. and A. Sica, *Macrophages, innate immunity and cancer: balance, tolerance, and diversity.* Curr Opin Immunol, 2010. **22**(2): p. 231-7.
75. Kaler, P., L. Augenlicht, and L. Klampfer, *Macrophage-derived IL-1beta stimulates Wnt signaling and growth of colon cancer cells: a crosstalk interrupted by vitamin D3.* Oncogene, 2009. **28**(44): p. 3892-902.
76. Zhao, H., X. Zhang, X. Chen, Y. Li, Z. Ke, T. Tang, H. Chai, A. Guo, H. Chen, and J. Yang, *Isoliquiritigenin, a flavonoid from licorice, blocks M2 macrophage polarization in colitis-associated tumorigenesis through downregulating PGE2 and IL-6.* Toxicology and Applied Pharmacology, 2014. **279**(3): p. 311-321.
77. Bu, L., M. Gao, S. Qu, and D. Liu, *Intraperitoneal injection of clodronate liposomes eliminates visceral adipose macrophages and blocks high-fat diet-induced weight gain and development of insulin resistance.* AAPS J, 2013. **15**(4): p. 1001-11.
78. Lee, B., L. Qiao, B. Kinney, G.S. Feng, and J. Shao, *Macrophage depletion disrupts immune balance and energy homeostasis.* PLoS One, 2014. **9**(6): p. e99575.
79. Hursting, S.D., S.M. Smith, L.M. Lashinger, A.E. Harvey, and S.N. Perkins, *Calories and carcinogenesis: lessons learned from 30 years of calorie restriction research.* Carcinogenesis, 2010. **31**(1): p. 83-9.
80. Gordon, S.R., R.L. Maute, B.W. Dulken, G. Hutter, B.M. George, M.N. McCracken, R. Gupta, J.M. Tsai, R. Sinha, D. Corey, A.M. Ring, A.J. Connolly, and I.L. Weissman, *PD-1 expression by tumour-associated macrophages inhibits phagocytosis and tumour immunity.* Nature, 2017. **545**(7655): p. 495-499.
81. Terabe, M., J.M. Park, and J.A. Berzofsky, *Role of IL-13 in regulation of anti-tumor immunity and tumor growth.* Cancer Immunol Immunother, 2004. **53**(2): p. 79-85.
82. Zhou, R., S. Qian, X. Gu, Z. Chen, and J. Xiang, *Interleukin-13 and its receptors in colorectal cancer (Review).* Biomed Rep, 2013. **1**(5): p. 687-690.
83. Legitimo, A., R. Consolini, A. Failli, G. Orsini, and R. Spisni, *Dendritic cell defects in the colorectal cancer.* Hum Vaccin Immunother, 2014. **10**(11): p. 3224-35.
84. Wang, Y., O.O. Braun, S. Zhang, E. Norstrom, and H. Thorlacius, *Monocytes regulate systemic coagulation and inflammation in abdominal sepsis.* Am J Physiol Heart Circ Physiol, 2015. **308**(5): p. H540-7.
85. Yu, H., D. Pardoll, and R. Jove, *STATs in cancer inflammation and immunity: a leading role for STAT3.* Nat Rev Cancer, 2009. **9**(11): p. 798-809.
86. Yu, H., H. Lee, A. Herrmann, R. Buettner, and R. Jove, *Revisiting STAT3 signalling in cancer: new and unexpected biological functions.* Nat Rev Cancer, 2014. **14**(11): p. 736-46.

87. Grossi, V., A. Peserico, T. Tezil, and C. Simone, *p38 alpha MAPK pathway: A key factor in colorectal cancer therapy and chemoresistance.* World Journal of Gastroenterology, 2014. **20**(29): p. 9744-9758.
88. Chiacchiera, F., V. Grossi, M. Cappellari, A. Peserico, M. Simonatto, A. Germani, S. Russo, M.P. Moyer, N. Resta, S. Murzilli, and C. Simone, *Blocking p38/ERK crosstalk affects colorectal cancer growth by inducing apoptosis in vitro and in preclinical mouse models.* Cancer Lett, 2012. **324**(1): p. 98-108.
89. Hassanzadeh, P., *Colorectal cancer and NF-kB signaling pathway.* Gastroenteralogy and Hepatology From Bed to Bench, 2011. **4**(3).
90. Tjalsma, H., A. Boleij, J.R. Marchesi, and B.E. Dutilh, *A bacterial driver-passenger model for colorectal cancer: beyond the usual suspects.* Nat Rev Microbiol, 2012. **10**(8): p. 575-82.
91. Yang, Y.H., X.M. Wang, T. Huycke, D.R. Moore, S.A. Lightfoot, and M.M. Huycke, *Colon Macrophages Polarized by Commensal Bacteria Cause Colitis and Cancer through the Bystander Effect.* Translational Oncology, 2013. **6**(5): p. 596-+.
92. Vipperia, K. and S. O'Keefe, *Diet, microbiota, and dysbiosis: a 'recipe' for colorectal cancer.* Food Funct., 2016. **7**: p. 1731-1740.
93. Sun, J. and I. Kato, *Gut microbiota, inflammation and colorectal cancer.* Genes Dis, 2016. **3**(2): p. 130-143.
94. Lu, Y., J. Chen, J. Zheng, G. Hu, J. Wang, C. Huang, L. Lou, X. Wang, and Y. Zeng, *Mucosal adherent bacterial dysbiosis in patients with colorectal adenomas.* Sci Rep, 2016. **6**: p. 26337.
95. Gagniere, J., J. Raisch, J. Veziant, N. Barnich, R. Bonnet, E. Buc, M.A. Bringer, D. Pezet, and M. Bonnet, *Gut microbiota imbalance and colorectal cancer.* World J Gastroenterol, 2016. **22**(2): p. 501-18.
96. Nguyen, D.M. and H.B. El-Serag, *The epidemiology of obesity.* Gastroenterol Clin North Am, 2010. **39**(1): p. 1-7.
97. Rastelli, M., C. Knauf, and P.D. Cani, *Gut Microbes and Health: A Focus on the Mechanisms Linking Microbes, Obesity, and Related Disorders.* Obesity (Silver Spring), 2018. **26**(5): p. 792-800.
98. Bessac, A., P.D. Cani, E. Meunier, G. Dietrich, and C. Knauf, *Inflammation and Gut-Brain Axis During Type 2 Diabetes: Focus on the Crosstalk Between Intestinal Immune Cells and Enteric Nervous System.* Front Neurosci, 2018. **12**: p. 725.
99. Bu, L., M. Gao, S. Qu, and D. Liu, *Intraperitoneal Injection of Clodronate Liposomes Eliminates Visceral Adipose Macrophages and Blocks High-fat Diet-induced Weight Gain and Development of Insulin Resistance.* The AAPS Journal, 2013. **15**(4): p. 1001-1011.
100. Feng, B., P. Jiao, Y. Nie, T. Kim, D. Jun, N. van Rooijen, Z. Yang, and H. Xu, *Clodronate Liposomes Improve Metabolic Profile and Reduce Visceral Adipose Macrophage Content in Diet-Induced Obese Mice.* PLoS ONE, 2011. **6**(9).
101. Lee, B., L. Qiao, B. Kinney, G.-S.S. Feng, and J. Shao, *Macrophage depletion disrupts immune balance and energy homeostasis.* PloS one, 2014. **9**(6).
102. Gordy, C., H. Pua, G.D. Sempowski, and Y.W. He, *Regulation of steady-state neutrophil homeostasis by macrophages.* Blood, 2011. **117**(2): p. 618-29.

103. Wu, C.L., J. McNeill, K. Goon, D. Little, K. Kimmerling, J. Huebner, V. Kraus, and F. Guilak, *Conditional Macrophage Depletion Increases Inflammation and Does Not Inhibit the Development of Osteoarthritis in Obese Macrophage Fas-Induced Apoptosis-Transgenic Mice.* Arthritis Rheumatol, 2017. **69**(9): p. 1772-1783.
104. Kumar, D., S.K. Pandya, S. Varshney, K. Shankar, S. Rajan, A. Srivastava, A. Gupta, S. Gupta, A.L. Vishwakarma, A. Misra, and A.N. Gaikwad, *Temporal immmunometabolic profiling of adipose tissue in HFD-induced obesity: manifestations of mast cells in fibrosis and senescence.* Int J Obes (Lond), 2018.
105. Hempenstall, S., L. Picchio, S.E. Mitchell, J.R. Speakman, and C. Selman, *The impact of acute caloric restriction on the metabolic phenotype in male C57BL/6 and DBA/2 mice.* Mech Ageing Dev, 2010. **131**(2): p. 111-8.
106. Cameron, K.M., S. Miwa, C. Walker, and T. von Zglinicki, *Male mice retain a metabolic memory of improved glucose tolerance induced during adult onset, short-term dietary restriction.* Longev Healthspan, 2012. **1**: p. 3.
107. Matyi, S., J. Jackson, K. Garrett, S.S. Deepa, and A. Unnikrishnan, *The effect of different levels of dietary restriction on glucose homeostasis and metabolic memory.* Geroscience, 2018. **40**(2): p. 139-149.
108. Park, S., N.Y. Park, G. Valacchi, and Y. Lim, *Calorie restriction with a high-fat diet effectively attenuated inflammatory response and oxidative stress-related markers in obese tissues of the high diet fed rats.* Mediators Inflamm, 2012. **2012**: p. 984643.
109. Enos, R.T., K.T. Velazquez, M.S. Carson, J.L. McClellan, P. Nagarkatti, M. Nagarkatti, J.M. Davis, and E.A. Murphy, *A Low Dose of Dietary Quercetin Fails to Protect against the Development of an Obese Phenotype in Mice.* PLoS One, 2016. **11**(12): p. e0167979.
110. Enos, R.T., K.T. Velazquez, J.L. McClellan, T.L. Cranford, M.D. Walla, and E.A. Murphy, *Reducing the dietary omega-6:omega-3 utilizing alpha-linolenic acid; not a sufficient therapy for attenuating high-fat-diet-induced obesity development nor related detrimental metabolic and adipose tissue inflammatory outcomes.* PLoS One, 2014. **9**(4): p. e94897.
111. Enos, R.T., K.T. Velazquez, J.L. McClellan, T.L. Cranford, M.D. Walla, and E.A. Murphy, *Lowering the dietary omega-6: omega-3 does not hinder nonalcoholic fatty-liver disease development in a murine model.* Nutr Res, 2015. **35**(5): p. 449-59.
112. Enos, R.T., K.T. Velazquez, and E.A. Murphy, *Insight into the impact of dietary saturated fat on tissue-specific cellular processes underlying obesity-related diseases.* J Nutr Biochem, 2014. **25**(6): p. 600-12.
113. Day, S.D., R.T. Enos, J.L. McClellan, J.L. Steiner, K.T. Velazquez, and E.A. Murphy, *Linking inflammation to tumorigenesis in a mouse model of high-fat-diet-enhanced colon cancer.* Cytokine, 2013. **64**(1): p. 454-62.
114. Lanthier, N., O. Molendi-Coste, P.D. Cani, N. van Rooijen, Y. Horsmans, and I.A. Leclercq, *Kupffer cell depletion prevents but has no therapeutic effect on metabolic and inflammatory changes induced by a high-fat diet.* FASEB J, 2011. **25**(12): p. 4301-11.

115. Folch, J., M. Lees, and G.H. Sloane Stanley, *A simple method for the isolation and purification of total lipides from animal tissues.* J Biol Chem, 1957. **226**(1): p. 497-509.
116. Velazquez, K.T., R.T. Enos, M.S. Carson, T.L. Cranford, J.E. Bader, A.T. Sougiannis, C. Pritchett, D. Fan, J.A. Carson, and E.A. Murphy, *miR155 deficiency aggravates high-fat diet-induced adipose tissue fibrosis in male mice.* Physiol Rep, 2017. **5**(18).
117. Woessner, J.F., Jr., *The determination of hydroxyproline in tissue and protein samples containing small proportions of this imino acid.* Arch Biochem Biophys, 1961. **93**: p. 440-7.
118. Cissell, D.D., J.M. Link, J.C. Hu, and K.A. Athanasiou, *A Modified Hydroxyproline Assay Based on Hydrochloric Acid in Ehrlich's Solution Accurately Measures Tissue Collagen Content.* Tissue Eng Part C Methods, 2017. **23**(4): p. 243-250.
119. Vandesompele, J., K. De Preter, F. Pattyn, B. Poppe, N. Van Roy, A. De Paepe, and F. Speleman, *Accurate normalization of real-time quantitative RT-PCR data by geometric averaging of multiple internal control genes.* Genome Biol, 2002. **3**(7): p. RESEARCH0034.
120. Sierra Rojas, J.X., M. Garcia-San Frutos, D. Horrillo, N. Lauzurica, E. Oliveros, J.M. Carrascosa, T. Fernandez-Agullo, and M. Ros, *Differential Development of Inflammation and Insulin Resistance in Different Adipose Tissue Depots Along Aging in Wistar Rats: Effects of Caloric Restriction.* J Gerontol A Biol Sci Med Sci, 2016. **71**(3): p. 310-22.
121. Soares, M.P. and I. Hamza, *Macrophages and Iron Metabolism.* Immunity, 2016. **44**(3): p. 492-504.
122. Ganz, T., *Macrophages and Iron Metabolism.* Microbiol Spectr, 2016. **4**(5).
123. Nairz, M., I. Theurl, F.K. Swirski, and G. Weiss, *"Pumping iron"-how macrophages handle iron at the systemic, microenvironmental, and cellular levels.* Pflugers Arch, 2017. **469**(3-4): p. 397-418.
124. Lee, Y.S., P. Li, J.Y. Huh, I.J. Hwang, M. Lu, J.I. Kim, M. Ham, S. Talukdar, A. Chen, W.J. Lu, G.K. Bandyopadhyay, R. Schwendener, J. Olefsky, and J.B. Kim, *Inflammation is necessary for long-term but not short-term high-fat diet-induced insulin resistance.* Diabetes, 2011. **60**(10): p. 2474-2483.
125. Kosteli, A., E. Sugaru, G. Haemmerle, J.F. Martin, J. Lei, R. Zechner, and A.W. Ferrante, Jr., *Weight loss and lipolysis promote a dynamic immune response in murine adipose tissue.* J Clin Invest, 2010. **120**(10): p. 3466-79.
126. Van Rooijen, N. and A. Sanders, *Liposome mediated depletion of macrophages: mechanism of action, preparation of liposomes and applications.* J Immunol Methods, 1994. **174**(1-2): p. 83-93.
127. Choe, S.S., K.C. Shin, S. Ka, Y.K. Lee, J.S. Chun, and J.B. Kim, *Macrophage HIF-2alpha ameliorates adipose tissue inflammation and insulin resistance in obesity.* Diabetes, 2014. **63**(10): p. 3359-71.
128. Lanthier, N., Y. Horsmans, and I.A. Leclercq, *Clodronate liposomes: all sites of injection are not equal.* Hepatology, 2010. **51**(2): p. 721-2; author reply 722.

129. Lanthier, N., O. Molendi-Coste, Y. Horsmans, N. van Rooijen, P.D. Cani, and I.A. Leclercq, *Kupffer cell activation is a causal factor for hepatic insulin resistance.* Am J Physiol Gastrointest Liver Physiol, 2010. **298**(1): p. G107-16.
130. Turner, N., G.M. Kowalski, S.J. Leslie, S. Risis, C. Yang, R.S. Lee-Young, J.R. Babb, P.J. Meikle, G.I. Lancaster, D.C. Henstridge, P.J. White, E.W. Kraegen, A. Marette, G.J. Cooney, M.A. Febbraio, and C.R. Bruce, *Distinct patterns of tissue-specific lipid accumulation during the induction of insulin resistance in mice by high-fat feeding.* Diabetologia, 2013. **56**(7): p. 1638-48.
131. Patsouris, D., P.P. Li, D. Thapar, J. Chapman, J.M. Olefsky, and J.G. Neels, *Ablation of CD11c-positive cells normalizes insulin sensitivity in obese insulin resistant animals.* Cell Metab, 2008. **8**(4): p. 301-9.
132. Hubler, M.J., K.R. Peterson, and A.H. Hasty, *Iron homeostasis: a new job for macrophages in adipose tissue?* Trends Endocrinol Metab, 2015. **26**(2): p. 101-9.
133. Aigner, E., A. Feldman, and C. Datz, *Obesity as an emerging risk factor for iron deficiency.* Nutrients, 2014. **6**(9): p. 3587-600.
134. Pollard, J.W., *Trophic macrophages in development and disease.* Nat Rev Immunol, 2009. **9**(4): p. 259-70.
135. McKercher, S.R., B.E. Torbett, K.L. Anderson, G.W. Henkel, D.J. Vestal, H. Baribault, M. Klemsz, A.J. Feeney, G.E. Wu, C.J. Paige, and R.A. Maki, *Targeted disruption of the PU.1 gene results in multiple hematopoietic abnormalities.* EMBO J, 1996. **15**(20): p. 5647-58.
136. Gribovskaja-Rupp, I., L. Kosinski, and K.A. Ludwig, *Obesity and colorectal cancer.* Clin Colon Rectal Surg, 2011. **24**(4): p. 229-43.
137. Rondini, E.A., A.E. Harvey, J.P. Steibel, S.D. Hursting, and J.I. Fenton, *Energy balance modulates colon tumor growth: Interactive roles of insulin and estrogen.* Mol Carcinog, 2011. **50**(5): p. 370-82.
138. Barzi, A., A.M. Lenz, M.J. Labonte, and H.J. Lenz, *Molecular pathways: Estrogen pathway in colorectal cancer.* Clin Cancer Res, 2013. **19**(21): p. 5842-8.
139. Rennert, G., H.S. Rennert, M. Pinchev, O. Lavie, and S.B. Gruber, *Use of hormone replacement therapy and the risk of colorectal cancer.* J Clin Oncol, 2009. **27**(27): p. 4542-7.
140. Donohoe, C.L., S.L. Doyle, and J.V. Reynolds, *Visceral adiposity, insulin resistance and cancer risk.* Diabetol Metab Syndr, 2011. **3**: p. 12.
141. Frezza, E.E., M.S. Wachtel, and M. Chiriva-Internati, *Influence of obesity on the risk of developing colon cancer.* Gut, 2006. **55**(2): p. 285-91.
142. Lysaght, J., E.P. van der Stok, E.H. Allott, R. Casey, C.L. Donohoe, J.M. Howard, S.A. McGarrigle, N. Ravi, J.V. Reynolds, and G.P. Pidgeon, *Pro-inflammatory and tumour proliferative properties of excess visceral adipose tissue.* Cancer Lett, 2011. **312**(1): p. 62-72.
143. Yan, H., W. Yang, F. Zhou, X. Li, Q. Pan, Z. Shen, G. Han, A. Newell-Fugate, Y. Tian, R. Majeti, W. Liu, Y. Xu, C. Wu, K. Allred, C. Allred, Y. Sun, and S. Guo, *Estrogen Improves Insulin Sensitivity and Suppresses Gluconeogenesis via the Transcription Factor Foxo1.* Diabetes, 2019. **68**(2): p. 291-304.
144. Enos, R.T., K.T. Velazquez, J.L. McClellan, T.L. Cranford, M. Nagarkatti, P.S. Nagarkatti, J.M. Davis, and E.A. Murphy, *High-fat diets rich in saturated fat*

protect against azoxymethane/dextran sulfate sodium-induced colon cancer. Am J Physiol Gastrointest Liver Physiol, 2016. **310**(11): p. G906-19.
145. Cassetta, L., R. Noy, A. Swierczak, G. Sugano, H. Smith, L. Wiechmann, and J.W. Pollard, *Isolation of Mouse and Human Tumor-Associated Macrophages.* Adv Exp Med Biol, 2016. **899**: p. 211-29.
146. Luu, Y.K., S. Lublinsky, E. Ozcivici, E. Capilla, J.E. Pessin, C.T. Rubin, and S. Judex, *In vivo quantification of subcutaneous and visceral adiposity by micro-computed tomography in a small animal model.* Med Eng Phys, 2009. **31**(1): p. 34-41.
147. Nimri, L., J. Saadi, I. Peri, E. Yehuda-Shnaidman, and B. Schwartz, *Mechanisms linking obesity to altered metabolism in mice colon carcinogenesis.* Oncotarget, 2015. **6**(35): p. 38195-209.
148. Guan, F., T. Tabrizian, A. Novaj, M. Nakanishi, D.W. Rosenberg, and D.M. Huffman, *Dietary Walnuts Protect Against Obesity-Driven Intestinal Stem Cell Decline and Tumorigenesis.* Front Nutr, 2018. **5**: p. 37.
149. Park, H., M. Kim, G.T. Kwon, D.Y. Lim, R. Yu, M.K. Sung, K.W. Lee, J.W. Daily, 3rd, and J.H. Park, *A high-fat diet increases angiogenesis, solid tumor growth, and lung metastasis of CT26 colon cancer cells in obesity-resistant BALB/c mice.* Mol Carcinog, 2012. **51**(11): p. 869-80.
150. Yakar, S., N.P. Nunez, P. Pennisi, P. Brodt, H. Sun, L. Fallavollita, H. Zhao, L. Scavo, R. Novosyadlyy, N. Kurshan, B. Stannard, J. East-Palmer, N.C. Smith, S.N. Perkins, R. Fuchs-Young, J.C. Barrett, S.D. Hursting, and D. LeRoith, *Increased tumor growth in mice with diet-induced obesity: impact of ovarian hormones.* Endocrinology, 2006. **147**(12): p. 5826-34.
151. Aggarwal, B.B., R.V. Vijayalekshmi, and B. Sung, *Targeting inflammatory pathways for prevention and therapy of cancer: short-term friend, long-term foe.* Clin Cancer Res, 2009. **15**(2): p. 425-30.
152. Prasad, S., J. Ravindran, and B.B. Aggarwal, *NF-kappaB and cancer: how intimate is this relationship.* Mol Cell Biochem. **336**(1-2): p. 25-37.
153. Aleksandrova, K., D. Drogan, H. Boeing, M. Jenab, H. Bas Bueno-de-Mesquita, E. Jansen, F.J. van Duijnhoven, S. Rinaldi, V. Fedirko, I. Romieu, R. Kaaks, E. Riboli, M.J. Gunter, D. Romaguera, S. Westhpal, K. Overvad, A. Tjonneland, J. Halkjaer, M.C. Boutron-Ruault, F. Clavel-Chapelon, A. Lukanova, A. Trichopoulou, D. Trichopoulos, P. Vidalis, S. Panico, C. Agnoli, D. Palli, R. Tumino, P. Vineis, G. Buckland, J.J. Sanchez-Cruz, M. Dorronsoro, M.J. Diaz, A. Barricarte, J. Ramon Quiros, P.H. Peeters, A.M. May, G. Hallmans, R. Palmqvist, F.L. Crowe, K.T. Khaw, N. Wareham, and T. Pischon, *Adiposity, mediating biomarkers and risk of colon cancer in the European prospective investigation into cancer and nutrition study.* Int J Cancer, 2014. **134**(3): p. 612-21.
154. Zhang, Y., A. Daquinag, D.O. Traktuev, F. Amaya-Manzanares, P.J. Simmons, K.L. March, R. Pasqualini, W. Arap, and M.G. Kolonin, *White adipose tissue cells are recruited by experimental tumors and promote cancer progression in mouse models.* Cancer Res, 2009. **69**(12): p. 5259-66.
155. Motylewska, E., O. Stasikowska, and G. Melen-Mucha, *The inhibitory effect of diarylpropionitrile, a selective agonist of estrogen receptor beta, on the growth of MC38 colon cancer line.* Cancer Lett, 2009. **276**(1): p. 68-73.

156. Motylewska, E. and G. Melen-Mucha, *Estrone and progesterone inhibit the growth of murine MC38 colon cancer line.* J Steroid Biochem Mol Biol, 2009. **113**(1-2): p. 75-9.
157. Guo, J.Y., X. Li, J.D. Browning, Jr., G.E. Rottinghaus, D.B. Lubahn, A. Constantinou, M. Bennink, and R.S. MacDonald, *Dietary soy isoflavones and estrone protect ovariectomized ERalphaKO and wild-type mice from carcinogen-induced colon cancer.* J Nutr, 2004. **134**(1): p. 179-82.
158. MJ, W., C. AM, M. NN, B. HL, R. H, B. RT, and M. Bertagnolli, *Reciprocal Expression of ERα and ERβ Is Associated with Estrogen-mediated Modulation of Intestinal Tumorigenesis.* Cancer Res, 2001. **61**(6): p. 2547–51.
159. Bowker, S.L., S.R. Majumdar, P. Veugelers, and J.A. Johnson, *Increased cancer-related mortality for patients with type 2 diabetes who use sulfonylureas or insulin.* Diabetes Care, 2006. **29**(2): p. 254-8.
160. Kasznicki, J., A. Sliwinska, and J. Drzewoski, *Metformin in cancer prevention and therapy.* Ann Transl Med, 2014. **2**(6): p. 57.
161. Hvid, H., M.J. Blouin, E. Birman, J. Damgaard, F. Poulsen, J.J. Fels, C. Fledelius, B.F. Hansen, and M. Pollak, *Treatment with insulin analog X10 and IGF-1 increases growth of colon cancer allografts.* PLoS One, 2013. **8**(11): p. e79710.
162. Hadad, S., T. Iwamoto, L. Jordan, C. Purdie, S. Bray, L. Baker, G. Jellema, S. Deharo, D.G. Hardie, L. Pusztai, S. Moulder-Thompson, J.A. Dewar, and A.M. Thompson, *Evidence for biological effects of metformin in operable breast cancer: a pre-operative, window-of-opportunity, randomized trial.* Breast Cancer Res Treat, 2011. **128**(3): p. 783-94.

APPENDIX A

PERMISSION TO REPRINT

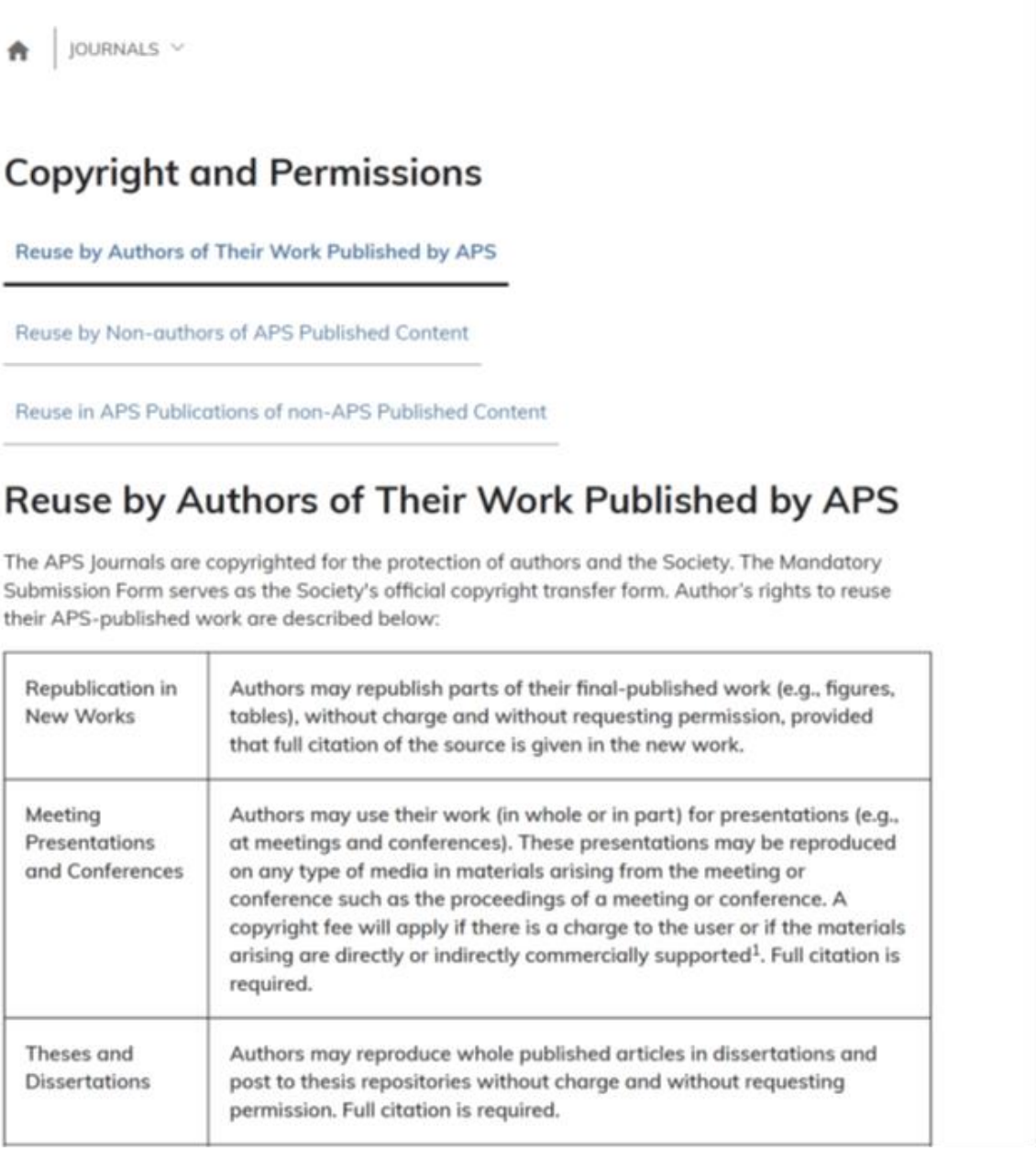

JOURNALS

Copyright and Permissions

Reuse by Authors of Their Work Published by APS

Reuse by Non-authors of APS Published Content

Reuse in APS Publications of non-APS Published Content

Reuse by Authors of Their Work Published by APS

The APS Journals are copyrighted for the protection of authors and the Society. The Mandatory Submission Form serves as the Society's official copyright transfer form. Author's rights to reuse their APS-published work are described below:

Republication in New Works	Authors may republish parts of their final-published work (e.g., figures, tables), without charge and without requesting permission, provided that full citation of the source is given in the new work.
Meeting Presentations and Conferences	Authors may use their work (in whole or in part) for presentations (e.g., at meetings and conferences). These presentations may be reproduced on any type of media in materials arising from the meeting or conference such as the proceedings of a meeting or conference. A copyright fee will apply if there is a charge to the user or if the materials arising are directly or indirectly commercially supported[1]. Full citation is required.
Theses and Dissertations	Authors may reproduce whole published articles in dissertations and post to thesis repositories without charge and without requesting permission. Full citation is required.

*Permission for reprint applies to Chapters 2 and 3.

Obtained from: https://www.physiology.org/author-info.permissions